JPTM
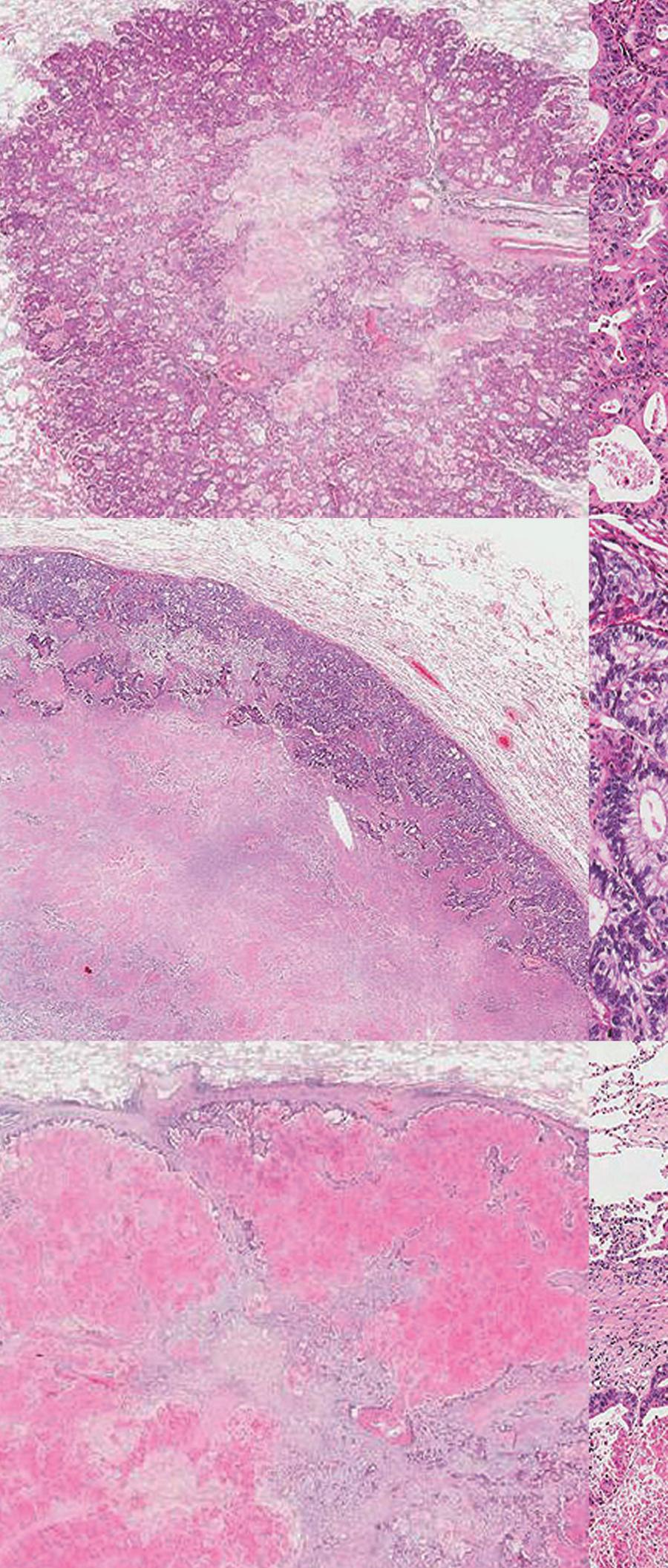
Prognostic Utility of Histological Growth Patterns of Colorectal Lung Oligometastasis

Aims & Scope

The Journal of Pathology and Translational Medicine is an open venue for the rapid publication of major achievements in various fields of pathology, cytopathology, and biomedical and translational research. The Journal aims to share new insights into the molecular and cellular mechanisms of human diseases and to report major advances in both experimental and clinical medicine, with a particular emphasis on translational research. The investigations of human cells and tissues using high-dimensional biology techniques such as genomics and proteomics will be given a high priority. Articles on stem cell biology are also welcome. The categories of manuscript include original articles, review and perspective articles, case studies, brief case reports, and letters to the editor.

Subscription Information

To subscribe to this journal, please contact the Korean Society of Pathologists/the Korean Society for Cytopathology. Full text PDF files are also available at the official website (http://jpatholtm.org). *Journal of Pathology and Translational Medicine* is indexed by Emerging Sources Citation Index (ESCI), PubMed, PubMed Central, Scopus, KoreaMed, KoMCI, WPRIM, Directory of Open Access Journals (DOAJ), and CrossRef. Circulation number per issue is 700.

Front cover image: Representative histologic features of the three different growth patterns of lung oligometastasis from colorectal adenocarcinoma (Fig. 1). p100.

CONTENTS

Instructions for Authors for *Journal of Pathology and Translational Medicine* are available at http://jpatholtm.org/authors/authors.php

Protein Phosphatase Magnesium-Dependent 1δ (PPM1D) Expression as a Prognostic Marker in Adult Supratentorial Diffuse Astrocytic and Oligodendroglial Tumors

Hui Jeong Jeong · Chang Gok Woo[1]
Bora Lee[2] · Shin Kwang Khang
Soo Jeong Nam · Jene Choi

Department of Pathology, Asan Medical Center, University of Ulsan College of Medicine, Seoul; [1]Department of Pathology, Chungbuk National University Hospital, Chungbuk National University College of Medicine, Cheongju; [2]Department of Biostatistics, Clinical Trial Center, Soonchunhyang Medical Center, Bucheon, Korea

Corresponding Author
Jene Choi, PhD
Department of Pathology, Asan Medical Center, University of Ulsan College of Medicine, 88 Olympic-ro 43-gil, Songpa-gu, Seoul 05505, Korea
Tel: +82-2-3010-4555
Fax: +82-2-472-7898
E-mail: jenec@amc.seoul.kr

Background: Protein phosphatase magnesium-dependent 1δ (PPM1D) is a p53-induced serine/threonine phosphatase, which is overexpressed in various human cancers. A recent study reported that a mutation in the *PPM1D* gene is associated with poor prognosis in brainstem gliomas. In this study, we evaluated the utility of PPM1D as a prognostic biomarker of adult supratentorial diffuse astrocytic and oligodendroglial tumors. **Methods:** To investigate PPM1D protein expression, mRNA expression, and copy number changes, immunohistochemistry, RNAscope *in situ* hybridization, and fluorescence *in situ* hybridization were performed in 84 adult supratentorial diffuse gliomas. We further analyzed clinical characteristics and overall survival (OS) according to PPM1D protein expression, and examined its correlation with other glioma biomarkers such as isocitrate dehydrogenase (*IDH*) mutation, and p53 expression. **Results:** Forty-six cases (54.8%) were PPM1D-positive. PPM1D expression levels were significantly correlated with PPM1D transcript levels (p = .035), but marginally with *PPM1D* gene amplification (p = .079). Patients with high-grade gliomas showed a higher frequency of PPM1D expression than those with low-grade gliomas (p < .001). Multivariate analysis demonstrated that PPM1D expression (hazard ratio [HR], 2.58; p = .032), age over 60 years (HR, 2.55; p = .018), and *IDH1* mutation (HR, 0.18; p = .002) were significantly independent prognostic factors; p53 expression had no prognostic significance (p = .986). The patients with tumor expressing PPM1D showed a shorter OS (p = .003). Moreover, patients with tumor harboring wild-type *IDH1* and PPM1D expression had the worst OS (p < .001). **Conclusions:** Our data suggest that a subset of gliomas express PPM1D; PPM1D expression is a significant marker of poor prognosis in adult supratentorial diffuse astrocytic and oligodendroglial tumors.

Key Words: PPM1D; IDH1; Mutation; Diffuse astrocytic and oligodendroglial tumors; Supratentorial gliomas; Molecular marker

Gliomas are the most common tumors of the brain and spinal cord, and account for the majority of brain cancer-related deaths.[1,2] Molecular-profiling studies have reported characteristic genetic alterations related with different gliomas. These biomarkers were subsequently incorporated in the 2016 World Health Classification (WHO) Classification of Tumours of the Central Nervous System (revised 4th edition).[3-9] Mutations in the isocitrate dehydrogenase 1 (*IDH1*) and *IDH2* genes occur in 70%–80% of grade II/III gliomas and most secondary glioblastomas.[10] Co-deletion of 1p/19q is typically related with tumors of the oligodendroglial lineage and is closely associated with *IDH* mutations.[11] Alterations in the *p53* and its pathway genes occur in 78% of glioblastomas, and are thought to promote progression to high-grade malignancy.[12,13]

Protein phosphatase magnesium-dependent 1δ (PPM1D),

also known as wild-type p53-induced phosphatase 1, is a member of the protein phosphatase type 2C and p53 target gene family and occurs in response to various stresses.[14-18] Activated PPM1D directly dephosphorylates Chk1, Chk2, p38 mitogen-activated protein kinase, uracil DNA glycosylase, MDM2, H2AX, and p53, suggesting that it acts as a homeostatic regulator.[19-22] The *PPM1D* gene is frequently amplified/overexpressed in various human cancers, all of which rarely carry a p53 mutation.[23-29] Recent studies have reported C-terminal truncating alterations in the *PPM1D* gene, which enhance the functional ability of PPM1D. *PPM1D* mutation was identified in 18.2% of pediatric brainstem gliomas, which were mutually exclusive with *p53* mutations detected in 57.6% of the same tumors. Moreover, *PPM1D* mutation was known to be associated with poor prognosis in pediatric brainstem gliomas.[30-32]

In this study, we intended to evaluate the utility of PPM1D expression as a prognostic biomarker of adult supratentorial diffuse astrocytic and oligodendroglial tumors. Other clinical characteristics were also analyzed to explore the relationship between the tumors and PPM1D expression. Moreover, we investigated brain lower grade gliomas (WHO grade II and III) from The Cancer Genome Atlas (TCGA) data to clarify the clinical effects according to the genetic alterations of PPM1D.

MATERIALS AND METHODS

Patients

We retrospectively reviewed data for 109 patients diagnosed with diffuse astrocytic and oligodendroglial tumors according to the 2016 WHO Classification of Tumours of the Central Nervous System (revised 4th edition) from August 2013 to July 2015 from the archives of the Department of Pathology at Asan Medical Center. Eighty-four patients were enrolled after excluding four cases of adult or pediatric brainstem glioma, one case of adult cerebellar glioma, and 20 cases without sufficient tissue. The medical records of 84 patients were reviewed, including sex, age, tumor locations, diagnoses, molecular parameters, treatments, and survival outcomes. This study adhered to the guidelines established by the Declaration of Helsinki and was approved by the Institutional Review Board of Asan Medical Center (2015-0151). Informed consents were obtained from all individual participants included in the study.

Tissue microarray construction and immunohistochemistry

Tissue microarrays (TMAs) consisting of two cylindrical cores (3-mm) from formalin-fixed, paraffin-embedded tissues obtained from surgically resected or stereotactic biopsy specimens were constructed using a Quick-Ray Manual Tissue Microarrayer (UT06, Unitma, Belrose, NSW, Australia). Immunohistochemistry (IHC) of 4-μm paraffin section of TMA blocks was performed using a Benchmark automatic immunostaining device (Ventana Medical Systems, Tucson, AZ, USA). The slides were incubated with primary antibodies against PPM1D (1:100, 2804D1a, Abcam, Cambridge, UK) and p53 (1:1,500, DO.7, DAKO, Glostrup, Denmark). IHC for PPM1D was scored as follows: 0, no reactivity or nuclear and cytoplasmic reactivity in less than 5% of the tumor cells; 1, reactivity in 5% to less than one-third of the tumor cells; 2, reactivity in one-third to two-thirds of the tumor cells; and 3, reactivity in more than two-thirds of the tumor cells.[33] Immunopositivity was determined to optimize the cutoff point for patient survival to dichotomize

the PPM1D expression data using the X-Tile software.[34] Scores of 0 and 1 indicated negative results, and scores of 2 and 3 indicated positive results. p53 immunoreactivity was also scored using this method.

IDH1 sequencing

The genomic region spanning codon 132 of *IDH1* was amplified using the polymerase chain reaction with the following primer set: 5'-TGAGAAGAGGGTTGAGGAGTTC-3' (forward) and 5'-CACATACAAGTTGGAAATTTCTGG-3' (reverse). The genomic region was then sequenced with the forward primer using the BigDye Terminator v3.1 Cycle Sequencing Kit (Applied Biosystems, Foster, CA, USA).

RNAscope *in situ* hybridization

PPM1D transcript was measured with the RNAscope assay using the Hs-PPM1D probe (602231; Advanced Cell Diagnostics, Hayward, CA, USA). Hybridization signals were amplified and visualized with the RNAscope 2.5 HD reagent kit-RED (322350, Advanced Cell Diagnostics). PPM1D mRNA molecules, shown as red spots, were quantified via light microscopy by manual counting. The signals per cell were divided into four groups according to the manufacturer's semi-quantitative scoring guideline: score 0, no staining or less than 1 dot in 10 cells; score 1, 1–3 dots in a cell; score 2, 4–9 dots in a cell; and score 3, ≥10 dots in a cell or the presence of gene clusters in ≥10% of the tumor cells. Based on a cutoff value of 1.5 determined by using the X-Tile software, scores of 2 and 3 were considered to indicate high PPM1D mRNA expression, and scores of 0 and 1 indicated no and low PPM1D mRNA expression, respectively.

Fluorescence *in situ* hybridization

Copy number status of the *PPM1D* gene was evaluated via fluorescence *in situ* hybridization (FISH) using the HYBrite denaturation/hybridization system (Abbott Molecular, Chicago, IL, USA). The PPM1D FISH probes in red and chromosome 17 control probes (CEP17) in green were purchased from Empire Genomics (Buffalo, NY, USA). Specimens that showed a PPM1D/CEP17 ratio ≥3 were considered positive for *PPM1D* amplification, and those with a PPM1D/CEP17 ratio >1 but <3 in ≥10% of tumor cells were defined as relative copy gain.

Statistical analysis

The independent t test, chi-square test, and Fisher exact test were carried out to assess the association between PPM1D protein expression and clinicopathological characteristics. To determine

the relationships among PPM1D alterations, we conducted a chi-square test and Fisher exact test. The Cox proportional hazards regression model was used to assess the dependency of survival duration on predictor variables. To estimate survival rates and compare survival distribution, we used the Kaplan-Meier method and log-rank test, respectively. All statistical analyses were performed using the R software (ver. 3.3.2, the R Foundation for Statistical Computing, Vienna, Austria). Any p-value < .05 was assumed to indicate a statistically significant difference.

RESULTS

Clinicopathological characteristics of the patients

A total of 84 patients with adult supratentorial diffuse astrocytic and oligodendroglial tumors were analyzed. The clinicopathological findings are summarized in Table 1. The 84 cases consisted of 26 glioblastomas, *IDH*-wildtype (31.0%), 16 ana-plastic oligodendrogliomas, *IDH*-mutant and 1p/19q-codeleted (19.0%), 12 oligodendrogliomas, *IDH*-mutant and 1p/19q-codeleted (14.3%), and 10 diffuse astrocytomas, *IDH*-mutant (11.9%). The majority (89.7%, 61/68) of the patients with high-grade gliomas or diffuse astrocytomas (*IDH*-mutant and wildtype) underwent surgery with adjuvant chemotherapy or chemoradiation therapy. Those with oligodendrogliomas, IDH-mutant and 1p/19q-codeleted were treated with surgery without any additional therapy (100%, 12/12). Over half of the enrolled patients showed PPM1D expression (54.8%, 46/84) and p53 expression (54.8%, 46/84) in IHC. Among the 36 patients (42.9%) with IDH1 mutations, 35 had R132H mutation and 1 had R132S mutation.

Clinicopathological characteristics according to PPM1D protein expression

IHC for PPM1D was performed in 84 cases of adult diffuse

Table 1. Baseline characteristics of the enrolled patients

Variable	Total (n = 84)	PPM1D (–) (n = 38)	PPM1D (+) (n = 46)	p-value
Age, median (range, yr)	51 (20–83)	45 (26–76)	52 (20–83)	.255
Sex				.327
Male	48 (57.1)	19 (50.0)	29 (63.0)	
Female	36 (42.9)	19 (50.0)	17 (37.0)	
Site				.165
Frontal lobe	41 (48.8)	20 (52.6)	21 (45.7)	
Temporal lobe	27 (32.1)	8 (21.1)	19 (41.3)	
Parietal lobe	12 (14.3)	8 (21.1)	4 (8.7)	
Occipital lobe	4 (4.8)	2 (5.3)	2 (4.3)	
Diagnosis				< .001
Diffuse astrocytoma, *IDH*-mutant	10 (11.9)	9 (23.7)	1 (2.2)	
Diffuse astrocytoma, *IDH*-wildtype	2 (2.4)	2 (5.3)	0 (0)	
Oligodendroglioma, *IDH*-mutant and 1p/19q-codeleted	12 (14.3)	9 (23.7)	3 (6.5)	
Anaplastic astrocytoma, *IDH*-mutant	3 (3.6)	1 (2.6)	2 (4.3)	
Anaplastic astrocytoma, *IDH*-wildtype	7 (8.3)	3 (7.9)	4 (8.7)	
Anaplastic oligodendroglioma, IDH-mutant and 1p/19q-codeleted	16 (19.0)	4 (10.5)	12 (26.1)	
Glioblastoma, *IDH*-mutant	5 (6.0)	3 (7.9)	2 (4.3)	
Glioblastoma, *IDH*-wildtype	26 (31.0)	6 (15.8)	20 (43.5)	
Oligodendroglioma, NOS	2 (2.4)	1 (2.6)	1 (2.2)	
Anaplstic oligodendroglioma, NOS	1 (1.2)	0 (0)	1 (2.2)	
Treatment				.156
Surgery	20 (23.8)	12 (31.6)	8 (17.4)	
Surgery with CTx and/or RTx	62 (73.8)	26 (68.4)	36 (78.3)	
CTx and/or RTx	2 (2.4)	0 (0)	2 (4.3)	
p53 expression				< .001
Negative	38 (45.2)	26 (68.4)	12 (26.1)	
Positive	46 (54.8)	12 (31.6)	34 (73.9)	
IDH1 mutation				.062
No	48 (57.1)	17 (44.7)	31 (67.4)	
Yes	36 (42.9)	21 (55.3)	15 (32.6)	

Values are presented as number (%).
PPM1D, protein phosphatase magnesium-dependent 1δ; IDH, isocitrate dehydrogenase; NOS, not otherwise specified; CTx, chemotherapy; RTx, radiotherapy.

astrocytic and oligodendroglial tumors (Fig. 1A). The relationships between PPM1D expression and clinicopathological characteristics are summarized in Table 1. The patients' characteristics were not significantly different according to PPM1D expression except for the diagnosis. High-grade gliomas showed a higher frequency of PPM1D expression than low-grade gliomas (70.2% vs 16.7%, p < .001). In terms of molecular profiles, p53 expression showed a positive correlation with PPM1D expression (p < .001). There was a marginally negative relationship between PPM1D expression and *IDH1* mutation (p = .062).

Relationships between PPM1D expression and its genetic alterations

To assess the relationships between PPM1D expression, mRNA levels, and DNA copy-number alterations, RNAscope *in situ* hybridization, and FISH were conducted. Informative results were obtained in 77 cases. Thirty-five cases (45.5%, 35/77) were classified as demonstrating high PPM1D mRNA levels (Fig. 1B). There was a significant correlation between PPM1D protein expression and PPM1D mRNA expression (p = .035)

(Table 2). Patients with PPM1D expression were found to have higher PPM1D mRNA expression than those without PPM1D expression (58.5%, 24/41 vs 31.4%, 11/35; p = .026). A large number of cases involving PPM1D positivity (90.2%, 37/41) showed mRNA expression (low or high expression), and over half of the cases (58.5%, 24/41) presented high PPM1D mRNA levels. The level of PPM1D positivity in the high PPM1D mRNA group was significantly higher than that in the low/no PPM1D mRNA group (68.6%, 24/35 vs 40.5%, 17/42; p = .026).

Of the cases examined using FISH analyses, 11 (14.3%) showed *PPM1D* gene amplification and four (5.2%) demonstrated relative copy gain (Fig. 1C). The majority of the cases with *PPM1D* gene amplification exhibited PPM1D positivity (81.8%, 9/11). The proportion of PPM1D positivity in the *PPM1D* amplification group was higher than that in the *PPM1D* non-amplification/relative copy gained group with borderline significance (81.8%, 9/11 vs 48.5%, 32/66; p = 0.053). However, there was a marginal correlation between PPM1D expression and *PPM1D* gene amplification (p = .079).
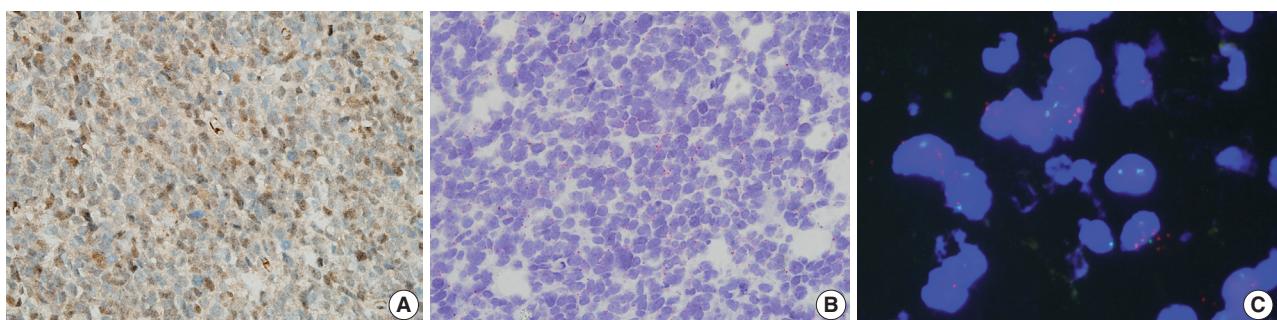
Fig. 1. A representative case of high-grade glioma. (A) Protein phosphatase magnesium-dependent 1δ (PPM1D) staining shows a high percentage of cells with positive protein expression in both the nucleus and cytoplasm in the anaplastic oligodendroglioma. (B) RNAscope *in situ* hybridization analysis shows positive expression of PPM1D shown as red dots. (C) Fluorescence *in situ* hybridization shows amplified *PPM1D* gene copies as red spots.

Table 2. Correlation between PPM1D protein expression and genetic variables of *PPM1D*

PPM1D gene	Total (n = 84)	PPM1D (–) (n = 38)	PPM1D (+) (n = 46)	p-value
mRNA expression				.035
No	13 (16.9)	9 (25.0)	4 (9.8)	
Low	29 (37.7)	16 (44.4)	13 (31.7)	
High	35 (45.5)	11 (30.6)	24 (58.5)	
NA	7	2	5	
DNA alteration				.079
No	62 (80.5)	31 (86.1)	31 (75.6)	
Relative copy gain	4 (5.2)	3 (8.3)	1 (2.4)	
Amplification	11 (14.3)	2 (5.6)	9 (22.0)	
NA	7	2	5	

Values are presented as number (%).
PPM1D, protein phosphatase magnesium-dependent 1δ; NA, not available.

Prognostic significance of PPM1D positivity in patients with supratentorial diffuse astrocytic and oligodendroglial tumors

Age, diagnosis, *IDH1* mutation, and PPM1D expression were significant predictors of survival in univariate Cox proportional hazard regression analyses (Table 3). The patients aged over 60 years presented an increased risk of poor prognosis (hazard ratio [HR] 3.97; 95% confidence interval [CI], 1.86 to 8.46; p < .001). Those diagnosed with glioblastoma, IDH-wildtype showed the worst prognosis (HR, 8.28; 95% CI, 1.71 to 40.01; p = .008). PPM1D expression was significantly associated with decreased survival (HR, 3.35; 95% CI, 1.42 to 7.90; p = .005), and survival in PPM1D-positive patients was significantly shorter than in PPM1D-negative patients (median overall survival [OS],

21 months [95% CI, 19 to not reached] vs not reached; p = .003) (Fig. 2A). Mutant *IDH1* was a significant protective factor when compared with wild-type *IDH1* (HR, 0.14; 95% CI, 0.05 to 0.38; p < .001), and the patients with mutant IDH1 showed significantly longer OS from the initial diagnosis (median OS, 102 months [95% CI, 102 to not reached] vs 19 months [95% CI, 14 to not reached]; p < .001) (Fig. 2B). In multivariate analyses, age (> 60 years) (HR, 2.55; 95% CI, 1.17 to 5.55; p = .018), PPM1D positivity (HR, 2.58; 95% CI, 1.08 to 6.17; p = .032), and *IDH1* mutation (HR, 0.18; 95% CI, 0.06 to 0.53; p = .002) were independent prognostic factors (Table 3). Thus, the prognostic significance of PPM1D protein expression was further analyzed. Patients with mutant *IDH1* and PPM1D-negative

Table 3. Cox proportional hazard regression analysis for overall survival of the patients with supratentorial glioma

Variable	Univariate		Multivariate	
	HR (95% CI)	p-value	HR (95% CI)	p-value
Age (yr)				
≤60	1 (Reference)		1 (Reference)	
>60	3.97 (1.86–8.46)	<.001	2.55 (1.17–5.55)	.018
Sex				
Female	1 (Reference)		-	
Male	1.03 (0.49–2.15)	.949	-	-
Site				
Frontal lobe	1 (Reference)		-	
Temporal lobe	1.81 (0.79–4.14)	.161	-	-
Parietal lobe	2.76 (0.94–8.01)	.064	-	-
Occipital lobe	0.86 (0.11–6.64)	.885	-	-
Diagnosis				
Diffuse astrocytoma, *IDH*-mutant	1 (Reference)		-	
Diffuse astrocytoma, *IDH*-wildtype	-	-	-	-
Oligodendroglioma, *IDH*-mutant and 1p/19q-codeleted	-	-	-	-
Anaplastic astrocytoma, *IDH*-mutant	1.83 (0.16–20.31)	.621	-	-
Anaplastic astrocytoma, *IDH*-wildtype	1.10 (2.07–58.12)	.005	-	-
Anaplstic oligodendroglioma, IDH-mutant and 1p/19q-codeleted	2.43 (0.43–13.63)	.312	-	-
Glioblastoma, *IDH*-mutant	-	-	-	-
Glioblastoma, *IDH*-wildtype	8.28 (1.71–40.01)	.008	-	-
Treatment				
Surgery	1 (Reference)			
Surgery+CTx and/or RTx	3.16 (0.95–10.52)	.060	-	-
CTx and/or RTx	18.75 (2.91–121.04)	.002	-	-
PPM1D expression				
Negative	1 (Reference)		1 (Reference)	
Positive	3.35 (1.42–7.90)	.005	2.58 (1.08–6.17)	.032
p53 expression				
Negative	1 (Reference)		1 (Reference)	
Positive	2.06 (0.96–4.43)	.064	1.01 (0.43–2.34)	.986
IDH1 mutation				
No	1 (Reference)		1 (Reference)	
Yes	0.14 (0.05–0.38)	<.001	0.18 (0.06–0.53)	.002

HR, hazard ratio; CI, confidence interval; IDH, isocitrate dehydrogenase; CTx, chemotherapy; RTx, radiotherapy; PPM1D, protein phosphatase magnesium-dependent 1δ.

(IDH1*mut*/PPM1D-negative) tumors had the best OS, whereas patients with wild-type *IDH1* and PPM1D expression (IDH1*wt*/PPM1D-positive) showed the worst OS (p < .001) (Fig. 2C).

DISCUSSION

Histologic diagnosis and grading were the gold standard for diagnosing gliomas. Recently, the well-established molecular markers, *IDH* and 1p/19q, were incorporated in the 2016 WHO classification.[7] In the present study, we explored the effect of PPM1D expression and its association with other molecular markers, including IDH and p53. To our knowledge, this is the first study regarding PPM1D expression in supratentorial diffuse astrocytic and oligodendroglial tumors. Patients with PPM1D-positive tumors had significantly worse OS than those without PPM1D-expressing tumors (p = .003) (Fig. 2A); in terms of prognostic utility, PPM1D expression was found to be comparable to *IDH* mutation status.

Genetic alterations of PPM1D are observed in various tumors, and are significantly associated with poor prognosis.[23-29] Our data showed that overexpression of p53 and that of PPM1D were positively correlated (p < .001) (Table 1). The results were in contrast to our expectation because *p53* mutation and PPM1D overexpression were exclusively detected in tumors. *p53* mutation status rather than p53 protein expression is clearly associated with poor prognosis in malignant gliomas.[35,36] In our study, PPM1D positivity was significantly correlated with its mRNA transcript levels (p = .035) and marginally associated with *PPM1D* gene amplification (p = .079). The degree of PPM1D-positivity in the PPM1D amplification group was greater than that in the PPM1D non-amplification/relative copy gained group (81.8% vs 48.5%, p = .053) (Table 2). Based on the data, we believe that PPM1D protein expression (55%, 46/84) may be increased by mRNA upregulation and DNA amplification of the *PPM1D* gene rather than functional wild-type p53 in this cohort. Recently, Zhang *et al*.[32] reported that *p53* (58%, 19/33) and *PPM1D* (18%, 6/33) mutations demonstrate a mutually exclusive pattern in brainstem gliomas; moreover, OS rates are similar in patients with *p53*-mutated gliomas and those with *PPM1D*-mutated gliomas. The genomic landscape of supratentorial diffuse astrocytic and oligodendroglial tumors could be different from that of brainstem gliomas, which have two main driver mutations, *p53* and *PPM1D*, in the absence of PPM1D overexpression. *PPM1D* mutation is very rare in gliomas arising outside the brainstem.[32,37] Our data suggest that PPM1D expression in supratentorial diffuse astrocytic and oligodendroglial tumors may have similar effects as *PPM1D* mutations in brainstem gliomas, resulting in stabilized and extended phosphatase activities of PPM1D.

In our study, multivariate analysis for OS according to various clinical and molecular parameters revealed that PPM1D is a significant molecular marker (HR, 2.58; p = .032) together with *IDH1* mutation (HR, 0.18; p = .002). In accordance with previous studies,[38,39] our data showed that p53 overexpression did not have prognostic effects, per univariate (p=.064) and multivariate (p = .986) analyses. The results suggest that p53
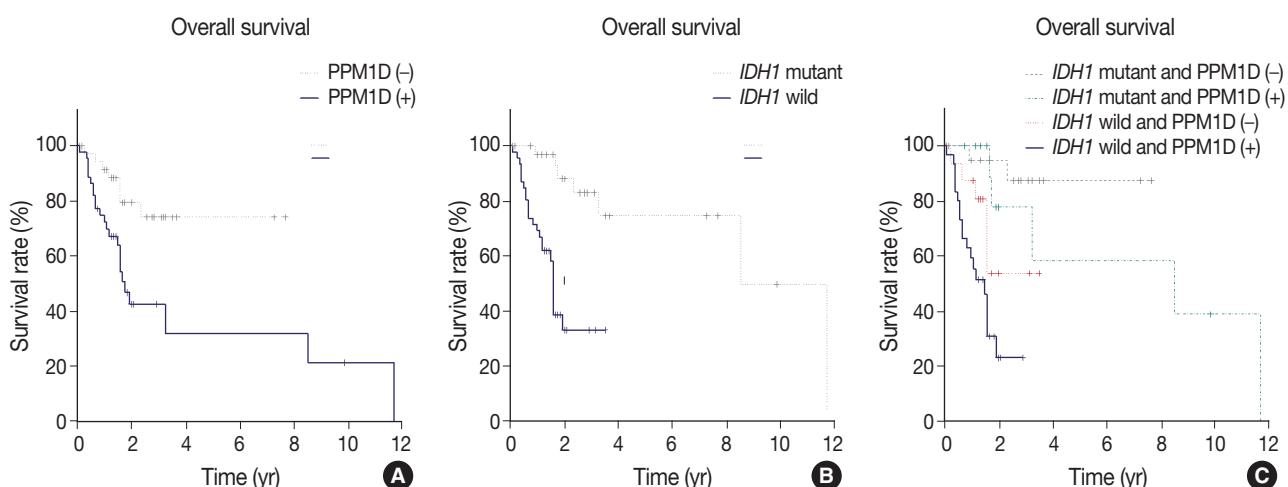
Fig. 2. Kaplan-Meier survival curves of patients with supratentorial diffuse astrocytic and oligodendroglial tumors. (A) Comparison of patients with protein phosphatase magnesium-dependent 1δ (PPM1D) expression and those without PPM1D expression. (B) Comparison of patients with isocitrate dehydrogenase 1 (*IDH1*) mutation versus those with wild-type *IDH1*. (C) Comparison of patients with PPM1D expression versus those without PPM1D expression with or without an additional *IDH1* mutation. Log-rank tests for a, b, and c yielded p = .003, p < .001, and p < .001, respectively.

expression did not enhance the negative prognostic effect in terms of survival, although we observed a positive correlation between PPM1D and p53 expressions. In addition, we analyzed mRNA expression and DNA alteration in the *PPM1D* gene in 516 lower grade gliomas including grades II and III available for the *PPM1D* gene, using the cBioPortal for Cancer Genomics from TCGA data (Supplementary Table S1).[40,41] Of the 40 cases with alterations, gene amplifications were found in 10 cases, deep deletion in 1, mRNA upregulation in 31, and mRNA down-regulation in 2 were found (Supplementary Table S2, Supplementary Fig. S1A). The patients with up-regulated PPM1D transcripts and/or DNA amplification had a shorter OS than those who did not demonstrate these alterations (p = .031) (Supplementary Fig. S1B). The results further confirm that PPM1D expression could be a novel prognostic marker in supratentorial diffuse astrocytic and oligodendroglial tumors. We further characterized two prognostic factors: *IDH1* mutation and PPM1D expression (Fig. 2C). Patients with *IDH1mut*/PPM1D-negative tumors had the most favorable OS; those with *IDH1wt*/PPM1D-positive tumors had the worst OS (p < .001). Considering the median OS for PPM1D-positive patients (21 months; 95% CI, 19 to not reached) and *IDH1wt* patients (19 months; 95% CI, 14 to not reached), these results suggest that PPM1D expression and wild-type *IDH1* status seem to have an additive negative prognostic effect on survival in supratentorial gliomas and may promote tumorigenesis via different mechanisms.

In conclusion, our results indicate that PPM1D has the potential to be a molecular prognostic marker of adult diffuse astrocytic and oligodendroglial tumors and its prediction abilities are independent of the *IDH1* and 1p19q co-deletion. Although these results need to be further validated, we hope to provide a basis for classifying this PPM1D-positive subset of gliomas and open up new opportunities for the treatment of such patients using PPM1D inhibitors.

Electronic Supplementary Material

Supplementary materials are available at Journal of Pathology and Translational Medicine (http://jpatholtm.org).

Conflicts of Interest

No potential conflict of interest relevant to this article was reported.

REFERENCES

1. Wen PY, Kesari S. Malignant gliomas in adults. N Engl J Med 2008; 359: 492-507.

2. DeAngelis LM. Brain tumors. N Engl J Med 2001; 344: 114-23.

3. Brennan CW, Verhaak RG, McKenna A, *et al*. The somatic genomic landscape of glioblastoma. Cell 2013; 155: 462-77.

4. Cancer Genome Atlas Research Network. Comprehensive genomic characterization defines human glioblastoma genes and core pathways. Nature 2008; 455: 1061-8.

5. Cancer Genome Atlas Research Network, Brat DJ, Verhaak RG, *et al*. Comprehensive, integrative genomic analysis of diffuse lower-grade gliomas. N Engl J Med 2015; 372: 2481-98.

6. Chen R, Smith-Cohn M, Cohen AL, Colman H. Glioma subclassifications and their clinical significance. Neurotherapeutics 2017; 14: 284-97.

7. Louis DN, Perry A, Reifenberger G, *et al*. The 2016 World Health Organization classification of tumors of the central nervous system: a summary. Acta Neuropathol 2016; 131: 803-20.

8. Reuss DE, Sahm F, Schrimpf D, *et al*. ATRX and IDH1-R132H immunohistochemistry with subsequent copy number analysis and IDH sequencing as a basis for an "integrated" diagnostic approach for adult astrocytoma, oligodendroglioma and glioblastoma. Acta Neuropathol 2015; 129: 133-46.

9. Suzuki H, Aoki K, Chiba K, *et al*. Mutational landscape and clonal architecture in grade II and III gliomas. Nat Genet 2015; 47: 458-68.

10. Lass U, Numann A, von Eckardstein K, *et al*. Clonal analysis in recurrent astrocytic, oligoastrocytic and oligodendroglial tumors implicates IDH1-mutation as common tumor initiating event. PLoS One 2012; 7: e41298.

11. Labussière M, Idbaih A, Wang XW, *et al*. All the 1p19q codeleted gliomas are mutated on IDH1 or IDH2. Neurology 2010; 74: 1886-90.

12. Nagpal J, Jamoona A, Gulati ND, *et al*. Revisiting the role of p53 in primary and secondary glioblastomas. Anticancer Res 2006; 26: 4633-9.

13. Tabouret E, Nguyen AT, Dehais C, *et al*. Prognostic impact of the 2016 WHO classification of diffuse gliomas in the French POLA cohort. Acta Neuropathol 2016; 132: 625-34.

14. Dudgeon C, Shreeram S, Tanoue K, *et al*. Genetic variants and mutations of PPM1D control the response to DNA damage. Cell Cycle 2013; 12: 2656-64.

15. Lee DH, Chowdhury D. What goes on must come off: phosphatases gate-crash the DNA damage response. Trends Biochem Sci 2011; 36: 569-77.

16. Le Guezennec X, Bulavin DV. WIP1 phosphatase at the crossroads of cancer and aging. Trends Biochem Sci 2010; 35: 109-14.

17. Lu X, Nguyen TA, Moon SH, Darlington Y, Sommer M, Donehower LA. The type 2C phosphatase Wip1: an oncogenic regulator of tumor suppressor and DNA damage response pathways. Cancer Metastasis Rev 2008; 27: 123-35.

18. Song JY, Ryu SH, Cho YM, *et al.* Wip1 suppresses apoptotic cell death through direct dephosphorylation of BAX in response to gamma-radiation. Cell Death Dis 2013; 4: e744.

19. Bulavin DV, Demidov ON, Saito S, *et al.* Amplification of PPM1D in human tumors abrogates p53 tumor-suppressor activity. Nat Genet 2002; 31: 210-5.

20. Kleiblova P, Shaltiel IA, Benada J, *et al.* Gain-of-function mutations of PPM1D/Wip1 impair the p53-dependent G1 checkpoint. J Cell Biol 2013; 201: 511-21.

21. Lu X, Nannenga B, Donehower LA. PPM1D dephosphorylates Chk1 and p53 and abrogates cell cycle checkpoints. Genes Dev 2005; 19: 1162-74.

22. Lu X, Ma O, Nguyen TA, Jones SN, Oren M, Donehower LA. The Wip1 phosphatase acts as a gatekeeper in the p53-Mdm2 autoregulatory loop. Cancer Cell 2007; 12: 342-54.

23. Hirasawa A, Saito-Ohara F, Inoue J, *et al.* Association of 17q21-q24 gain in ovarian clear cell adenocarcinomas with poor prognosis and identification of PPM1D and APPBP2 as likely amplification targets. Clin Cancer Res 2003; 9: 1995-2004.

24. Hu W, Feng Z, Modica I, *et al.* Gene amplifications in well-differentiated pancreatic neuroendocrine tumors inactivate the p53 pathway. Genes Cancer 2010; 1: 360-8.

25. Lambros MB, Natrajan R, Geyer FC, *et al. PPM1D* gene amplification and overexpression in breast cancer: a qRT-PCR and chromogenic in situ hybridization study. Mod Pathol 2010; 23: 1334-45.

26. Loukopoulos P, Shibata T, Katoh H, *et al.* Genome-wide array-based comparative genomic hybridization analysis of pancreatic adenocarcinoma: identification of genetic indicators that predict patient outcome. Cancer Sci 2007; 98: 392-400.

27. Saito-Ohara F, Imoto I, Inoue J, *et al. PPM1D* is a potential target for 17q gain in neuroblastoma. Cancer Res 2003; 63: 1876-83.

28. Tan DS, Lambros MB, Rayter S, *et al.* PPM1D is a potential therapeutic target in ovarian clear cell carcinomas. Clin Cancer Res 2009; 15: 2269-80.

29. Yu E, Ahn YS, Jang SJ, *et al.* Overexpression of the wip1 gene abrogates the p38 MAPK/p53/Wip1 pathway and silences p16 expression in human breast cancers. Breast Cancer Res Treat 2007; 101: 269-78.

30. Liang C, Guo E, Lu S, *et al.* Over-expression of wild-type p53-induced phosphatase 1 confers poor prognosis of patients with gliomas. Brain Res 2012; 1444: 65-75.

31. Wang P, Rao J, Yang H, Zhao H, Yang L. Wip1 over-expression correlated with TP53/p14(ARF) pathway disruption in human astrocytomas. J Surg Oncol 2011; 104: 679-84.

32. Zhang L, Chen LH, Wan H, *et al.* Exome sequencing identifies somatic gain-of-function PPM1D mutations in brainstem gliomas. Nat Genet 2014; 46: 726-30.

33. Chuman Y, Kurihashi W, Mizukami Y, Nashimoto T, Yagi H, Sakaguchi K. PPM1D430, a novel alternative splicing variant of the human PPM1D, can dephosphorylate p53 and exhibits specific tissue expression. J Biochem 2009; 145: 1-12.

34. Camp RL, Dolled-Filhart M, Rimm DL. X-tile: a new bio-informatics tool for biomarker assessment and outcome-based cut-point optimization. Clin Cancer Res 2004; 10: 7252-9.

35. Wang X, Chen JX, Liu JP, You C, Liu YH, Mao Q. Gain of function of mutant *TP53* in glioblastoma: prognosis and response to temozolomide. Ann Surg Oncol 2014; 21: 1337-44.

36. Watanabe T, Katayama Y, Yoshino A, Komine C, Yokoyama T. Deregulation of the TP53/p14ARF tumor suppressor pathway in low-grade diffuse astrocytomas and its influence on clinical course. Clin Cancer Res 2003; 9: 4884-90.

37. Jones C, Baker SJ. Unique genetic and epigenetic mechanisms driving paediatric diffuse high-grade glioma. Nat Rev Cancer 2014; 14: 651-61.

38. Karsy M, Neil JA, Guan J, Mahan MA, Colman H, Jensen RL. A practical review of prognostic correlations of molecular biomarkers in glioblastoma. Neurosurg Focus 2015; 38: E4.

39. Ludwig K, Kornblum HI. Molecular markers in glioma. J Neurooncol 2017; 134: 505-12.

40. Cerami E, Gao J, Dogrusoz U, *et al.* The cBio cancer genomics portal: an open platform for exploring multidimensional cancer genomics data. Cancer Discov 2012; 2: 401-4.

41. Gao J, Aksoy BA, Dogrusoz U, *et al.* Integrative analysis of complex cancer genomics and clinical profiles using the cBioPortal. Sci Signal 2013; 6: pl1.

Extramural Perineural Invasion in pT3 and pT4 Gastric Carcinomas

Alejandro España-Ferrufino
Leonardo S. Lino-Silva
Rosa A. Salcedo-Hernández[1]

Departments of Gastrointestinal Pathology and [1]Surgical Oncology, Instituto Nacional de Cancerología (INCan), Mexico City, Mexico

Corresponding Author
Leonardo S. Lino-Silva, MD
Department of Gastrointestinal Pathology,
Instituto Nacional de Cancerología, Av. San
Fernando 22 Col. Sección XVI, CP. 14080, México
City, México
Tel: +52-55-5628-0400 (ext. 11068)
Fax: +52-55-56280401
E-mail: saul.lino.sil@gmail.com

Background: Perineural invasion (PNI) is widely studied in malignant tumors, and its prognostic significance is well demonstrated. Most studies have focused on evaluating the mural PNI (mPNI); however, extramural PNI (ePNI) may influence the prognosis in gastric cancer. We evaluated the prognostic value of ePNI compared with mPNI in gastric cancer in this observational comparative cross-sectional study. **Methods:** Seventy-three pT3 and pT4 gastric carcinomas with PNI were evaluated. Forty-eight (65.7%) were in the mPNI group and the remaining in the ePNI group. **Results:** Clinicopathologic characteristics between the two groups were similar, except for the outcomes. The 5-year disease-specific survival (DSS) rate was 64% for the mPNI group and 50% for the ePNI group (p = .039), a difference that did not remain significant in multivariate analysis. The only independent adverse prognostic factor in multivariate analysis was the presence of lymph node metastasis (hazard ratio, 1.757; 95% confidence interval, 1.082 to 2.854; p = .023). **Conclusions:** We demonstrated the prognostic effect of ePNI for DSS in surgically resected pT3–pT4 gastric cancer patients. ePNI could be considered in the staging and prognostic systems of gastric cancer to stratify patients with a high risk of recurrence.

Key Words: Stomach neoplasms; Perineural invasion; Survival; Prognostic factor; Neoplasms

Gastric cancer is the fifth most common cancer worldwide, with about one million new cases reported in 2012 (6.8% of the total).[1] About 70% of cases occur in developed and developing countries a half of them are presented in East Asia (mainly in China) and twice as often in men over women. Although the incidence of gastric cancer has declined in recent decades, it remains the third leading cancer-related cause of death worldwide with 723,000, deaths representing 8.8% of all cancer deaths.[1] The prognosis in advanced stages of gastric cancer is poor, even with the use of chemotherapy or other adjuvant treatments.

Perineural invasion (PNI) is one of the pathological factors widely studied in malignant neoplasms with a well-established prognostic significance in head and neck neoplasia and prostate cancer.[2] PNI is related to a more aggressive behavior of the neoplasia and poor prognosis in several malignancies.[3] However, there is no universal definition of PNI. Several pathologists simply define PNI as the presence of neoplastic cells in, around or through the nerves, while others require the presence of tumor cells within any of the epineurium, perineurium, or endoneurium. The most accepted one was defined by Batsakis,[4] defining it as the invasion of tumor cells in, around, and through nerves. Other authors define PNI according to the location of the neoplastic cells with regards to the layers of the nerve sheath (outer epineurium, perineurium, and inner endoneurium). Liebig *et al*.[5] defined PNI as the presence of neoplastic cells in any three layers of the nerve sheath or in foci outside the nerve sheath with the involvement of 33% of the nerve circumference. The criterion of PNI defined as cancer cells inside the perineurium and surrounding at least 33% of the nerve circumference showed a perfect interobserver concordance.

PNI was once thought to be an extension of lymphatic metastasis, but recent studies have shown that lymphatic channels do not penetrate the layers of the nerve sheath.[6-8] Studies on prostate and pancreatic cancer showed that in PNI there is an interaction of reciprocal neurotrophic factors between the neoplastic cells and the nerves, like nerve growth factor (NGF), brain-derived neurotrophic factor, neurotrophin 3, and neurotrophin.[9,10] Okada *et al*.[11] reported that exogenous NGF leads to a dose-dependent increase in matrix metalloproteinase 2 expression and invasion in neoplastic cells of the pancreas.

In a systematic review and meta-analysis of 30,590 cases on PNI in gastric cancer, Deng *et al*.[12] found PNI as an independent predictor of recurrence, as well as to affecting disease-free survival and overall survival in patients with gastric cancer undergoing

curative resection. Although most authors focus their attention on evaluating mural perineural invasion (mPNI, invasion of the nerve plexus in the proper muscle and submucosal muscle), there are studies in gastrointestinal cancers (especially colon cancer) that demonstrate that the PNI outside the muscular wall (extramural PNI [ePNI]) has a worse prognosis.[13] To date, there are no studies subclassifying PNI into mPNI and ePNI in gastric carcinoma.

Our goal was to confirm whether the prognosis associated with PNI is determined by ePNI rather than mPNI under the hypothesis that the patients with ePNI will show worse disease-specific survival (DSS) than those with mPNI, in pT3–pT4 carcinomas in clinical stages II and III.

MATERIALS AND METHODS

From the database of patients with gastric adenocarcinomas from 2005 to 2015 at the national referral cancer center in Mexico, we searched for patients who underwent curative resection of gastric adenocarcinoma in clinical stages II and III, with pathological tumor stages pT3 and pT4 and with PNI described in the pathological report. Most patients at our institution were at stage IV disease at presentation or in poor clinical conditions and they did not receive surgery. In our center, the same surgical team performs around 30 gastric surgeries per year. Gastrectomy with D2 lymphadenectomy was the standard surgical procedure in all cases. The standard adjuvant therapy was capecitabine/oxaliplatin in selected patients (especially in those who had pathological risk factors and/or low lymph node counts). Data on patient demographics, tumor localization, operation, and histopathological study were recorded. The staging was determined by clinical, radiological, and histopathological data according to the American Joint Commission on Cancer pTNM system (7th edition, 2010).[14]

For the selected cases (n = 73), two pathologists with expertise in gastrointestinal pathology separately evaluated a median of five hematoxylin and eosin stained slides (range, 3 to 8) for evaluation of PNI and other pathologic features. Each pathologist was blind to the patient data and the diagnosis of the other pathologist. The criterion of PNI was cancer cells inside the perineuroum involving at least 33% of the nerve circumference (Fig. 1).[5,15] When PNI was present in the submucosa or *muscularis propria*, the pathologist classified the case as mPNI. If the the tumor invaded a nerve located beyond the *muscularis propria* (subserosal tissue or adventitia), it was classified as ePNI. When the muscular layer could not be identified due to tumor destruction, an imaginary line was drawn between the breakpoints of
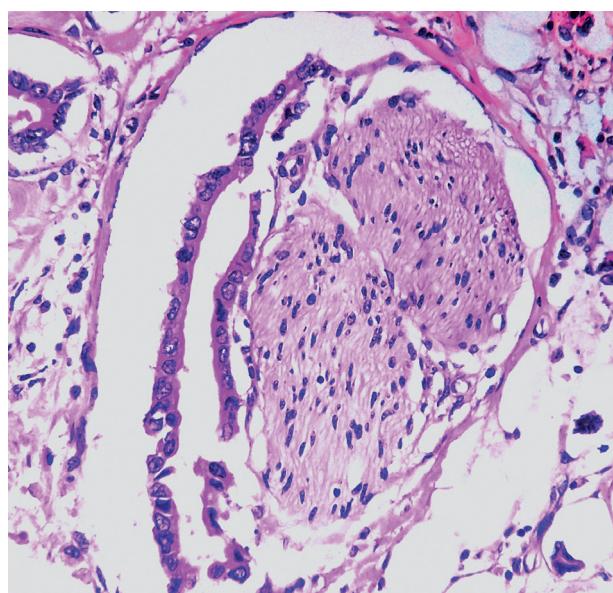
Fig. 1. Histologic microphotography showing perineural space invasion. Note that neoplastic glands invade perineurium and encases at least 33% of the circumference of the nerve.

intact *muscularis propria*. Discordant cases were reviewed by both pathologists under the same microscope for consensus. The tumor was classified as intestinal adenocarcinoma when glandular differentiation was clearly demonstrated and as diffuse adenocarcinoma when there was no glandular differentiation and the tumor was composed of individual cells with or without signet ring cells.

Statistic analysis

Data were analyzed using the Statistical Package for Social Sciences ver.12.0 (SPSS Inc., Chicago, IL, USA). Kappa statistic for interobserver concordance regarding PNI was performed before consensus between the pathologists. A comparison of the means was performed with an unpaired Student t test. Chi-square and Fisher exact tests were performed to examine associations between categorical variables. In all cases, p-values were two-sided, and a statistical significance was accepted when $p < .05$.

Survival analysis

The primary end-point was DSS defined as cancer death, determined from the date of the first treatment, including palliative care (event) or last follow-up (censored). The DSS curves were estimated using the Kaplan-Meier method. The univariate Cox regression model was used to examine the association of variables with DSS. Significant characteristics in the univariate analysis (variables with a $p < .05$) were introduced into a multi-

variate model of Cox proportional hazards in addition to age and sex.

This study was approved by the Institutional Review Board and Ethics Committe of the National Cancer Institute of Mexico with a waiver of informed consent because of the retrospective nature of the study (IRB No. CEI.16/117).

Table 1. Clinicopathologic data comparison between 73 gastric carcinomas in pT3 and pT4 stage according perineural invasion

Variable	Intramural (n = 25)	Extramural (n = 48)	p-value[a]
Median age (Q1–Q3 range)	56 (46–65)	58 (47–65)	.783
Sex			
Female	12 (48)	23 (47.9)	.617
Male	13 (52)	25 (52.1)	
pT			
pT3	15 (60)	21 (43.8)	.247
pT4a	10 (40)	24 (50)	
pT4b	0	3 (6.3)	
Nodal metastasis			
N0	5 (20)	8 (16.7)	.423
N1	12 (48)	25 (52.1)	
N2	8 (32)	14 (29.2)	
N3	0	1 (2.1)	
Location			
Proximal third	5 (20)	11 (22.9)	.759
Medim third	7 (28)	12 (25)	
Distal third	13 (52)	25 (52.1)	
Median number of dissected lymph nodes (Q1–Q3 range)	26 (19–36)	26 (19–39)	.818
Median number of positive lymph nodes (Q1–Q3 range)	7 (2–11)	10 (3–22)	.933
Distant metastases			
No	18 (72)	33 (68.8)	.774
Yes	7 (28)	15 (31.2)	
Lymphovascular invasion			
No	4 (16)	7 (14.6)	.872
Yes	21 (84)	41 (85.4)	
Grade			
Well differentiated	2 (8)	4 (8.3)	.405
Moderately differentiated	19 (76)	41 (85.4)	
Poorly differentiated	4 (16)	3 (6.3)	
Clinical stage			
Stage II	7 (28)	10 (20.8)	.770
Stage III	11 (44)	22 (45.8)	
Stage IV	7 (28)	16 (33.4)	
Resection			
R0	24 (96)	44 (91.7)	.487
R1	1 (4)	4 (8.3)	
Adjuvant treatment			
No	3 (12)	16 (33.3)	.137
Yes	22 (88)	32 (66.7)	
Overall recurrence			
No	12 (48)	18 (37.5)	.231
Yes	13 (52)	30 (62.5)	
Outcome			
Alive free of disease	9 (36)	5 (10.4)	.023
Dead with disease	6 (24)	14 (29.2)	
Alive with disease	10 (40)	22 (45.8)	
Dead without disease	0	7 (14.6)	
Median follow-up (Q1–Q3 range, mo)	13 (8–51)	11 (5–19)	.052
5-Year disease-specific survival (%)	64	50	.039

Values are presented as median (range) or number (%).
[a]Chi square test or Kruskal-Wallis test.

RESULTS

Clinicopathologic characteristics

Features of the patient cohort (n = 73) are summarized in Table 1. The median age was 56 years old, ranging from 46 to 65 years. Thirty-eight patients (52%) were male and 35 (48%) were female. In total, 68 patients (93%) received total gastrectomy and five received subtotal gastrectomy. Surgery was performed by laparoscopy in 15 cases (20.5%). During the laparotomy or laparoscopy, 22 patients (30.1%) presented with resectable peritoneal, hepatic or splenic metastasis, and all of them were fully resected. Major complications occurred in nine patients (12.3%; i.e., anastomotic leakage, septicemia, dehiscence). PNI was verified in all cases, with a majority (65.7%) in the ePNI group, and the kappa statistic was 1.0 for concordance between observers. There was no difference in clinicopathologic features between the groups including pT and pN stage (Table 1). Patients with ePNI were less likely to be free of disease (10.4% vs 36%). The percentage of each histologic type of the tumor was also similar between the groups.

Outcome

The median follow-up time was 12 ± 24.6 months, ranging from 5 to 116 months. In this timeframe, 43 patients had recurrence (48.9%): 33 distant and 10 local. The median time to recurrence was 5 months, with a range from 3 to 20 months. The incidence of recurrence was similar between the groups. Of the patient cohort, 19.2% of all patients were alive and free of disease, 27.4% died from the disease, 43.8% were alive with disease, and 9.6% died from causes not related to gastric carcinoma. Patients with ePNI had a higher mortality rate than patients with mPNI (29.2% vs 24%) (p = .023).

Survival analysis

The 5-year DSS was 60%. Univariate analysis is summarized in Table 2. Lymph node metastasis, tumor stage pT4b, presence of ePNI and recurrence were predictors of increased mortality. Patients with PNI showed differences in survival between the groups, with 5-year DSS of 64% for 25 patients with mPNI compared with 50% for 48 patients in the ePNI group (p = .039) (Fig. 2). Among the patients in the ePNI group, 14 were dead of disease with a median of 16 months, and 22 patients were alive with disease (recurrence). The median DSS of the patients in the ePNI group was 16 months and for the patients in the mPNI group was 46 months. Most patients (74%) received adjuvant therapy with heterogeneous modalities for subanalysis. All patients

Table 2. Univariate analysis of 73 gastric carcinomas[a]

Variable	5-Year disease-specific survival (%)	p-value
Sex		
Male	49	.591
Female	65	
Pathologic tumoral category		
pT3	67	.023
pT4a	43	
pT4b	0	
Clinical stage		
II	85	
III	36	.116
IV	27	
Lymph node metastasis		
No	90	.001
Yes	42	
Distant metastases		
No	56	.880
Yes	46	
Lymphovascular invasion		
No	90	.290
Yes	50	
Perineural invasion		
Intramural	64	.039
Extramural	49	
Grade		
Well differentiated	50	.619
Moderately differentiated	56	
Poorly differentiated	50	
Adjuvant therapy		
No	62	.713
Yes	66	
Resection		
R0	52	.783
R1	60	
Recurrence		
No	87	.007
Yes	42	

[a]Mantel-Cox test.

with nodal metastasis, lymphovascular invasion and R1 resections received adjuvant therapy. R1 resections had a higher 5-year survival than R0 resections, which can be explained by the rate of adjuvant therapy in the R1 group; however, the difference was not statistically significant.

The only independent adverse prognostic factor identified in multivariate analysis was lymph node metastasis (hazard ratio, 1.757; 95% confidence interval, 1.082 to 2.854; p = .023). The remaining factors including ePNI were not associated with poor DSS as independent factors (Table 3).
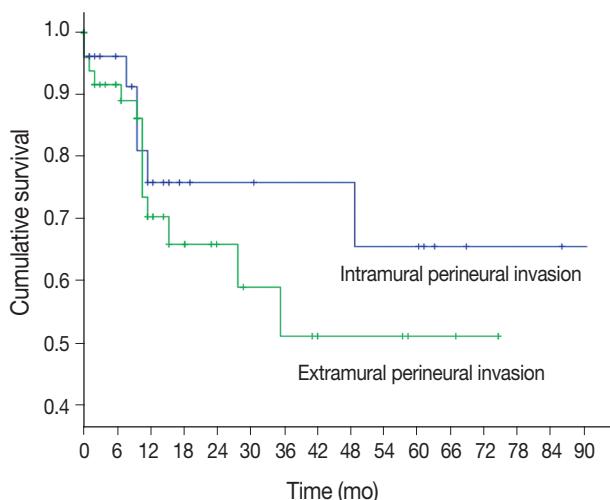
Fig. 2. Five-year disease-specific survival of 73 patients with gastric carcinoma divided by perineural invasion.

Table 3. Multivariate analysis of 73 gastric carcinomas

Variable	Cox hazard ratio	95% CI	p-value
Lymph node metastasis (yes vs no)	1.757	1.082–2.854	.023
Recurrence (yes vs no)	1.594	0949–2.676	.078
Pathologic T category (pT3 vs pT4).	1.187	0.453–3.110	.727
Extramural perineural invasion (yes vs no).	1.096	0.393–3.054	.861

CI, confidence interval.

DISCUSSION

PNI has been identified in gastric cancer with a median of 40.9% (6.8%–75.6%).[12] This is the first study subclassifying PNI into mPNi and ePNI in gastric cancer. We found ePNI to be present in equal sex distribution, with a median age of 58 years, more frequent in pT4a tumors, in patients with lymphovascular invasion and associated with a lower DSS compared with mPNI.

In gastric cancer, the prognostic significance of PNI is clear. Tanaka *et al*.[16] reported that PNI is a determinant in the prognosis of advanced cancer and found that 80% of patients with peritoneal recurrence had PNI whereas Duraker *et al*.[17] showed that PNI was present in 59.9% of patients with disease progression. Bilici *et al*.[18] found that the mean survival of patients with PNI was shorter than patients without PNI (60.3 months vs 27.9 months, respectively). Tianhang *et al*.[19] found a significant relationship between clinical stage and PNI; both were independent prognostic factors. Finally, Selcukbiricik *et al*.[20] and Jiang *et al*.[21] demosntrated that PNI is an independent prognostic factor associated with tumor size (> 5 cm), lymphovascular invasion, pT4 tumors, lymph node metastasis, and advanced stage.[21]

However, we think that this observations are due to ePNI rather than mPNI based on findings like those by Ueno *et al*.,[13] who analyzed 364 patients with rectal cancer, dividing PNI into PNI-0 (absence of IPN), PN-1 (less than five PNI foci in the first 10 mm measured from the outer muscle layer), PN-2 (five or more foci or 10 mm or more from the muscularis propria), and reported a 5-year survival of 74%, 50%, and 22%, respectively. They showed that the degrees of PNI were independently associated with local recurrence and long-term survival regardless of tumor depth and lymph node metastasis.[13] We applied a similar approach to gastric cancer, demonstrating similar results; an independent worse DSS of patients with ePNI compared with those with mPNI.

The perineural space is a potential route for tumor spread in gastric adenocarcinoma, especially outside muscularis propria in patients with pT3 and pT4 tumors. While in multivariate analysis their association could not be demonstrated as an independent factor for survival, it is clear that it is associated with lower median survival and 5-year DSS. We believe that this difference does not have significance in multivariate analysis in part because of the poor prognosis of these patients due to the advanced pathological stage and possibly inaccurate lymph node stage (some cases in our series had less than 25 lymph nodes in "D2" gastrectomy). However, in order to decrease these potential biases, we only used cases in pT3 and pT4 stages because these are the tumors that invade beyond muscularis propria.

It is plausible that ePNI could be considered in the staging and prognostic systems in gastric cancer to stratify patients with a high risk of recurrence. Our results need to be confirmed in a larger series; however, this study provide us with information on the possibility that PNI behaves differently depending on how it is evaluated, which can explain the lack of consensus on the true prognostic value of PNI.

Conflicts of Interest

No potential conflict of interest relevant to this article was reported.

REFERENCES

1. Ferlay J, Soerjomataram I, Ervik M, *et al*. GLOBOCAN 2012 v1.0, cancer incidence and mortality worldwide: IARC CancerBase No. 11. IARC CancerBase No. 11 [Internet]. Lyon: International Agency for Research on Cancer, 2013 [cited 2017 Dec 10]. Available from:

http://globocan.iarc.fr.

2. Fagan JJ, Collins B, Barnes L, D'Amico F, Myers EN, Johnson JT. Perineural invasion in squamous cell carcinoma of the head and neck. Arch Otolaryngol Head Neck Surg 1998; 124: 637-40.

3. Liebig C, Ayala G, Wilks JA, Berger DH, Albo D. Perineural invasion in cancer: a review of the literature. Cancer 2009; 115: 3379-91.

4. Batsakis JG. Nerves and neurotropic carcinomas. Ann Otol Rhinol Laryngol 1985; 94(4 Pt 1): 426-7.

5. Liebig C, Ayala G, Wilks J, *et al*. Perineural invasion is an independent predictor of outcome in colorectal cancer. J Clin Oncol 2009; 27: 5131-7.

6. Hassan MO, Maksem J. The prostatic perineural space and its relation to tumor spread: an ultrastructural study. Am J Surg Pathol 1980; 4: 143-8.

7. Reina MA, López A, Villanueva MC, de Andrés JA, León GI. Morphology of peripheral nerves, their sheaths, and their vascularization. Rev Esp Anestesiol Reanim 2000; 47: 464-75.

8. Ayala GE, Wheeler TM, Shine HD, *et al*. In vitro dorsal root ganglia and human prostate cell line interaction: redefining perineural invasion in prostate cancer. Prosate 2001; 49: 213-23.

9. Boyd JG, Gordon T. Neurotrophic factors and their receptors in axonal regeneration and functional recovery after peripheral nerve injury. Mol Neurobiol 2003; 27: 277-324.

10. Ketterer K, Rao S, Friess H, Weiss J, Büchler MW, Korc M. Reverse transcription-PCR analysis of laser-captured cells points to potential paracrine and autocrine actions of neurotrophins in pancreatic cancer. Clin Cancer Res 2003; 9: 5127-36.

11. Okada Y, Eibl G, Guha S, Duffy JP, Reber HA, Hines OJ. Nerve growth factor stimulates MMP-2 expression and activity and increases invasion by human pancreatic cancer cells. Clin Exp Metastasis 2004; 21: 285-92.

12. Deng J, You Q, Gao Y, *et al*. Prognostic value of perineural invasion in gastric cancer: a systematic review and meta-analysis. PLoS One 2014; 9: e88907.

13. Ueno H, Hase K, Mochizuki H. Criteria for extramural perineural invasion as a prognostic factor in rectal cancer. Br J Surg 2001; 88: 994-1000.

14. Edge SB, Byrd DR, Compton CC, Fritz AG, Greene FL, Trotti A. American Joint Committee on Cancer Cancer staging manual. New York: Springer, 2010.

15. Ceyhan GO, Liebl F, Maak M, *et al*. The severity of neural invasion is a crucial prognostic factor in rectal cancer independent of neoadjuvant radiochemotherapy. Ann Surg 2010; 252: 797-804.

16. Tanaka A. Watabe T, Okuno K, Yasutomi M. Perineural invasion as a predictor of recurrence of gastric cancer. Cancer 1994; 73: 550-5.

17. Duraker N, Sişman S, Can G. The significance of perineural invasion as a prognostic factor in patients with gastric carcinoma. Surg Today 2003; 33: 95-100.

18. Bilici A, Seker M, Ustaalioglu BB, *et al*. Prognostic significance of perineural invasion in patients with gastric cancer who underwent curative resection. Ann Surg Oncol 2010; 17: 2037-44.

19. Tianhang L, Guoen F, Jianwei B, Liye M. The effect of perineural invasion on overall survival in patients with gastric carcinoma. J Gastrointest Surg 2008; 12: 1263-7.

20. Selçukbiricik F, Tural D, Büyükünal E, Serdengeçti S. Perineural invasion independent prognostic factors in patients with gastric cancer undergoing curative resection. Asian Pac J Cancer Prev 2012; 13: 3149-52.

21. Jiang N, Deng JY, Liu Y, Ke B, Liu HG, Liang H. Incorporation of perineural invasion of gastric carcinoma into the 7th edition tumor-node-metastasis staging system. Tumour Biol 2014; 35: 9429-36.

The Clinicopathological and Prognostic Significance of the Gross Classification of Hepatocellular Carcinoma

Yangkyu Lee · Hyunjin Park[1]
Hyejung Lee[1] · Jai Young Cho[2]
Yoo-Seok Yoon[2] · Young-Rok Choi[2]
Ho-Seong Han[2] · Eun Sun Jang[3]
Jin-Wook Kim[3] · Sook-Hyang Jeong[3]
Soomin Ahn · Haeryoung Kim[1]

Department of Pathology, Seoul National University Bundang Hospital, Seoul National University College of Medicine, Seongnam; [1]Department of Pathology, Seoul National University Hospital, Seoul National University College of Medicine, Seoul; Departments of [2]Surgery and [3]Internal Medicine, Seoul National University Bundang Hospital, Seoul National University College of Medicine, Seongnam, Korea

Corresponding Author
Haeryoung Kim, MD, PhD
Department of Pathology, Seoul National University Hospital, Seoul National University College of Medicine, 103 Daehak-ro, Jongno-gu, Seoul 03080, Korea
Tel: +82-2-740-8322
Fax: +82-2-765-5600
E-mail: haeryoung.kim@snu.ac.kr

Background: We aimed to determine the clinicopathological significance of the gross classification of hepatocellular carcinoma (HCC) according to the Korean Liver Cancer Association (KLCA) guidelines. **Methods:** A retrospective analysis was performed on 242 cases of consecutively resected solitary primary HCC between 2003 and 2012 at Seoul National University Bundang Hospital. The gross classification (vaguely nodular [VN], expanding nodular [EN], multinodular confluent [MC], nodular with perinodular extension [NP], and infiltrative [INF]) was reviewed for all cases, and were correlated with various clinicopathological features and the expression status of "stemness"-related (cytokeratin 19 [CK19], epithelial cell adhesion molecule [EpCAM]), and epithelial-mesenchymal transition (EMT)–related (urokinase plasminogen activator receptor [uPAR] and Ezrin) markers. **Results:** Significant differences were seen in overall survival (p = .015) and disease-free survival (p = .034) according to the gross classification; INF type showed the worst prognosis while VN and EN types were more favorable. When the gross types were simplified into two groups, type 2 HCCs (MC/NP/INF) were more frequently larger and poorly differentiated, and showed more frequent microvascular and portal venous invasion, intratumoral fibrous stroma and higher pT stages compared to type 1 HCCs (EN/VN) (p < .05, all). CK19, EpCAM, uPAR, and ezrin expression was more frequently seen in type 2 HCCs (p < .05, all). Gross classification was an independent predictor of both overall and disease-free survival by multivariate analysis (overall survival: p = .030; hazard ratio, 4.118; 95% confidence interval, 1.142 to 14.844; disease-free survival: p = .016; hazard ratio, 1.617; 95% confidence interval, 1.092 to 2.394). **Conclusions:** The gross classification of HCC had significant prognostic value and type 2 HCCs were associated with clinicopathological features of aggressive behavior, increased expression of "stemness"- and EMT-related markers, and decreased survival.

Key Words: Carcinoma, hepatocellular; Gross classification; Prognosis

Hepatocellular carcinomas (HCCs) vary in their macroscopic appearances, from well-circumscribed expansile nodules to those with multinodular features and irregular margins; however, the gross classification of HCC has not received much attention in the literature. Although the macroscopic classification was first described by Eggel in 1901 based on an autopsy series, it was not until the late 1980's that the gross classification was proposed and adopted by the Liver Cancer Study Group of Japan (LCSGJ) in the General Rules of the Clinical and Pathologic Study of Primary Liver Cancer.[1,2] Since then, there have been several clinicopathological studies that focused on the gross features of HCC, mainly from Asian countries, and most studies

have demonstrated that HCCs with single nodular morphology have more favorable outcomes compared with those with multinodular or infiltrative (INF) growth patterns.[3-11] As the gross appearance of HCCs can be recognized preoperatively by imaging studies, it could have translational impact on clinical practice, such as guiding treatment decisions. However, the gross appearance was only reflected in the Cancer of the Liver Italian Program (CLIP) score (uninodular versus multinodular) which is not deemed suitable for the current population of HCC patients,[12] and the current widely used staging systems, such as the modified Union for International Cancer Control (UICC), Barcelona Clinic Liver Cancer (BCLC), and American Joint Committee on Cancer

(AJCC) TNM classifications focus on the multiplicity, size and vascular/bile duct invasion status of the HCCs.

In this study, we analyzed the differences in the clinicopathological features and survival between the different gross morphological types of HCC in a single cohort of surgically resected solitary HCCs. The gross morphology was classified according to The General Rules for the Study of Primary Liver Cancer published by the Korean Liver Cancer Association (KLCA).[13]

MATERIALS AND METHODS

Patient selection and clinicopathological analysis

Two hundred and ninety-eight consecutive cases of primary HCCs that were surgically resected between 2003 and 2012 at Seoul National University Bundang Hospital, Seongnam, Republic of Korea were evaluated in this study. This study was approved by the Institutional Review Board of Seoul National University Bundang Hospital (IRB No. B-1708-412-304), and patient consent was waived due to the retrospective nature of this study. Clinicopathological data were analyzed by reviewing electronic medical records, pathology reports and glass slides, and included patient sex, age at operation, tumor size, gross type, histologic

differentiation (Edmondson-Steiner grade), serum α-fetoprotein (AFP) levels and the pathological T and N categories according to AJCC TNM staging system (7th edition). The presence of intratumoral fibrous stroma was also noted; we defined the presence of intratumoral fibrous stroma as fibrous stroma occupying more than 30% of the tumor area.[14] Cases with multiple HCCs were excluded from the study, leaving a total of 242 cases for further analysis. Follow-up data was retrieved from the electronic medical records, including the status at last follow up and occurrence of distant or intrahepatic metastasis or local recurrence.

The gross type was determined by examining the largest cross section of the tumor by two pathologists (Y.L. and H.K.), according to the General Rules for the Study of Primary Liver Cancer by the KLCA (Fig. 1).[13] "Vaguely nodular" (VN) type was defined as a nodule with indistinct margins. While VN type morphology is an important characteristic of early HCC,[15] we classified HCCs as VN type purely by gross appearance, regardless of the tumor size and histologic differentiation status. "Expanding nodular" (EN) type was defined by as a round expansile nodule with a distinct margin. "Multinodular confluent" (MC) type was defined as a cluster of small and confluent nodules. "Nodular with perinodular extension" (NP) type was defined as an expanding
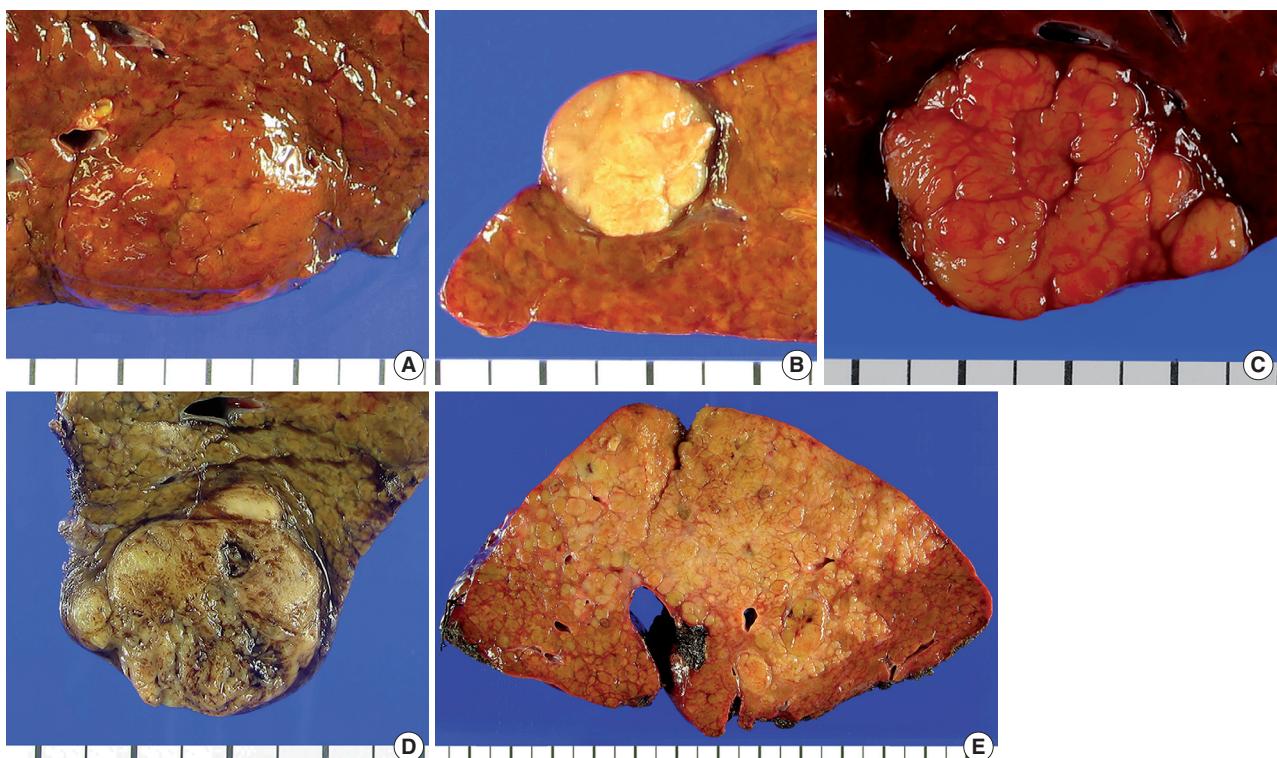
Fig. 1. Examples of the different gross types of hepatocellular carcinoma. (A) Vaguely nodular type. (B) Expanding nodular type. (C) Multinodular confluent type. (D) Nodular with perinodular extension type. (E) Infiltrative type.

nodule similar to EN type HCCs that had extranodular growth in less than 50% of the tumor circumference. INF type HCCs showed extranodular growth in more than 50% of the tumor circumference. The gross types were correlated with the clinico-pathological features of the HCCs.

Tissue microarray construction and immunohistochemistry

Two-millimeter-core tissue microarrays were constructed from the HCCs (Superbiochips Laboratories, Seoul, Korea), and 4 μm-thick tissue sections obtained from the tissue microarray blocks. Immunohistochemical staining was performed for "stemness"-related markers (cytokeratin 19 [CK19]; 1:100, mouse mono-clonal, Dako, Glostrup, Denmark), epithelial cell adhesion mol-ecule (EpCAM; 1:3,000, mouse monoclonal, Millipore, Billerica, MA, USA), and epithelial-mesenchymal transition (EMT)–related markers (urokinase plasminogen activator receptor [uPAR; 1:40, mouse monoclonal, Abcam, Cambridge, UK] and ezrin [1:100, mouse monoclonal, Abcam]). Briefly, after deparaffinization in xylene and rehydration in graded alcohol, antigen retrieval was performed on tissue sections using citrate buffer (pH 6.0) for CK19, EpCAM, and ezrin, and protease for uPAR. Incubation with primary antibodies was performed for 1 hour at room temperature, and with secondary antibody (EnVision kit, Dako) for 30 minutes. The presence of cytoplasmic expression in > 5% of the tumor cells was regarded as positive for CK19, ezrin, and uPAR expression. EpCAM was expressed in the tumor cell membranes.

Statistical analysis

All statistical analyses were performed using SPSS ver. 19.0 K (SPSS Korea, Seoul, Korea). Chi-square tests and Fisher exact tests were performed as deemed appropriate. Survival analyses for overall and disease-free survivals were performed by the Kaplan-Meier method and log-rank test. The Cox regression models were used for multivariate analysis. Statistical significance was defined as p < .05.

RESULTS

Clinicopathological characteristics according to HCC gross classification

The clinicopathological characteristics of the 242 cases studied are summarized in Table 1. The most common etiologic factor was hepatitis B virus (HBV) infection (171/242, 70.7%), fol-lowed by alcohol (35/242, 14.5%), hepatitis C virus (HCV) infec-tion (17/242, 7.0%) and combined HBV + HCV infection (1/242, 0.4%). The etiology was uncertain for the remainder of

Table 1. Summary of the clinicopathological characteristics

Characteristic	No. (%) (n = 242)
Sex	
Male	181 (74.8)
Female	61 (25.2)
Age at operation, median (range, yr)	59 (29-87)
Preoperative serum AFP level, median (range, ng/mL)	14.35 (1–40,000)
Etiology	
Hepatitis B virus (HBV)	171 (70.7)
Alcohol	35 (14.5)
Hepatitis C virus (HCV)	17 (7.0)
HBV + HCV	1 (0.4)
Uncertain etiology	18 (7.4)
Tumor size, median (range, cm)	3.0 (0.9–17.0)
≤ 2	52 (21.5)
> 2 and ≤ 5	145 (59.9)
> 5	45 (18.6)
Gross type	
Vaguely nodular	9 (3.7)
Expanding nodular	107 (44.2)
Multinodular confluent	78 (32.2)
Nodular with perinodular extension	32 (13.2)
Infiltrative	16 (6.6)
Edmondson-Steiner grade	
Grade I	2 (0.8)
Grade II	74 (30.6)
Grade III	142 (58.7)
Grade IV	24 (9.9)
Microvascular invasion	
Absent	154 (63.6)
Present	88 (36.4)
Portal vein invasion	
Absent	225 (93.0)
Present	17 (7.0)
Cirrhosis in background liver	
Absent	109 (45.0)
Present	126 (52.1)
Intratumoral fibrous stroma (> 30%)	
Absent	187 (77.3)
Present	55 (22.7)
Pathologic T category (AJCC 7th edition)	
pT1	140 (57.9)
pT2	82 (33.9)
pT3	17 (7.0)
pT4	3 (1.2)
Pathologic N category (AJCC 7th edition)	
pN0	240 (99.2)
pN1	2 (0.8)
Recurrence on follow-up	
Absent	138 (57.0)
Present	104 (43.0)
Status at last follow-up	
Alive	160 (66.1)
Deceased of disease	19 (7.9)
Deceased of other cause	5 (2.1)
Follow-up loss	58 (24.0)

AFP, α-fetoprotein; AJCC, American Joint Committee on Cancer.

patients (18/298, 7.4%). The most common gross type of HCCs was the EN type (107/242, 44.2%), followed by the MC type (78/242, 32.2%), NP type (32/242, 13.2%), INF type (16/242, 6.6%), and the VN type (9/242, 3.7%).

When the clinicopathological features were compared among the five different gross types, we found that INF type HCCs were associated with larger tumor size, poor histologic differentiation, more frequent microvascular and portal venous invasion and higher pathologic T stage compared to the other gross types (Table 2). Large tumor size, microvascular and portal venous invasion and high T stage were rare or absent in VN or EN type HCCs. The clinicopathological features of MC and NP type HCCs were similar. We regrouped the five gross types into type 1 and type 2, as previously described by Gong *et al.*[5]: type 1 HCCs consisted of VN and EN type, and type 2 HCCs consisted of MC, NP, and INF types. On comparing the clinicopathological findings between the two types, we found that type 2 HCCs were more frequently larger (p < .001) and poorly differentiated (p =

.001), and showed more frequent microvascular invasion (p < .001), portal venous invasion (p < .001), higher pT stages (p < .001), and intratumoral fibrous stroma (p < .001) compared to type 1 HCCs.

Differences in expression status of "stemness"- and EMT-related markers in HCC according to gross classification

The immunohistochemical stain results are summarized in Table 2 and Fig. 2. The expression of "stemness"-related markers, CK19 and EpCAM, was seen in 18.6% and 43.4% of HCCs, respectively. CK19 and EpCAM expression rates were significantly higher in INF type HCCs compared to EN type HCCs (CK19, 37.5% vs 9.3%; EpCAM, 75.0% vs 34.6%). Significant differences were seen in the frequencies of CK19 and EpCAM positivity between type 1 and type 2 HCCs (CK19, p = .002; EpCAM, p = .009). uPAR and ezrin, EMT-related markers, were more frequently expressed in type 2 HCCs compared to type 1 HCCs (uPAR, p < .001; ezrin, p = .036).

Table 2. Clinicopathological features and immunohistochemical stain results according to gross type

	VN (n = 9)	EN (n = 107)	MC (n = 78)	NP (n = 32)	INF (n = 16)	Type 1 (VN, EN) (n = 116)	Type 2 (MC, NP, INF) (n = 126)	p-value (type 1 vs 2)
Tumor size (> 5 cm)	0	11 (10.3)	21 (26.9)	7 (21.9)	6 (37.5)	11 (9.5)	34 (27.0)	< .001
HBV etiology	5 (55.6)	73 (68.2)	58 (74.4)	21 (65.6)	15 (93.8)	78 (67.2)	94 (74.6)	.207
Edmondson-Steiner grade III/IV	4 (44.4)	64 (59.8)	58 (74.4)	25 (78.1)	15 (93.8)	68 (58.6)	98 (77.8)	.001
Microvascular invasion	1 (11.1)	29 (27.1)	34 (43.6)	14 (43.8)	10 (62.5)	30 (25.9)	58 (46.0)	< .001
Portal vein invasion	0	0	4 (5.1)	5 (15.6)	8 (50.0)	0	17 (13.55)	< .001
High T category (pT3 or pT4)	0	1 (0.9)	7 (9.0)	5 (15.6)	7 (43.8)	1 (0.9)	19 (15.1)	< .001
Cirrhosis in background liver	6 (66.7)	49 (46.7)	42 (57.5)	15 (46.9)	14 (87.5)	55 (48.2)	71 (58.1)	.118
Serum AFP level > 1,000 ng/mL	0	12 (13.6)	10 (14.7)	6 (20.7)	6 (37.5)	12 (12.6)	22 (19.5)	.194
Fibrous stroma (> 30%)	1 (11.1)	14 (13.1)	25 (32.1)	9 (28.1)	6 (37.5)	15 (12.9)	40 (31.7)	< .001
CK19 positive	2 (22.2)	10 (9.3)	20 (25.6)	7 (21.9)	6 (37.5)	12 (10.3)	33 (26.2)	.002
EpCAM positive	3 (33.3)	37 (34.6)	34 (43.6)	19 (59.4)	12 (75.0)	40 (34.5)	65 (51.6)	.009
uPAR positive	1 (11.1)	16 (15.2)	22 (28.2)	14 (43.8)	12 (75.0)	17 (14.9)	48 (38.1)	< .001
Ezrin positive	4 (44.4)	34 (32.4)	40 (51.3)	12 (37.5)	7 (43.8)	38 (33.3)	59 (46.8)	.036

VN, vaguely nodular; EN, expanding nodular; MC, multinodular confluent; NP, nodular with perinodular extension; INF, infiltrative; HBV, hepatitis B virus; AFP, α-fetoprotein; CK19, cytokeratin 19; EpCAM, epithelial cell adhesion molecule; uPAR, urokinase plasminogen activator receptor.
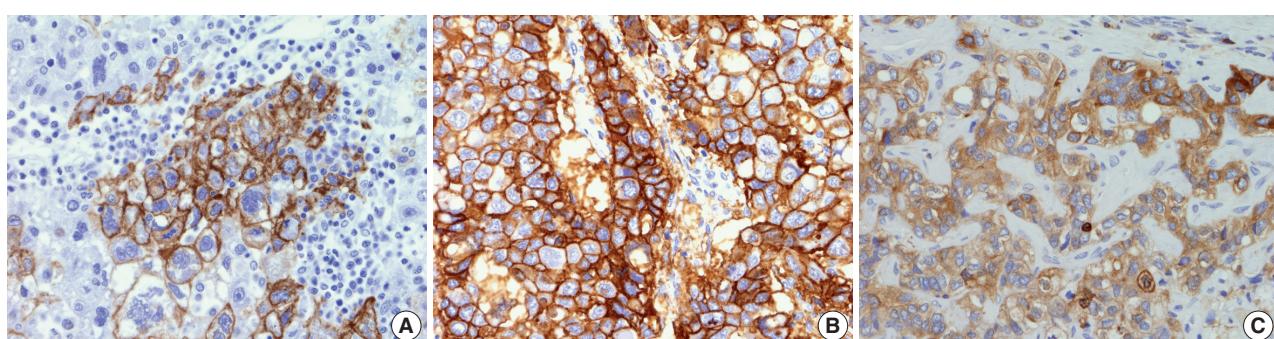
Fig. 2. Immunohistochemical stain results for stemness- and epithelial-mesenchymal transition-related markers: cytokeratin 19 (A), epithelial cell adhesion molecule (B), and ezrin (C).

Table 3. Survival analysis results

Variable	Overall survival		Disease-free survival	
	Hazard ratio (95% confidence interval)	p-value	Hazard ratio (95% confidence interval)	p-value
Univariate analysis				
Gross type (type 1 vs type 2)[a]	5.439 (1.583–18.683)	.007	1.617 (1.092–2.394)	.016
Tumor size (>5 cm)	1.229 (0.407–3.712)	.714	1.590 (1.013–2.495)	.044
High E-S grade (III or IV)	0.636 (0.256–1.583)	.331	1.054 (0.694–1.599)	.805
Microvascular invasion	2.178 (0.881–5.383)	.092	1.445 (0.977–2.138)	.065
Portal vein invasion	5.311 (1.906–14.796)	<.001	1.702 (0.858–3.376)	.128
High T category (pT3 or pT4)	5.206 (1.974–13.728)	<.001	1.795 (0.982–3.284)	.057
Intratumoral stromal fibrosis	2.037 (0.801–5.179)	.135	0.973 (0.608–1.559)	.973
Multivariate analysis				
Gross type (type 1 vs type 2)	4.118 (1.142–14.844)	.030	1.617 (1.092–2.394)	.016
Tumor size (>5 cm)	0.586 (0.166–2.060)	.404	1.303 (0.802–2.115)	.285
Microvascular invasion	1.953 (0.765–4.982)	.161	1.300 (0.866–1.952)	.205
Portal vein invasion	1.091 (0.150–7.931)	.931	0.954 (0.292–3.124)	.938
High T category (pT3 or pT4)	3.173 (1.156–8.710)	.025	1.462 (0.500–4.275)	.487

E-S grade, Edmondson-Steiner grade.

[a]Type 1: vaguely nodular and expanding nodular types, type 2: multinodular confluent, nodular with perinodular extension and infiltrative types.
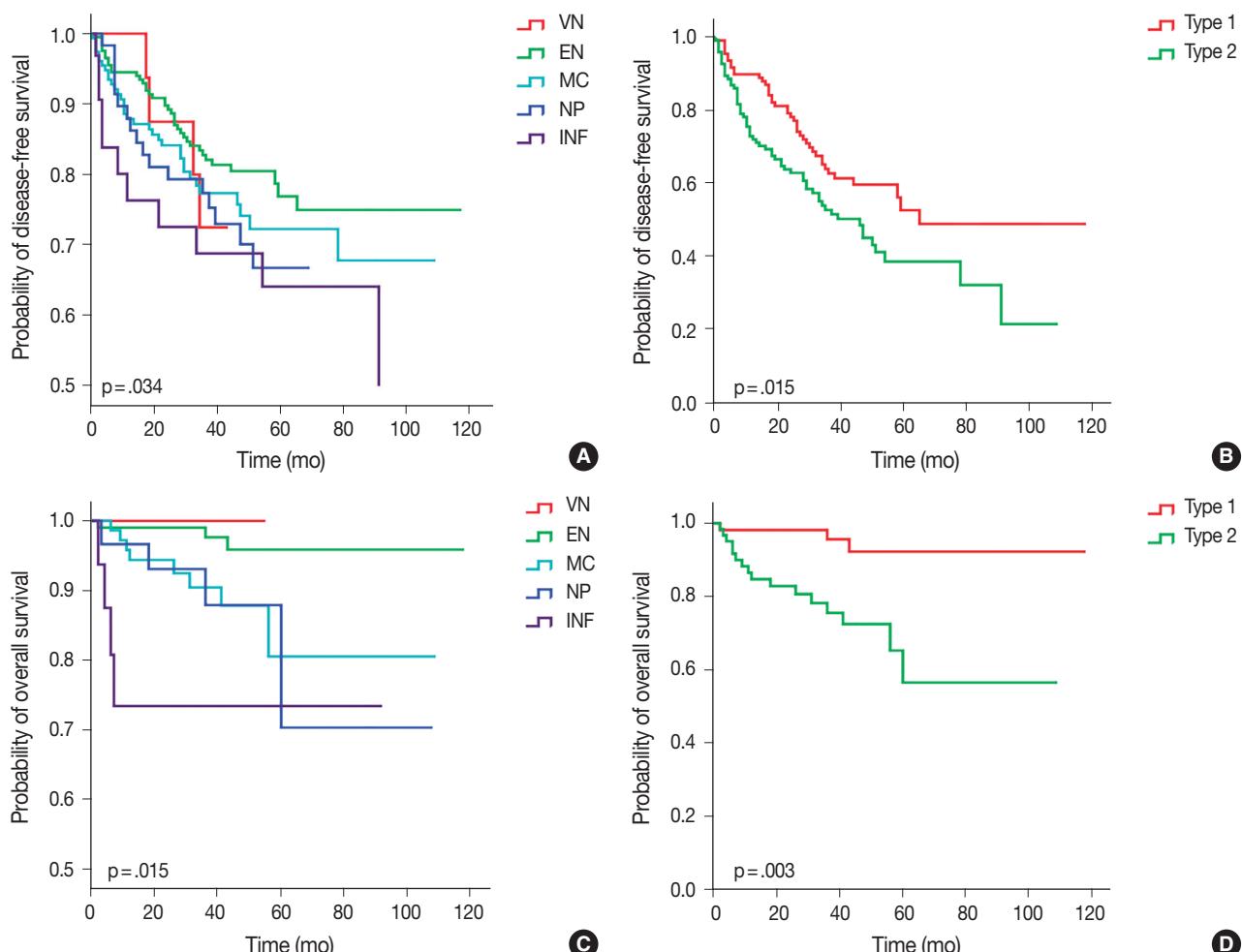
Fig. 3. Kaplan-Meier curves demonstrating differences in disease-free survival and overall survival according to gross classification of hepatocellular carcinoma. (A, B) Disease-free survival. (C, D) Overall survival. VN, vaguely nodular; EN, expanding nodular; MC, multinodular confluent; NP, nodular with perinodular extension; INF, infiltrative.

Survival analysis results

Of the five different gross types, the INF type demonstrated the worst overall survival (p = .015) and disease-free survival (p=.034) compared to other types (Table 3, Fig. 3). The most favorable outcome was seen for EN and VN types, and the survival curves for MC and NP types were in between that of EN and INF type HCCs. When the gross types were simplified into two groups, type 2 HCCs showed significantly decreased disease-free (p = .015) and overall survival (p = .003) compared to type 1 HCCs. Of the other clinicopathological variables, tumor size of larger than 5 cm was associated with a decreased disease-free survival (p = .041), portal venous invasion (p < .001) and higher pT stage (p < .001) were associated with decreased overall survival, and microvascular invasion was marginally associated with decreased disease-free and overall survivals although not statistically significant.

Multivariate analysis demonstrated that gross classification (type 1 vs 2) was a significant independent predictor of both overall and disease-free survival, after adjusting for patient sex and age. Type 2 HCCs showed significantly decreased overall survival (p = .030; hazard ratio, 4.118; 95% confidence interval, 1.142 to 14.844) and disease-free survival (p = .016; hazard ratio, 1.617; 95% confidence interval, 1.092 to 2.394). High pathologic T stage also remained a significant predictive factor for overall survival (p = .025; hazard ratio, 3.173; 95% confidence interval, 1.156 to 8.710).

DISCUSSION

In this study, we found that INF type HCCs had the worst prognosis out of the five different gross types, and when the HCCs were further grouped into types 1 and 2, gross type 2 HCCs more frequently showed clinicopathological features of aggressive behavior and poor prognosis compared to type 1 HCCs. The gross classification had a strong impact on patient survival; type 2 gross morphology was a significant independent predictor of decreased overall and disease-free survivals on multivariate analysis.

Our findings are similar to the results of a few previous studies. Increased overall and disease-free survival was noted for single nodular type HCCs compared to those with extranodular growth or MC growth patterns.[6,9] Interestingly, Shimada *et al.*[9] analyzed small HCCs (< 3 cm) separately and found similar associations between gross morphology and prognosis, and in another analysis[3] on huge HCCs (> 10 cm), single nodular type HCCs showed more favorable outcomes compared to non-single nodular

HCCs. Taken together, it could be suggested that the gross classification may be an important predictor of prognosis regardless of tumor size. When tumor size was entered into our multivariate analysis model, we found that gross type 2 was a strong independent predictor of both overall survival and disease-free survival.

The gross classification consists of five different morphological types of HCCs and clear definitions for the different types have been proposed in the guidelines of both the LCSGJ and KLCA. However, in practice, the distinction between NP, MC, and INF type HCCs is not always clear cut, and prone to interobserver variability. On the other hand, EN and VN types (known as "single nodular with distinct margin" and "single nodular with indistinct margin" types in the LCSGJ guidelines, respectively) are relatively easier to discriminate from the other types as they lack the multilobulated irregular contour. If the gross classification is an important prognostic factor for HCC on surgically resected specimens, this could also be implemented in the preoperative evaluation of HCC patients, as the gross features can be determined on preoperative imaging. Therefore, it may be sufficient and more practical to classify HCCs as single nodular types (type 1) and non-single nodular types (type 2) for guiding patient management strategies. Interestingly, Fu *et al.*[4] analyzed the survival of patients with small HCCs (< 5 cm) treated with radiofrequency ablation according to the gross type on imaging, and found that HCCs with single nodular HCCs without extranodular growth or irregular margins were associated with favorable survival.

A subset of HCCs that have morphological features consistent with HCC have been demonstrated to express immunophenotypes associated with "stemness," such as CK19, EpCAM, CD133, and c-kit positivity. These tumors have been associated with higher preoperative serum AFP levels, less frequent fibrous capsule formation, intratumoral fibrous stroma, frequent vascular invasion and poor prognosis compared to typical HCCs that do not express these markers.[16,17] As expected, we found in this study that larger tumor size, poor histological differentiation, microvascular and portal venous invasion, intratumoral fibrous stroma, "stemness" and EMT-related marker expression and higher T stages were significantly more frequent in type 2 HCCs compared to type 1 HCCs. Therefore, HCCs that have a solitary, well-circumscribed and expansile growth pattern were less likely to exhibit features associated with "stemness." The higher prevalence of CK19 expression in type 2 HCCs has been recently demonstrated by another group.[5]

EMT refers to the process in which tumor epithelial cells lose their epithelial characteristics (e.g., loss of membranous E-cad-

herin expression) and acquire mesenchymal features, facilitating tumor invasion and distant metastasis.[18] This process has been described in HCCs, and HCCs expressing ezrin and uPAR have been associated with poor prognoses.[19,20] We found in this study that INF type HCCs showed frequent uPAR expression (75%) compared to other types, especially VN and EN types which were uPAR positive in 11% and 15%, respectively. MC and NP types showed uPAR expression frequency intermediate between INF types and EN/VN types. In a previous study from Japan, E-cadherin loss was more frequently seen in single nodular with extranodal growth type and confluent multinodular type HCCs of less than 6 cm in diameter (which can be translated to NP and MC type HCCs according to the KLCA classification).[7] Taken together, it could be suggested that invasiveness and metastatic ability of HCCs could be reflected by the gross appearance.

On examining the Kaplan-Meier curves for overall and disease-free survival according to the five different gross types of our cohort, significant differences in survival were noted between the EN types and INF types. The MC and NP types showed survivals intermediate between the EN and INF types, without significant differences between the two types. Interestingly, while the VN type showed the best overall survival (no HCC-related deaths), early recurrences were noted for two VN type HCCs (at 17 and 18 months) for the disease-free survival analysis. Although VN type morphology is a characteristic feature of early HCC,[15] we included all cases that were macroscopically of VN type regardless of the histological differentiation or tumor size; indeed, poor histological differentiation was noted in 4/9 (44.4%) cases and 2/9 (22.2%) cases were larger than 3 cm. Therefore, the VN type in this study does not refer to early HCC, and we grouped VN and EN types together into type 1 (single nodular) HCCs for analytical purposes.

Although this is not the first report on the clinicopathological significance of the gross classification of HCCs, this is a large-scale cohort study of 242 surgically resected solitary HCCs using the definitions in the guidelines of the KLCA, and we also demonstrate for the first time the associations between the different gross types and the expression status of "stemness"- and EMT-related markers. A limitation of this study is that we excluded multiple HCCs (including multicentricity and intrahepatic metastasis) from the study cohort in order to exclude cases showing multiple gross types in the same liver. This resulted in the lower percentage of cases with higher pT stage, and the exclusion of pT3a cases using the current AJCC staging system (seventh edition). Nevertheless, we demonstrate that the gross classification of HCCs according to the KLCA guidelines has prognostic value,

and that gross type 2 HCCs with non-single nodular patterns are associated with clinicopathological features of aggressive behavior, increased expression of "stemness"- and EMT-related markers and decreased survival. Further validation would be required in independent cohorts and also radio-pathological correlation studies would be needed to validate the utility of the gross classification in HCC patient management.

REFERENCES

1. Liver Cancer Study Group of Japan. General rules for the clinical and pathological study of primary liver cancer. 2nd ed. Tokyo: Kanehara & Co., 2003.

2. Kanai T, Hirohashi S, Upton MP, *et al*. Pathology of small hepatocellular carcinoma: a proposal for a new gross classification. Cancer 1987; 60: 810-9.

3. Choi GH, Han DH, Kim DH, *et al*. Outcome after curative resection for a huge (>or=10 cm) hepatocellular carcinoma and prognostic significance of gross tumor classification. Am J Surg 2009; 198: 693-701.

4. Fu X, Mao L, Tang M, *et al*. Gross classification of solitary small hepatocellular carcinoma on preoperative computed tomography: prognostic significance after radiofrequency ablation. Hepatol Res 2016; 46: 298-305.

5. Gong SC, Cho MY, Lee SW, Kim SH, Kim MY, Baik SK. The meaning of gross tumor type in the aspects of cytokeratin 19 expression and resection margin in patients with hepatocellular carcinoma. J Gastroenterol Hepatol 2016; 31: 206-12.

6. Hui AM, Takayama T, Sano K, *et al*. Predictive value of gross classification of hepatocellular carcinoma on recurrence and survival after hepatectomy. J Hepatol 2000; 33: 975-9.

7. Inayoshi J, Ichida T, Sugitani S, *et al*. Gross appearance of hepatocellular carcinoma reflects E-cadherin expression and risk of early recurrence after surgical treatment. J Gastroenterol Hepatol 2003; 18: 673-7.

8. Murakata A, Tanaka S, Mogushi K, *et al*. Gene expression signature of the gross morphology in hepatocellular carcinoma. Ann Surg 2011; 253: 94-100.

9. Shimada M, Rikimaru T, Hamatsu T, *et al*. The role of macroscopic classification in nodular-type hepatocellular carcinoma. Am J Surg 2001; 182: 177-82.

10. Trevisani F, Caraceni P, Bernardi M, *et al*. Gross pathologic types of hepatocellular carcinoma in Italian patients: relationship with demographic, environmental, and clinical factors. Cancer 1993; 72: 1557-63.

11. Tsujita E, Yamashita Y, Takeishi K, *et al*. The clinicopathological impact of gross classification on solitary small hepatocellular carcinoma. Hepatogastroenterology 2013; 60: 1726-30.

12. A new prognostic system for hepatocellular carcinoma: a retrospective study of 435 patients: the Cancer of the Liver Italian Program (CLIP) investigators. Hepatology 1998; 28: 751-5.

13. Jang JY, Lee JS, Kim HJ, *et al*. The general rules for the study of primary liver cancer. J Liver Cancer 2017; 17: 19-44.

14. Kurogi M, Nakashima O, Miyaaki H, Fujimoto M, Kojiro M. Clinicopathological study of scirrhous hepatocellular carcinoma. J Gastroenterol Hepatol 2006; 21: 1470-7.

15. International Consensus Group for Hepatocellular Neoplasia. Pathologic diagnosis of early hepatocellular carcinoma: a report of the international consensus group for hepatocellular neoplasia. Hepatology 2009; 49: 658-64.

16. Kim H, Choi GH, Na DC, *et al*. Human hepatocellular carcinomas with "stemness"-related marker expression: keratin 19 expression and a poor prognosis. Hepatology 2011; 54: 1707-17.

17. Kim H, Park YN. Hepatocellular carcinomas expressing 'stemness'-related markers: clinicopathological characteristics. Dig Dis 2014; 32: 778-85.

18. Lee JM, Dedhar S, Kalluri R, Thompson EW. The epithelial-mesenchymal transition: new insights in signaling, development, and disease. J Cell Biol 2006; 172: 973-81.

19. Okamura D, Ohtsuka M, Kimura F, *et al*. Ezrin expression is associated with hepatocellular carcinoma possibly derived from progenitor cells and early recurrence after surgical resection. Mod Pathol 2008; 21: 847-55.

20. Zhou L, Hayashi Y, Itoh T, Wang W, Rui J, Itoh H. Expression of urokinase-type plasminogen activator, urokinase-type plasminogen activator receptor, and plasminogen activator inhibitor-1 and -2 in hepatocellular carcinoma. Pathol Int 2000; 50: 392-7.

Myoferlin Expression and Its Correlation with FIGO Histologic Grading in Early-Stage Endometrioid Carcinoma

Min Hye Kim[1] · Dae Hyun Song[2,3,4]
Gyung Hyuck Ko[1,2,3] · Jeong Hee Lee[1,2,3]
Dong Chul Kim[1,2,3] · Jung Wook Yang[1]
Hyang Im Lee[4] · Hyo Jung An[4]
Jong Sil Lee[1,2,3]

[1]Department of Pathology, Gyeongsang
National University Hospital, Jinju; [2]Gyeongsang
National University School of Medicine, Jinju;
[3]Gyeongsang Institute of Health Science, Jinju;
[4]Department of Pathology, Gyeongsang National
University Changwon Hospital, Changwon, Korea

Corresponding Author
Jong Sil Lee, MD
Department of Pathology, Gyeongsang National
University School of Medicine, 15 Jinju-daero
816beon-gil, Jinju 52727, Korea
Tel: +82-55-750-8231
Fax: +82-55-759-7952
E-mail: jongsil25@gnu.ac.kr

Background: For endometrioid carcinoma patients, International Federation of Gynecologists and Obstetricians (FIGO) histologic grading is very important for identifying the appropriate treatment method. However, the interobserver discrepancy with this three-tiered grading system is a serious potential problem. In this study, we used immunohistochemistry to analyze the relationship between FIGO histologic grading score and myoferlin expression. **Methods:** We studied the endometrioid carcinoma tissues of 60 patients from Gyeongsang National University Hospital between January 2002 and December 2009. Immunohistochemical analysis of myoferlin was performed on tissue microarray blocks from surgical specimens. **Results:** Myoferlin expression was observed in 58 of 60 patients. Moderate and strong myoferlin expression was observed in low-grade endometrioid carcinoma, while there was a tendency toward loss of myoferlin expression in high-grade endometrioid carcinoma (p < .001). **Conclusions:** Our study revealed that myoferlin loss is significantly correlated with high FIGO grade of endometrioid carcinoma.

In endometrioid carcinoma patients, International Federation of Gynecologists and Obstetricians (FIGO) histologic grading is very important in determining the treatment method and predicting the patient's prognosis.[1-3] Particularly, it is recommended that patients with FIGO stage I and histologic grade 3 endometrioid carcinoma undergo adjuvant radiotherapy after surgery,[3] while patients with FIGO stage I and histologic grade 1 or 2 endometrioid carcinoma should be treated with surgery only. However, the interobserver discrepancy of this three-tiered FIGO grading system can pose a serious potential problem. Thus, many authors have used immunohistochemical (IHC) staining,[4-6] genetic molecular testing,[7-9] and other two-tiered systems[10,11] to reduce the discrepancy.

Myoferlin, a protein in the cellular membrane, is involved in cellular regeneration after injury.[12] Recent studies have reported a correlation between the prognosis of cancer patients and myoferlin expression in breast, lung, oropharyngeal, and pancreatic cancer.[13-16]

In this study, we used IHC staining to analyze the relationship between FIGO histologic grading and myoferlin expression.

MATERIALS AND METHODS

Case selection

We collected clinical data from the charts of endometrioid carcinoma patients treated at Gyeongsang National University Hospital, Jinju, Korea, between January 2002 and December 2009. A total of 60 patients who underwent hysterectomy were enrolled. The tumor stage and histologic grade of each case were assessed using the FIGO system. All gross photographs and hematoxylin and eosin–stained glass slides of surgical specimens were reviewed by two pathologists.

This study was approved by the Institutional Review Board of Gyeongsang National University Hospital with a waiver of informed consent (IRB No. GNUH-2015-12-003).

Tissue microarray

Tumor samples were fixed overnight in 20% neutral-buffered formalin and were examined grossly, dissected, and embedded in paraffin blocks. One or two representative blocks were selected by microscopic examination. One representative core (3 mm in diameter) tissue was obtained from each paraffin block and arranged in new recipient tissue microarray blocks. Representative areas of the donor blocks were selected from near the invasive front.

IHC analysis

A primary antibody for myoferlin (1:100, 7D6, Abcam, Cambridge, UK) was used to investigate protein expression. The IHC method used was described in detail in our previous report.[14]

The positive control for myoferlin was normal endometrial tissue. Tissues showing an intensity equal to or stronger than that of normal endometrial tissue were classified as grade 3. The IHC slides were scored using the three-tiered FIGO system by two pathologists.

Statistical analysis

Correlation analyses were performed using the chi-square test. A p-value of < .05 was considered statistically significant. All statistics were analyzed using SPSS ver. 24.0 (IBM Corp., Armonk, NY, USA).

RESULTS

Clinicopathological features of the patients

The clinicopathological features of 60 endometrioid carcinoma patients are summarized in Table 1. The mean age was 51 years. All patients underwent hysterectomy. Among 60 cases, 43 (71.7%) were classified as FIGO stage Ia after surgery, whereas 40 (66.7%) were considered FIGO histologic grade 1.

Myoferlin expression in nontumorous endometrial tissue

Nontumorous endometrial tissues were obtained from leiomyoma or adenomyosis patients who underwent hysterectomy. In normal epithelial tissues, moderate and strong myoferlin expression was observed. Specifically, endometrial tissue in secretory phase showed strong expression (Fig. 1).

Myoferlin expression in endometrioid carcinoma

The clinicopathological features of the cases included in this study are summarized in Table 1. Myoferlin expression in the cytoplasm and cellular membrane of cancer cells was observed in 58 of the 60 patients (Fig. 1). Similarly, cytoplasmic and membra-

Table 1. Clinical and pathological features of 60 endometrioid carcinoma patients

Variable	No. of patients (%)
Mean age (yr)	51 (35–78)
T category	
Ia	43 (71.7)
Ib	12 (20)
II	3 (5)
IIIa	1 (1.7)
IIIb	1 (1.7)
Histologic grade	
1	40 (66.7)
2	15 (25)
3	5 (8.3)
Myoferlin expression	
Negative	2 (3.3)
Weak (+1)	4 (6.6)
Moderate (+2)	9 (15)
Strong (+3)	45 (75)
Total	60

nous expression of myoferlin was evident in normal endometrial glands in proliferative and secretory phases. Forty-five patients (75%) exhibited strong myoferlin expression, similar to that in normal endometrial glands.

Correlation between myoferlin expression and FIGO histologic grading

The correlation is described in Table 2. In the chi-square test, moderate and strong myoferlin expression was observed in low-grade endometrioid carcinoma, while there was a tendency toward loss of myoferlin expression in high-grade endometrioid carcinoma (p < .001).

Correlation between myoferlin expression and FIGO staging

The correlation is shown in Table 3. In the chi-square test, most patients with FIGO stage III endometrioid carcinoma exhibited negative or weak myoferlin expression (+1). A tendency toward loss of myoferlin expression was also observed in late-stage endometrioid carcinoma (p < .001).

DISCUSSION

Myoferlin is a little known protein. To our knowledge, this study is the first to identify myoferlin expression in endometrial tissue. Recent studies have reported that myoferlin contributes to the proliferation, migration, and invasion of cancer cells and is over-expressed in several types of cancer. However, in this study, endometrial cancer showed the opposite result; myoferlin expression was decreased in high-grade endometrioid carcinoma, probably
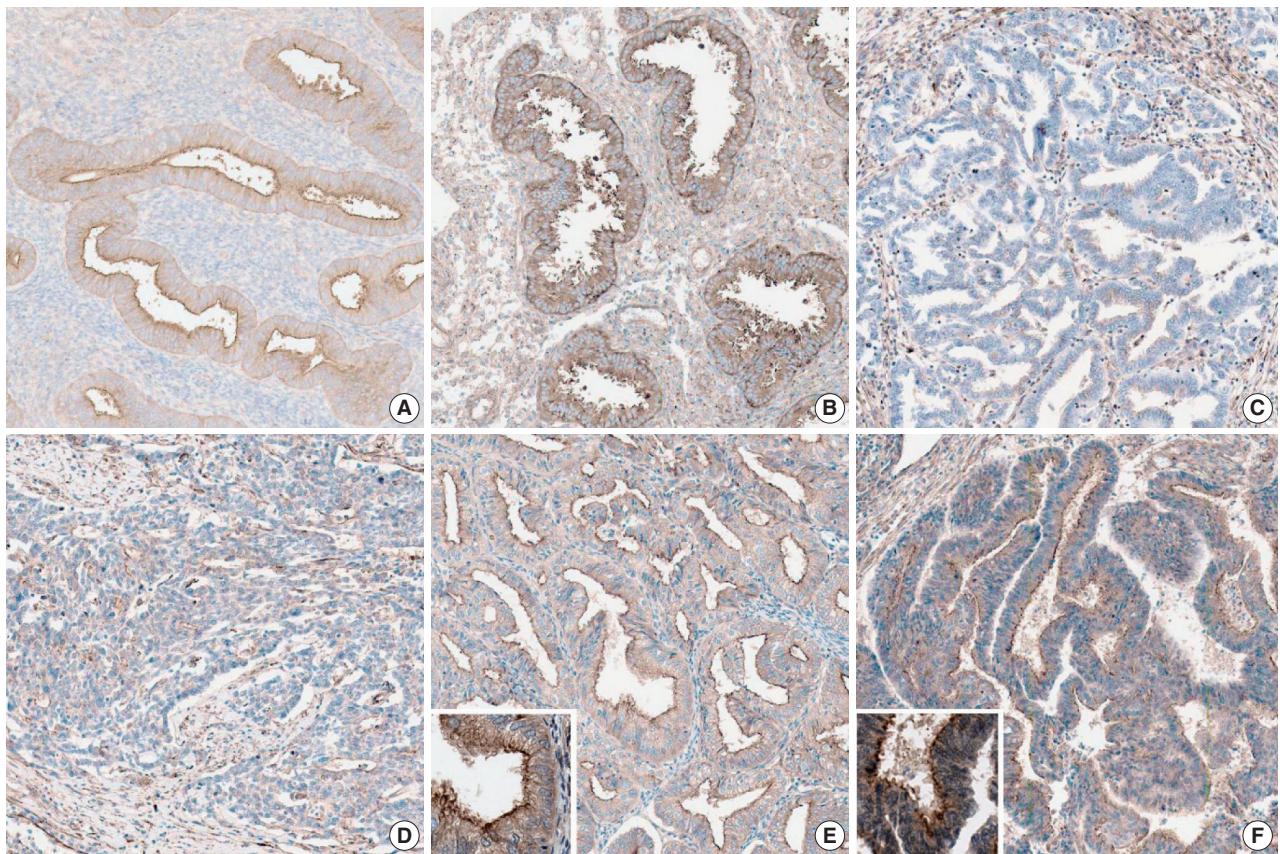
Fig. 1. Myoferlin expression in nontumorous endometrial tissue in proliferative phase (A) and secretory phase (B). (C) Loss of myoferlin expression in high-grade endometrioid carcinoma. Weak (+1, International Federation of Gynecologists and Obstetricians [FIGO] grade 3) (D), moderate (+2, FIGO grade 2) (E), and strong (+3, FIGO grade 1) (F) expression of myoferlin in endometrioid carcinoma.

Table 2. Correlation between myoferlin expression and FIGO histologic grading

Histologic grade	≤+1	≥+2	Total
1	1	39	40
2	2	13	15
3	37	2	5
Total	6	54	

p < .001.
FIGO, International Federation of Gynecologists and Obstetricians.

Table 3. Correlation between myoferlin expression and FIGO staging

T category	Myoferlin		Total
	≤+1	≥+2	
Ia	1	42	43
Ib	3	9	12
II	0	3	3
IIIa	1	0	1
IIIb	1	0	1
Total	6	54	

p < .001.
FIGO, International Federation of Gynecologists and Obstetricians.

because normal endometrial tissue undergoes a continuous cycle of regeneration. Moreover, myoferlin has been reported to be involved in cellular regeneration after injury.[14] The tumorigenesis of endometrioid carcinoma is associated with noncyclic continuous exposure to sex hormones. Our results implicate a correlation among cellular regeneration, hormonal effect, and myoferlin expression.

Though FIGO grading is important in guiding patient treatment, the interobserver discrepancy of this three-tiered grading system is a potential problem. Hence, many authors have attempted grading using IHC staining,[4-6] genetic molecular testing,[7-9] other two-tiered systems,[10,11] and curettage and cytology[17] to decrease

discrepancies.

In a previous study, Daniilidou *et al.*[5] investigated *PTEN* and *p53* gene expression in endometrioid and serous papillary carcinoma and showed that these biomarkers contribute to accurate diagnosis and therapeutic decisions in relation to tumor stage and grade. In another notable study on the cytologic scoring of endometrioid carcinoma of the endometrium, Nishimura *et al.*[17] examined 64 cytologic samples and scored them using 10 cytology character-

istics. The cytologic grade was closely related to histologic grade, and a high cytologic score was correlated with *p53* mutation and myometrial invasion. The study implied that the cytologic scoring system for endometrioid carcinoma is useful for predicting histologic grade and malignant potential of the tumor.

Guan *et al.*[10] tried a new binary grading system for endometrial carcinoma and compared it with an existing binary grading system and FIGO grading in hysterectomy specimens. They examined 254 hysterectomies and graded them according to the new grading system including architecture pattern and nuclear atypia. They concluded that the three-tiered FIGO grading system retained superior prognostic power. However, the new binary grading system is an attractive option due to its good reproducibility and the elimination of ambiguity of intermediate grades.

In the present study, we also tried to decrease discrepancies by determining the FIGO grade according to myoferlin expression. Our statistically significant (p < .001) finding was that moderate and strong myoferlin expression was observed in low-grade endometrioid carcinoma, and loss of myoferlin expression was noted in high-grade endometrioid carcinoma. Here, we found that myoferlin could be a valuable marker for the accurate grading of uterine endometrioid carcinoma.

In this study, the level of myoferlin expression in endometrioid carcinoma was opposite that observed in other studies, suggesting a hidden mechanism underlying the continuous regeneration of tissue in the endometrium. Thus, further investigation in the role of myoferlin in the endometrium and in tumorigenesis of endometrioid carcinoma is recommended.

This study had some limitations. The number of patients involved was only 60, and the cases consisted of mostly early-stage endometrioid carcinoma. Therefore, further studies with larger sample sizes are necessary to validate the significance of myoferlin expression in early- and late-stage endometrioid carcinoma.

In conclusion, our study revealed that myoferlin loss is significantly correlated with high FIGO grade of endometrioid carcinoma. To our knowledge, this is the first report on myoferlin expression in endometrial tissue, and our results could help in the management of patients with endometrioid carcinoma.

Conflicts of Interest

No potential conflict of interest relevant to this article was reported.

REFERENCES

1. Dvalishvili I, Charkviani L, Turashvili G, Burkadze G. Clinical characteristics of prognostic factors in uterine endometrioid adenocarcinoma of various grade. Georgian Med News 2006; (132): 24-7.

2. Zaki MA, Robbins JR, Fatteh S, Mahan MG, Hanna RK, Elshaikh MA. Histological grade predicts for recurrence in patients with uterine endometrioid carcinoma without myometrial involvement. Anticancer Res 2012; 32: 4061-5.

3. Creasman WT, Odicino F, Maisonneuve P, *et al.* Carcinoma of the corpus uteri. FIGO 26th Annual Report on the Results of Treatment in Gynecological Cancer. Int J Gynaecol Obstet 2006; 95 Suppl 1: S105-43.

4. Apostolou G, Apostolou N, Biteli M, Kavantzas N, Patsouris E, Athanassiadou P. Utility of Ki-67, p53, Bcl-2, and Cox-2 biomarkers for low-grade endometrial cancer and disordered proliferative/benign hyperplastic endometrium by imprint cytology. Diagn Cytopathol 2014; 42: 134-42.

5. Daniilidou K, Frangou-Plemenou M, Grammatikakis J, Grigoriou O, Vitoratos N, Kondi-Pafiti A. Prognostic significance and diagnostic value of PTEN and p53 expression in endometrial carcinoma: a retrospective clinicopathological and immunohistochemical study. J BUON 2013; 18: 195-201.

6. Kounelis S, Kapranos N, Kouri E, Coppola D, Papadaki H, Jones MW. Immunohistochemical profile of endometrial adenocarcinoma: a study of 61 cases and review of the literature. Mod Pathol 2000; 13: 379-88.

7. Abdalla N, Piorkowski R, Stanirowski P, Slomka A, Cendrowski K, Sawicki W. Assessment of levels of the tumor markers HE4 and CA125 considering staging, grading and histological types of endometrial cancer. Prz Menopauzalny 2016; 15: 133-7.

8. Coenegrachts L, Schrauwen S, Van Bree R, *et al.* Increased expression of placental growth factor in high-grade endometrial carcinoma. Oncol Rep 2013; 29: 413-8.

9. Kashima H, Wu RC, Wang Y, *et al.* Laminin C1 expression by uterine carcinoma cells is associated with tumor progression. Gynecol Oncol 2015; 139: 338-44.

10. Guan H, Semaan A, Bandyopadhyay S, *et al.* Prognosis and reproducibility of new and existing binary grading systems for endometrial carcinoma compared to FIGO grading in hysterectomy specimens. Int J Gynecol Cancer 2011; 21: 654-60.

11. Kapucuoglu N, Bulbul D, Tulunay G, Temel MA. Reproducibility of grading systems for endometrial endometrioid carcinoma and their relation with pathologic prognostic parameters. Int J Gynecol

Cancer 2008; 18: 790-6.

12. Leung C, Yu C, Lin MI, Tognon C, Bernatchez P. Expression of myoferlin in human and murine carcinoma tumors: role in membrane repair, cell proliferation, and tumorigenesis. Am J Pathol 2013; 182: 1900-9.

13. Blomme A, Costanza B, de Tullio P, *et al*. Myoferlin regulates cellular lipid metabolism and promotes metastases in triple-negative breast cancer. Oncogene 2017; 36: 2116-30.

14. Song DH, Ko GH, Lee JH, *et al*. Myoferlin expression in non-small cell lung cancer: prognostic role and correlation with VEGFR-2 expression. Oncol Lett 2016; 11: 998-1006.

15. Kumar B, Brown NV, Swanson BJ, *et al*. High expression of myoferlin is associated with poor outcome in oropharyngeal squamous cell carcinoma patients and is inversely associated with HPV-status. Oncotarget 2016; 7: 18665-77.

16. Wang WS, Liu XH, Liu LX, *et al*. iTRAQ-based quantitative proteomics reveals myoferlin as a novel prognostic predictor in pancreatic adenocarcinoma. J Proteomics 2013; 91: 453-65.

17. Nishimura Y, Watanabe J, Jobo T, Hattori M, Arai T, Kuramoto H. Cytologic scoring of endometrioid adenocarcinoma of the endometrium. Cancer 2005; 105: 8-12.

Prognostic Utility of Histological Growth Patterns of Colorectal Lung Oligometastasis

Son Jae Yeong · Min Gyoung Pak Hyoun Wook Lee[1] · Seung Yeon Ha[2] Mee Sook Roh

Department of Pathology, Dong-A University College of Medicine, Busan; [1]Department of Pathology, Samsung Changwon Hospital, Sungkyunkwan University School of Medicine, Changwon; [2]Department of Pathology, Gachon University of Medicine and Science, Incheon, Korea

Corresponding Author
Mee Sook Roh, MD, PhD
Department of Pathology, Dong-A University College of Medicine, 32 Daesingongwon-ro, Seo-gu, Busan 49201, Korea
Tel: +82-51-240-2833
Fax: +82-51-243-7396
E-mail: msroh@dau.ac.kr

Background: Patients with resectable colorectal lung oligometastasis (CLOM) demonstrate a heterogeneous oncological outcome. However, the parameters for predicting tumor aggressiveness have not yet been fully investigated in CLOM. This study was performed to determine the prognostic value of histological growth patterns in patients who underwent surgery for CLOM. **Methods:** The study included 92 patients who were diagnosed with CLOM among the first resection cases. CLOMs grow according to three histological patterns: aerogenous, pushing, and desmoplastic patterns. The growth patterns were evaluated on archival hematoxylin and eosin–stained tissue sections. **Results:** The aerogenous pattern was found in 29.4% (n = 27) of patients, the pushing pattern in 34.7% (n = 32), the desmoplastic pattern in 6.5% (n = 6), and a mix of two growth patterns in 29.4% (n = 27). The size of the aerogenous pattern was significantly smaller than that of metastases with other patterns (p = .033). Kaplan-Meier analysis demonstrated that patients showing an aerogenous pattern appeared to have a poorer prognosis, which was calculated from the time of diagnosis of the CLOM (p = .044). The 5-year survival rate from the diagnosis of colorectal cancer tended to be lower in patients with an aerogenous pattern than in those who had a non-aerogenous pattern; however, the difference was marginally significant (p = .051). In the multivariate Cox analysis, the aerogenous pattern appeared as an independent predictor of poor overall survival (hazard ratio, 3.122; 95% confidence interval, 1.196 to 8.145; p = .020). **Conclusions:** These results suggest that the growth patterns may play a part as a histology-based prognostic parameter for patients with CLOM.

Key Words: Colorectal neoplasms; Lung; Oligometastasis; Growth pattern; Prognosis

The term "oligometastasis" indicates an intermediate state (≤ 5 metastases) of malignancy that lies between a localized tumor and widespread metastases.[1] The implication of the concept of an oligometastatic condition is that metastatic disease may be cured with metastasis-directed, locally ablative therapies.[2] Colorectal cancer (CRC) is one of the most frequently reported malignant tumors in a surgical series of oligometastasis,[2] and early metastatic progression of CRC may present with oligometastatic disease.[3]

The lung is the most common extra-abdominal organ of metastases from CRC, involved in 10%–25% of all patients with CRC.[4,5] Evidence suggests that pulmonary metastasectomy is the standard therapy for patients with resectable lesions and has a better prognosis, with a 5-year overall survival rate of 36%– 63%.[4,6] However, patients who undergo complete surgical resection of these lesions reveal a heterogeneous oncological outcome; some experience recurrent disease and die within a short duration after pulmonary metastasectomy, whereas other patients live without recurrence of disease.[4-8]

In previous studies, many authors have tried to clarify various prognostic parameters in patients undergoing pulmonary metastasectomies, including the number of metastatic lesions, disease-free interval, pretreatment carcinoembryonic antigen level, and degree of mediastinal lymph node involvement.[5,9] However, factors for classifying the potential aggressiveness have not yet been fully evaluated in colorectal lung oligometastasis (CLOM). Moreover, little is known about the histopathological features that determine prognosis after pulmonary metastasectomy.[10]

Vermeulen *et al.*[11] reported three histological growth patterns with biological differences for colorectal liver metastases: (1) a replacement growth pattern, where tumor cells infiltrate the liver cell plates by replacing the hepatocytes and co-opting hepatic stroma and sinusoids; (2) a pushing growth pattern, where the metastatic tumor expands by compression of the surrounding liver parenchyma with parallel running to the tumor liver interface; and (3) a desmoplastic growth pattern, in which the metastatic

tumor is separated by a fibrous rim from the liver parenchyma. Although the morphological classification described by Vermeulen *et al.*[11] has been reported in a few studies, the prognostic significance remains controversial in patients with colorectal liver metastasis.[12-15]

Furthermore, the significance of similar histological growth patterns has not yet been assessed in patients with CLOM. Therefore, we hypothesized that these histological growth patterns could help predict survival in patients with CLOM. This study was performed to determine the association of these three growth patterns of CLOM with standard clinicopathological parameters and also to determine the prognostic value of these growth patterns in patients who underwent surgery for CLOM.

MATERIALS AND METHODS

Patients and tissue samples

This study included 92 consecutive patients who were diagnosed with lung oligometastasis from colorectal adenocarcinoma among the first resection cases. The patients underwent curative lung resection for CLOM between 2004 and 2013 at Dong-A University Medical Center. We excluded patients who had another active cancer, more than five progressive metastatic sites, and a diagnosis of hereditary nonpolyposis CRC syndrome or familial polyposis. In addition, we excluded patients whose metastases showed a positive margin or cautery artifact due to the surgical procedure.[12] The final sample included 57 men and 35 women, with ages ranging from 31 to 83 years (mean age, 60.8 years). For each patient, the following demographic and clinicopathological factors were collected through a review of medical records: age, sex, differentiation grade of the primary tumor, location of the primary tumor, invasion depth of the primary tumor, lymph node status of the primary tumor, detection timing of CLOM in relation to detection of the primary tumor (synchronous or metachronous), number of CLOMs, diameter of the largest metastasis, and recurrence status. Synchronous lung metastasis had to be diagnosed during the diagnostic work-up or within 3 months following the diagnosis of CRC. CLOMs were defined as metachronous when they occurred at least 3 months after the diagnosis of CRC.[7] In patients who had undergone multiple resections for metastatic tumors, only the first resection was included in this study. The follow-up of patients began the month following CRC operation and ended at death or completion of follow-up (30 April 2017). All patients signed a written informed consent form to permit the use of their clinicopathological data for the purpose of the study. This retrospective study was approved by the required institutional review boards (IRB No. DAMC 15-141).

Histopathological evaluation

The growth pattern of CLOM was evaluated on archival 4 μm hematoxylin and eosin (H&E)–stained tissue sections cut from formalin-fixed, paraffin-embedded specimens from the tumor-lung boundary. In patients with multiple metastases, sections of the lesion with the largest diameter were examined. The histological growth pattern of CLOM was characterized as the "aerogenous-type," the "pushing-type," or the "desmoplastic-type," according to the modified Vermeulen's procedure.[11] Briefly, in the aerogenous pattern, tumor clusters, nests, or single tumor cells spread into the air spaces in the lung parenchyma surrounding the edge of the tumor without destruction of the lung architecture and lung parenchyma, which were in close approximation, and showed no compression of the air spaces, desmoplastic stroma or inflammatory infiltrate. In the pushing pattern, the metastasis grew by compression of the lung parenchyma with parallel running to the tumor-lung interface without desmoplastic stroma, and only a mild inflammatory infiltrate. In the desmoplastic pattern, the metastatic tumor was separated from the lung parenchyma by a desmoplastic fibrous rim infiltrated with lymphocytes. There was no direct contact between tumor cells and lung parenchyma. Hence, a "mixed-type" growth pattern was defined as a histologic feature where at least two growth patterns existed, both patterns appearing in at least 20% of the tumor-lung interface.[13] Mixed-type metastases were included with a predominant primary growth pattern and one or two secondary growth patterns (Fig. 1). Two pathologists (S.Y.H. and M.S.R.) blinded to the clinicopathological information and outcome evaluated the H&E-stained slides of metastatic tumor nodules. The third pathologist (H.W.L.), who was also blinded to the clinicopathological information and outcome, resolved any discrepancy between the first two pathologists.

Statistical analysis

Comparisons between the growth pattern and clinicopathological factors were analyzed using a chi-square test for proportions and analysis of variance (ANOVA) test for continuous variables as appropriate. The patient survival rate was analyzed using the Kaplan-Meier method, and the log-rank test was used to determine if there were any significant differences between the survival curves. All variables that revealed a statistically significant difference on univariate analysis were entered into the multivariate analysis. A $p < .05$ was considered statistically significant. All statistical analyses were performed using the Statistical Package

for the Social Sciences (SPSS) ver. 21 (IBM Co., Armonk, NY, USA).

RESULTS

Clinicopathological characteristics

The clinicopathological characteristics of the study participants

are summarized in Table 1. The patient population included 57 (62.0%) men and 35 (38.0%) women with a mean age of 60.8 years (range, 31 to 83 years). The diameter of the largest CLOM ranged from 0.4 to 7.0 cm, with a mean size of 1.8 cm. The histology of the primary tumor included 86 well- or moderately-differentiated adenocarcinomas (93.5%) and six poorly differen-
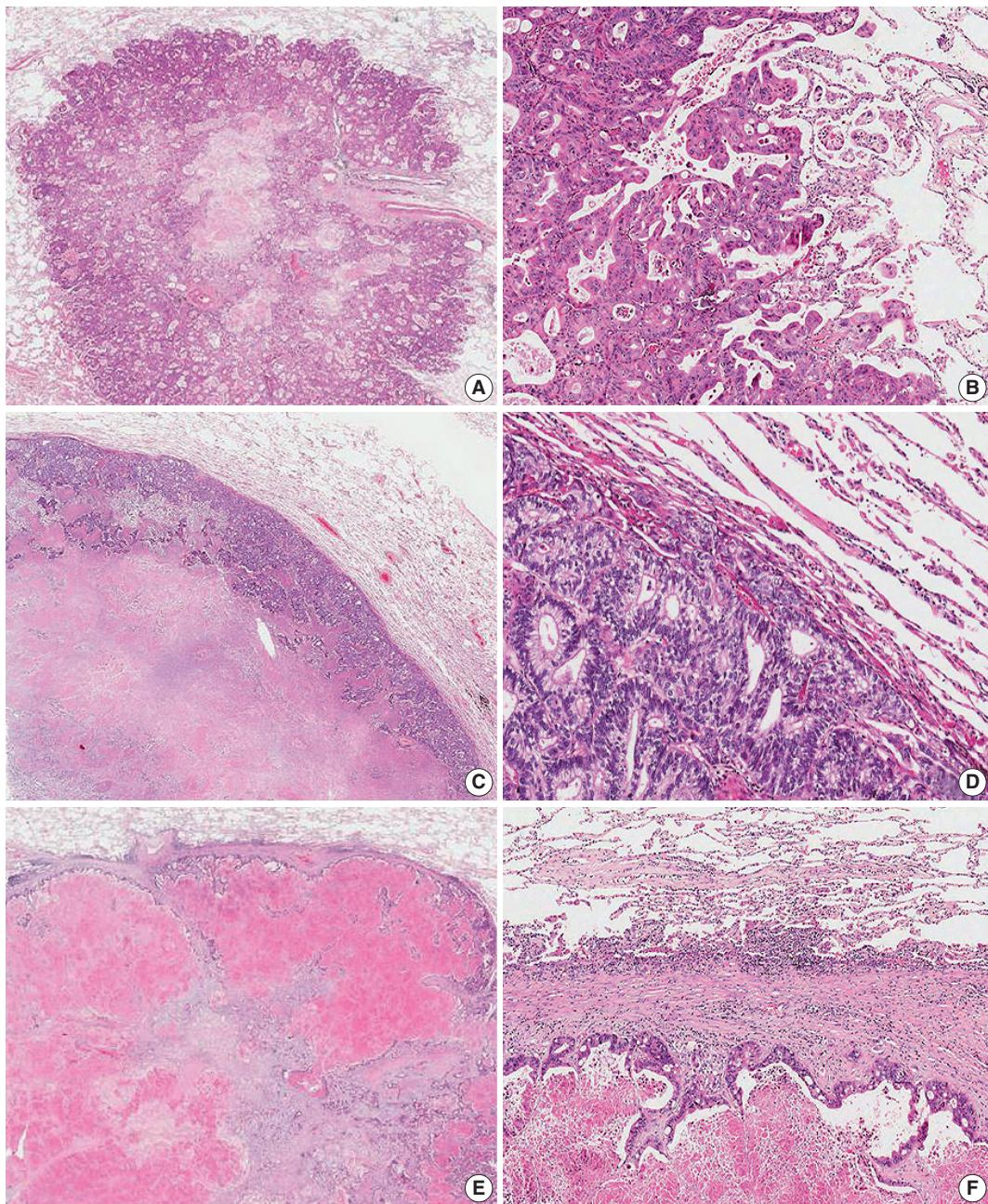
Fig. 1. Representative histologic features of the three different growth patterns of lung oligometastasis from colorectal adenocarcinoma. (A, B) In the aerogenous pattern, tumor clusters, nests, or single tumor cells spread into the air spaces of the lung parenchyma surrounding the edge of the tumor without destruction of the lung architecture, desmoplastic stroma, or inflammatory infiltrate. (C, D) In the pushing pattern, the metastasis grows by compression of the lung parenchyma, running parallel to the tumor-lung interface without desmoplastic stroma, and with only a mild inflammatory infiltrate. (E, F) In the desmoplastic pattern, the metastatic tumor is separated from the lung parenchyma by a desmoplastic rim infiltrated with lymphocytes. There is no direct contact between the tumor cells and lung parenchyma.

Table 1. Relationship between histological growth patterns of colorectal lung oligometastasis and clinicopathological characteristics

Clinicopathological characteristic	Growth pattern				p-value
	Aerogenous (n = 27)	Pushing (n = 32)	Desmoplastic (n = 6)	Mixed (n = 27)	
Age at CLOM (yr)					
Mean ± SD	57.63 ± 11.32	61.25 ± 10.52	69.50 ± 11.50	61.78 ± 11.30	.110[a]
Sex					
Male	16 (59.3)	20 (62.5)	3 (50.0)	18 (66.7)	.872[b]
Female	11 (40.7)	12 (37.5)	3 (50.0)	9 (33.3)	
Size of CLOM (cm)					
Mean ± SD	1.49 ± 0.54	2.03 ± 1.40	2.68 ± 1.78	1.66 ± 0.59	.033[a]
No. of CLOMs					
Single	15 (55.6)	19 (59.4)	2 (33.3)	18 (66.7)	.491[b]
Multiple (2 to ≤5)	12 (44.4)	13 (40.6)	4 (66.7)	9 (33.3)	
Detection timing of CLOM					
Synchronous	8 (29.6)	9 (28.1)	0	7 (25.9)	.501[b]
Metachronous	19 (70.4)	23 (71.9)	6 (100)	20 (74.1)	
Frequency of CLOM					
One time	24 (88.9)	28 (87.5)	6 (100)	22 (81.5)	.635[b]
More than one time	3 (11.1)	4 (12.5)	0	5 (18.5)	
Location of CRC					
Colon	11 (40.7)	14 (43.8)	3 (50.0)	9 (33.3)	.182[b]
Rectosigmoid	1 (3.7)	8 (25.0)	0	7 (25.9)	
Rectum	15 (55.6)	10 (31.3)	3 (50.0)	11 (40.7)	
Differentiation grade of CRC					
Well	15 (55.6)	21 (65.6)	2 (33.3)	12 (44.4)	.570[b]
Moderately	11 (40.7)	9 (28.1)	3 (50.0)	13 (48.2)	
Poorly	1 (3.7)	2 (6.3)	1 (16.7)	2 (7.4)	
T category of CRC					
T1	0	1 (3.1)	0	2 (7.4)	.566[b]
T2	1 (3.7)	2 (6.3)	1 (16.7)	3 (11.1)	
T3	22 (81.5)	25 (78.1)	4 (66.7)	15 (55.6)	
T4	3 (11.1)	2 (6.3)	1 (16.7)	5 (18.5)	
Unknown	1 (3.7)	2 (6.3)	0	2 (7.4)	
N category of CRC					
N0	8 (29.6)	14 (43.8)	1 (16.7)	11 (40.7)	.617[b]
N1	8 (29.6)	8 (25.0)	3 (50.0)	9 (33.3)	
N2	10 (37.0)	8 (25.0)	2 (33.3)	5 (18.5)	
Unknown	1 (3.7)	2 (6.3)	0	2 (7.4)	

Values are presented as number (%) unless otherwise indicated.
CLOM, colorectal lung oligometastasis; SD, standard deviation; CRC, colorectal cancer.
[a]One-way ANOVA analysis; [b]Chi-square test.

tiated adenocarcinomas (6.5%). Fifty-four (58.7%) patients had a single CLOM, while 38 (41.3%) had multiple (2 to ≤5 metastases) CLOMs. Twenty-four patients (26.1%) had synchronous CLOM, and 68 (73.9%) patients had metachronous CLOM. Further, 42.4% of our cases were located in the rectum, 83.7% had a locally advanced tumor (stage T3 or higher), and 57.6% demonstrated lymph node metastasis at the time of diagnosis.

Histological growth patterns

Overall, the aerogenous pattern was found in 29.4% (n = 27) of the CLOMs, the pushing pattern was present in 34.7% (n = 32) of the CLOMs, the desmoplastic pattern was identified in 6.5% (n = 6) of the CLOMs, and the mixed pattern was found in 29.4% (n = 27) of the CLOMs (Table 1). Among the CLOMs with a mixed pattern, the pushing pattern (63.0%) was the most predominant, and a combination of the pushing and aerogenous patterns (48.2%) was the most common mixed pattern. Only one metastasis displayed all three growth patterns.

Relationships between growth patterns and clinicopathological characteristics

The size of the aerogenous pattern (1.49 ± 0.54 cm) was sig-

nificantly smaller than that of metastases with the pushing pattern (2.03 ± 1.40 cm) or the desmoplastic (2.68 ± 1.78 cm) pattern (p = .033). The number of CLOMs (single vs. multiple) per patient was not different among the growth patterns (p > .05). The detection timing (synchronous vs metachronous) and frequency (one time vs. more than once) of CLOM also did not show any significant difference among the growth patterns (each p > .05). Although there was no significant correlation between the location of CRC and the growth pattern, the aerogenous pattern seemed to occur more frequently in the rectum than the non-aerogenous pattern, and this difference was marginally significant (p = .058). The differentiation grade and invasion depth of the primary tumor (T category of CRC) and primary tumor lymph node status (N category of CRC) were not significantly correlated with the growth pattern of CLOM (each p > .05).

Survival analysis

Of the 92 patients included, 23 (25.0%) died during follow-up. Median survival was 61.0 months, and the median follow-up time was 52.1 months (range, 0.2 to 155 months). When matched against all four growth patterns, a Kaplan-Meier analysis demonstrated no significant differences in overall survival according to the four growth patterns calculated from the diagnosis of CLOM or CRC (data not shown). However, the difference was more significant when patients were divided into two groups, with one group including patients with metastases having an aerogenous pattern and the other group including those with metastases having a pushing, desmoplastic, or mixed pattern. Patients showing an aerogenous pattern appeared to have a poorer prognosis with a median survival time of 58 months compared to a median survival of 64 months in patients with a non-aerogenous pattern, which was calculated from the time of diagnosis of CLOM (p = .044) (Fig. 2A). The 5-year survival rate calculated from the diagnosis of CRC tended to be lower in patients with CLOM having an aerogenous pattern than in those with CLOM having a non-aerogenous pattern; however, the difference was marginally significant (p = .051) (Fig. 2B). In the multivariate Cox analysis, the aerogenous pattern was associated with a significantly poorer survival compared to the non-aerogenous pattern (hazard ratio [HR], 3.122; 95% confidence interval [CI], 1.196 to 8.145; p = .020), as the aerogenous pattern appeared to be an independent prognostic factor for poor overall survival (Table 2). The Cox regression analysis also showed the effects of the specific T category of CRC (HR, 5.412; 95% CI, 1.961 to 14.938; p = .001) and the detection timing of CLOM (HR, 3.008; 95% CI, 1.106 to 8.185; p = .031) on survival time (Table 2).

Table 2. Multivariate Cox regression analysis for overall survival

Variable	Cox regression		
	HR	95% CI	p-value
Growth pattern			
Aerogenous	3.122	1.196–8.145	.020
Non-aerogenous	1		
T category of CRC			
T3–T4	5.412	1.961–14.938	.001
T1–T2	1		
Detection timing of CLOM			
Synchronous	3.008	1.106–8.185	.031
Metachronous	1		

HR, hazard ratio; CI, confidence interval; CRC, colorectal cancer; CLOM, colorectal lung oligometastasis.
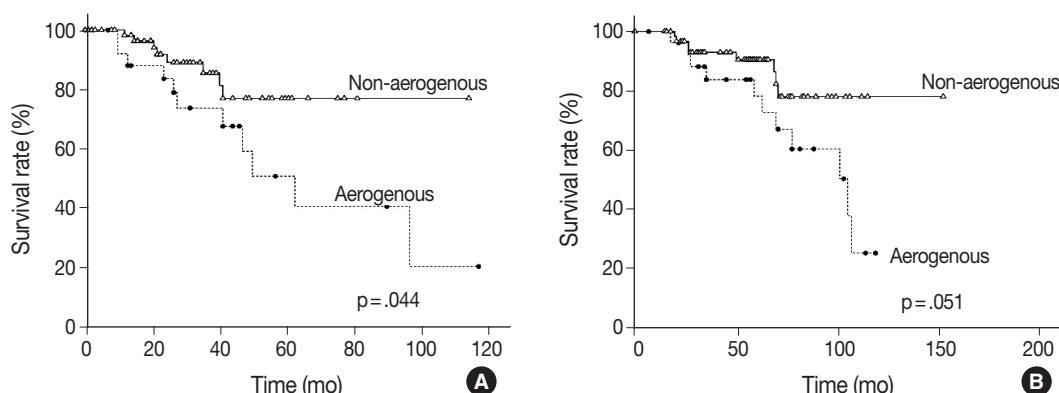
Fig. 2. Kaplan-Meier curves illustrating the overall survival of patients with colorectal lung oligometastasis (CLOM) in relation to growth patterns. (A) The overall survival rate calculated from the diagnosis of CLOM shows a shorter survival time in patients with CLOM having an aerogenous pattern than in those with CLOM having a non-aerogenous pattern (p = .044). (B) Although the difference was marginally significant (p = .051), the overall survival rate calculated from the time of diagnosis of colorectal cancer tends to show a shorter survival length in patients with CLOM having an aerogenous pattern than in those with CLOM with a non-aerogenous pattern.

DISCUSSION

In the present study, Kaplan-Meier and Cox regression analyses showed the prognostic significance of the histological growth patterns, as the aerogenous pattern seemed to be an independent prognostic factor for poor overall survival. This is one of few works to analyze the histopathological prognostic factors for classifying the potential of tumor aggressiveness in CLOM after pulmonary metastasectomy. If the present results can be reaffirmed, we recommend recoding the aerogenous pattern as a routine prognostic biomarker in the pathology report of CLOM.

The first possible mechanism behind these findings is explained by the new concept of spread through air spaces (STAS). Prior to the definition of STAS, one early study indicated that an aerogenous tumor spread and free floating cell clusters from metastatic CRC are unfavorable prognostic features.[10] In a new statement regarding the invasiveness of primary lung adenocarcinoma, STAS have been recognized as an additional pattern of tumor invasiveness. Although the concept of STAS is still evolving, STAS consists of micropapillary clusters, solid nests or single cells beyond the edge of the tumor into the air spaces in the surrounding lung parenchyma.[16] The loss of cell-to-cell adhesion or anchorage-independent growth of cancer cells may contribute to STAS.[10] The presence of STAS in lung adenocarcinoma suggests a high risk of recurrence and invasion and is thus an important prognostic factor.[17] We consider CLOM that has an aerogenous pattern to be comparable with STAS in primary lung cancer tumors. Although the definition of cancer infiltration into the surrounding lung parenchyma is different from that occurring in the liver, the aerogenous pattern is compatible with the replacement pattern of Vermeulen's procedure.[11] The second possible explanation is that non-aerogenous metastases offer a benefit by incorporating the supporting architecture endogenous to the lung, as in colorectal liver metastasis. At the leading edge of CLOM, direct dynamic interaction between metastatic tumor and host cells, mediated by various kinds of cytokines, chemokines, or growth factors, may show tumor-promoting properties.[12,18,19]

Although our findings are interesting, there are several limitations to the present study. First, our study is retrospective, and it is limited by the fact that there was variation in the treatment protocol and modality before and after resection and also by the fact that responses to each treatment option were not evaluated in the survival analysis, possibly resulting in selection bias. Preoperative neoadjuvant therapy may also have influenced the morphology of growth patterns. However, we feel these limitations are outweighed based on Nielsen's opinion[13] that the histologic findings of a growth pattern are really relevant, as the cohort reflects the actual patient status from a clinical point of view, although the survival data may not completely reflect the prognostic significance of growth patterns. Second, growth patterns were evaluated on the basis of only one tissue section per patient and included only the first metastasectomy, even for patients with multiple metastases that took place at different times. One study assessed the growth pattern of recurrent liver metastases and reported that 27.3% of recurrent metastases showed a different growth pattern than the first metastasis, while 31.8% of recurrent metastases had a partly new growth pattern.[13] Therefore, the growth pattern does not appear to be a host-specific feature.[20] As the metastasis advances, the morphology of the tumor-lung interface can change either with the accumulation of desmoplastic stroma or with STAS when the speed of tumor growth exceeds the spread rate at the invasive front, which has been similarly reported in the liver.[13,21] Third, a mixed-type was found in 29.4% of cases, and the pushing growth pattern was predominant (63.0% of these cases). Moreover, 48.2% of these cases showed a combination of pushing and aerogenous growth patterns. Regarding the idea of STAS, the quantity of the aerogenous pattern might also be an important prognostic parameter.[22] However, we could not demonstrate the intermediate survival rates for patients with CLOM having a mixed pattern, which reflects a heterogeneous tumor with both an aggressive aerogenous pattern and other more indolent patterns. Moreover, the case numbers of the combination subgroups of mixed pattern were too small for statistical evaluation to determine the prognostic effect according to the constituent parts of growth pattern. Another limitation of our study was that the number of patients showing each growth pattern was small, especially the desmoplastic subgroup, as previously discussed; therefore, this study may have been underpowered to detect some differences.

Despite these limitations, this study is the first to evaluate the histology-based prognostic factors for classifying the potential of tumor aggressiveness in the setting of pulmonary metastasectomy for CLOM. However, the current findings must be reproduced, and further investigation is needed to determine the clinical implications and the biological mechanism of growth patterns of CLOM in a well-adjusted study. A concomitant study of diverse metastatic mechanisms, including the complicated interaction with the lung microenvironment, might be helpful to understand the significance of histologic growth patterns of CLOM.

REFERENCES

1. Weichselbaum RR, Hellman S. Oligometastases revisited. Nat Rev Clin Oncol 2011; 8: 378-82.

2. Corbin KS, Hellman S, Weichselbaum RR. Extracranial oligometastases: a subset of metastases curable with stereotactic radiotherapy. J Clin Oncol 2013; 31: 1384-90.

3. Comito T, Cozzi L, Clerici E, *et al.* Stereotactic ablative radiotherapy (SABR) in inoperable oligometastatic disease from colorectal cancer: a safe and effective approach. BMC Cancer 2014; 14: 619.

4. Inoue M, Ohta M, Iuchi K, *et al.* Benefits of surgery for patients with pulmonary metastases from colorectal carcinoma. Ann Thorac Surg 2004; 78: 238-44.

5. Rama N, Monteiro A, Bernardo JE, Eugénio L, Antunes MJ. Lung metastases from colorectal cancer: surgical resection and prognostic factors. Eur J Cardiothorac Surg 2009; 35: 444-9.

6. Pfannschmidt J, Dienemann H, Hoffmann H. Surgical resection of pulmonary metastases from colorectal cancer; a systemic review of published series. Ann Thorac Surg 2007; 84: 324-38.

7. Mitry E, Guiu B, Cosconea S, Jooste V, Faivre J, Bouvier AM. Epidemiology, management and prognosis of colorectal cancer with lung metastases: a 30-year population-based study. Gut 2010; 59: 1383-8.

8. Lee KS, Nam SK, Koh J, *et al.* Stromal expression of microRNA-21 in advanced colorectal cancer patients with distant metastases. J Pathol Transl Med 2016; 50: 270-7.

9. Iizasa T, Suzuki M, Yoshida S, *et al.* Prediction of prognosis and surgical indications for pulmonary metastasectomy from colorectal cancer. Ann Thorac Surg 2006; 82: 254-60.

10. Shiono S, Ishii G, Nagai K, *et al.* Histopathologic prognostic factors in resected colorectal lung metastases. Ann Thorac Surg 2005; 79: 278-82.

11. Vermeulen PB, Colpaert C, Salgado R, *et al.* Liver metastases from colorectal adenocarcinomas grow in three patterns with different angiogenesis and desmoplasia. J Pathol 2001; 195: 336-42.

12. Van den Eynden GG, Bird NC, Majeed AW, Van Laere S, Dirix LY, Vermeulen PB. The histological growth pattern of colorectal cancer liver metastases has prognostic value. Clin Exp Metastasis 2012; 29: 541-9.

13. Nielsen K, Rolff HC, Eefsen RL, Vainer B. The morphological growth patterns of colorectal liver metastases are prognostic for overall survival. Mod Pathol 2014; 27: 1641-8.

14. Nagashima I, Oka T, Hamada C, Naruse K, Osada T, Muto T. Histopathological prognostic factors influencing long-term prognosis after surgical resection for hepatic metastases from colorectal cancer. Am J Gastroenterol 1999; 94: 739-43.

15. Lunevicius R, Nakanishi H, Ito S, *et al.* Clinicopathological significance of fibrotic capsule formation around liver metastasis from colorectal cancer. J Cancer Res Clin Oncol 2001; 127: 193-9.

16. Travis WD, Brambilla E, Burke AP, Marx A, Nicholson AG. WHO classification of tumours of the lung, pleura, thymus and heart. 4th ed. Lyon: IARC Press, 2015.

17. Dai C, Xie H, Su H, *et al.* Tumor spread through air spaces affects the recurrence and overall survival in patients with lung adenocarcinoma >2 to 3 cm. J Thorac Oncol 2017; 12: 1052-60.

18. Paku S. Current concepts of tumor-induced angiogenesis. Pathol Oncol Res 1998; 4: 62-75.

19. Ueno H, Konishi T, Ishikawa Y, *et al.* Histological categorization of fibrotic cancer stroma in the primary tumor is an independent prognostic index in resectable colorectal liver metastasis. Am J Surg Pathol 2014; 38: 1380-6.

20. Eefsen RL, Van den Eynden GG, Høyer-Hansen G, *et al.* Histopathological growth pattern, proteolysis and angiogenesis in chemonaive patients resected for multiple colorectal liver metastases. J Oncol 2012; 2012: 907971.

21. Terayama N, Terada T, Nakanuma Y. Histologic growth patterns of metastatic carcinomas of the liver. Jpn J Clin Oncol 1996; 26: 24-9.

22. Warth A. Spread through air spaces (STAS): a comprehensive update. Transl Lung Cancer Res 2017; 6: 501-7.

Preoperative Cytologic Diagnosis of Warthin-like Variant of Papillary Thyroid Carcinoma

Jisup Kim · Beom Jin Lim
Soon Won Hong · Ju Yeon Pyo

Department of Pathology, Gangnam Severance
Hospital, Yonsei University College of Medicine,
Seoul, Korea

Corresponding Author
Ju Yeon Pyo, MD, PhD
Department of Pathology, Gangnam Severance
Hospital, Yonsei University College of Medicine,
211 Eonju-ro, Gangnam-gu, Seoul 06273, Korea
Tel: +82-2-2019-3540
Fax: +82-2-3463-2103
E-mail: jypyo@yuhs.ac

Background: Warthin-like variant of papillary thyroid carcinoma (WLV-PTC) is a relatively rare variant of papillary thyroid carcinoma with favorable prognosis. However, preoperative diagnosis using fine-needle aspiration (FNA) specimens is challenging especially with lymphocytic thyroiditis characterized by Hürthle cells and lymphocytic background. To determine a helpful cytological differential point, we compared WLV-PTC FNA findings with conventional papillary thyroid carcinoma with lymphocytic thyroiditis (PTC-LT) and conventional papillary thyroid carcinoma without lymphocytic thyroiditis (PTC) regarding infiltrating inflammatory cells and their distribution. Preoperative diagnosis or potential for WLV-PTC will be helpful for surgeons to decide the scope of operation. **Methods:** Of the 8,179 patients treated for papillary thyroid carcinoma between January 2007 and December 2012, 16 patients (0.2%) were pathologically confirmed as WLV-PTC and four cases were available for cytologic review. For comparison, we randomly selected six PTC-LT cases and five PTC cases during the same period. The number of intratumoral and background lymphocytes, histiocytes, neutrophils, and the presence of giant cells were evaluated and compared using conventional smear and ThinPrep preparations. **Results:** WLV-PTC showed extensive lymphocytic smear with incorporation of thyroid follicular tumor cell clusters and frequent histiocytes. WLV-PTC was associated with higher intratumoral and background lymphocytes and histiocytes compared with PTC-LT or PTC. The difference was more distinct in liquid-based cytology. **Conclusions:** The lymphocytic smear pattern and the number of inflammatory cells of WLV-PTC are different from those of PTC-LT or PTC and will be helpful for the differential diagnosis of WLV-PTC in preoperative FNA.

Key Words: Warthin-like variant; Thyroid cancer, papillary; Hashimoto disease; Biopsy, fine-needle

Warthin-like variant of papillary thyroid carcinoma (WLV-PTC) was first described by Apel *et al*.[1] in 1995 and named "warthin-like" due to the presence of abundant lymphocytes interspersed in oncocytic follicular epithelial cells resembling the warthin tumor of salivary glands. It is a relatively rare variant of papillary thyroid carcinoma with only 95 cases published in the English literature.[2] This tumor expresses the product of the *RET/PTC* fusion gene, indicating that it is a variant of papillary thyroid carcinoma.[3] WLV-PTC is a favorable prognostic variant[1,3,4] although ominous behavior has also been reported.[5] The diagnosis of WLV-PTC is relatively simple due to its characteristic morphology. However, preoperative diagnosis using fine-needle aspiration (FNA) samples is challenging because abundant lymphocytes and oncocytic follicular epithelial cells (Hürthle cells) are observed in various lesions associated with lymphocytic thyroiditis. In this study, we compared FNA findings of WLV-PTC, conventional papillary thyroid carcinoma with lympho-

cytic thyroiditis (PTC-LT), and conventional papillary thyroid carcinoma without lymphocytic thyroiditis (PTC). The characteristics of infiltrating inflammatory cells and their distribution were analyzed to evaluate their usefulness for differential diagnosis. Preoperative differential diagnosis of WLV-PTC will be helpful for surgeons to determine the optimal scope of operation.

MATERIALS AND METHODS

Patients and cases

We retrieved 8,179 papillary thyroid carcinoma cases from the Thyroid Cancer Center database, Gangnam Severance Hospital, Yonsei University College of Medicine, Seoul, Korea between January 2007 and December 2012. Based on the final pathological diagnosis, 16 patients (0.2%) were WLV-PTC including outside consultation cases. We were able to reexamine cytology slides from four of the patients. Six PTC-LT cases and five PTC

cases were randomly selected for comparison (Table 1). Each case had been prepared for both conventional smear and liquid-based cytology (ThinPrep, Hologic, Bedford, MA, USA). The Institutional Review Board of Gangnam Severance Hospital (local IRB number: 3-2017-0235) approved this retrospective study and informed consent was waived.

Microscopic evaluation

Three slides (two conventional smears and one ThinPrep) were reviewed in each case. The number of background lymphocytes within tumor clusters as well as the number of histiocytes and neutrophils was counted in 10 high power fields (HPFs, ×200) in each sample slide. Tumor clusters composed of at least five tumor cells were included in this counting. The presence or absence of background giant cells was recorded. In each case, the average number of inflammatory cells per one HPF was recorded and separated into low and high groups for comparison. The cut-off points are shown in Tables 2 and 3.

Table 1. Baseline clinicopathologic characteristics of each case

Case No.	Age (yr)/Sex	Tumor size (cm)	Sonographic feature	FNA diagnosis[a]	Pathologic diagnosis	Associated thyroiditis
1	46/F	1.0	Irregular shaped calcified nodule	VI. PTC	PTC-LT	Present
2	45/F	0.9	Suspicious malignant nodule	VI. PTC	PTC-LT	Present
3	46/F	0.6	Suspicious malignant nodule	V. Suspicious PTC	PTC-LT	Present
4	53/F	0.4	Suspicious lesion	VI. PTC	PTC-LT	Present
5	53/F	0.6	Suspicious nodule	V. Suspicious PTC	PTC-LT	Present
6	62/F	0.4	Taller than wider hypoechoic nodule	VI. PTC	PTC-LT	Present
7	76/F	0.5	Suspicious nodule	VI. PTC	PTC	Absent
8	44/F	0.7	Suspicious malignant nodule	V. Suspicious PTC	PTC	Absent
9	49/F	0.6	Suspicious lesion	VI. PTC	PTC	Absent
10	70/M	1.0	Cancer nodule	VI. PTC	PTC	Absent
11	57/F	0.3	Suspicious lesion	VI. PTC	PTC	Absent
12	33/F	1.4	Suspicious nodule	VI. PTC	WLV-PTC	Present
13	59/F	0.3	Low suspicious nodule	V. Suspicious PTC	WLV-PTC	Absent
14	40/F	0.6	Oval shaped mass with poor enhancement	V. Suspicious PTC	WLV-PTC	Absent
15	48/F	0.4	Suspicious nodule	VI. PTC	WLV-PTC	Present

FNA, fine-needle aspiration; F, female; PTC, conventional papillary thyroid carcinoma without lymphocytic thyroiditis around the tumor; PTC-LT, conventional papillary thyroid carcinoma with lymphocytic thyroiditis around the tumor; M, male; WLV-PTC, Warthin-like variant of papillary thyroid carcinoma.
[a]Diagnostic categories according to the Bethesda system for reporting thyroid cytopathology.

Table 2. Comparison of inflammatory cell components among the papillary thyroid cancer groups in conventional smears

Inflammatory cell component	WLV-PTC (n=4)	PTC-LT (n=6)	PTC (n=5)	WLV-PTC vs PTC-LT p-value	WLV-PTC vs PTC p-value
Lymphocyte					
Background	38.00 (1–154)	7.50 (1–41)	14.00 (5–22)	.524[a]	.206[a]
Low (≤30)	1 (25)	5 (83)	5 (100)	.190[b]	.048[b]
High (>30)	3 (75)	1 (17)	0		
Within tumor	11.50 (0–51)	1.50 (0–3)	0.00 (0–2)	.999[a]	.524[a]
Low (≤10)	2 (50)	6 (100)	5 (100)	.133[b]	.167[b]
High (>10)	2 (50)	0	0		
Histiocyte	5.00 (1–9)	1.00 (0–2)	1.00 (1–29)	.999[a]	.999[a]
Low (<1)	1 (25)	2 (33)	0	.999[b]	.444[b]
High (≥1)	3 (75)	4 (67)	5 (100)		
Giant cell					
Absent	2 (50)	3 (50)	3 (60)	.999[b]	.999[b]
Present	2 (50)	3 (50)	2 (40)		
Neutrophil	3.50 (0–6)	5.00 (1–22)	4.00 (1–26)	.999[a]	.999[a]
Low (≤10)	4 (100)	4 (67)	4 (80)	.467[b]	.999[b]
High (>10)	0	2 (33)	1 (20)		

Values are presented as median (range) or number (%).
WLV-PTC, Warthin-like variant of papillary thyroid carcinoma; PTC-LT, conventional papillary thyroid carcinoma with lymphocytic thyroiditis around the tumor; PTC, conventional papillary thyroid carcinoma without lymphocytic thyroiditis around the tumor.
[a]Mann–Whitney U test; [b]Fisher exact test.

Table 3. Comparison of inflammatory cell components among the papillary thyroid cancer groups in liquid-based cytology (ThinPrep)

	WLV-PTC (n=4)	PTC-LT (n=6)	PTC (n=5)	WLV-PTC vs PTC-LT p-value	WLV-PTC vs PTC p-value
Lymphocyte					
Background	38.00 (17–47)	23.50 (6–71)	4.00 (2–8)	.999[a]	.008[a]
Low (≤10)	0	3 (50)	5 (100)	.200[b]	.008[b]
High (>10)	4 (100)	3 (50)	0		
Within tumor	14.50 (5–22)	3.50 (0–10)	0 (0–0)	.190[a]	.008[a]
Low (<1)	0 (0)	2 (33)	5 (100)	.467[b]	.008[b]
High (≥1)	4 (100)	4 (66)	0		
Histiocyte	11.00 (8–12)	1.50 (0–13)	1.00 (0–91)	.048[a]	.206[a]
Low (≤10)	1 (25)	5 (83)	4 (80)	.190[b]	.206[b]
High (>10)	3 (75)	1 (17)	1 (20)		
Giant cell				.400[b]	.524[b]
Absent	1 (25)	0	3 (60)		
Present	3 (75)	6 (100)	2 (40)		
Neutrophil	3.00 (1–12)	16.00 (1–47)	2.00 (0–10)	.524[a]	.999[a]
Low (≤10)	3 (75)	3 (50)	5 (100)	.571[b]	.444[b]
High (>10)	1 (25)	3 (50)	0		

Values are presented as median (range) or number (%).
WLV-PTC, Warthin-like variant of papillary thyroid carcinoma; PTC-LT, conventional papillary thyroid carcinoma with lymphocytic thyroiditis around the tumor; PTC, conventional papillary thyroid carcinoma without lymphocytic thyroiditis around the tumor.
[a]Mann–Whitney U test; [b]Fisher exact test.

Statistical analysis

The median number of inflammatory cells per one HPF was compared using the Mann-Whitney U test. Binary group distribution regarding inflammatory cell infiltration was compared using the Fisher's exact test. All statistical analyses were performed using SPSS ver. 23.0 (IBM Corp, Armonk, NY, USA) and p-values less than 0.05 were considered statistically significant.

RESULTS

The baseline clinicopathologic characteristics of each case such as age, gender, preoperative sonographic finding, preoperative FNA diagnosis, surgical pathologic diagnosis, tumor size, and associated thyroiditis are shown in Table 1. The WLV-PTC, PTC-LT, and PTC microscopic findings are shown in Fig. 1. Conventional smear and ThinPrep WLV-PTC samples showed irregular and papillary clusters with oncocytic cytoplasm and many lymphocytes within the tumor clusters and background (Fig. 1B–E) contrary to those of PTC-LT (Fig. 1G–J) and PTC (Fig. 1L–O) showing rare intratumoral and background lymphocytes. In WLV-PTC, the lymphocytic smear pattern was not different between the conventional and ThinPrep preparations.

The median number, range, and group distributions of inflammatory cells in WLV-PTC, PTC-LT, and PTC in conventional smears and in liquid-based smears are summarized in Tables 2 and 3. In conventional smears, WLV-PTC showed a tendency for association with higher numbers of lymphocytes within tumor clusters and in the background compared with PTC-LT or PTC. WLV-PTC was significantly associated with a high number of background lymphocytes compared with PTC (p = .048). In ThinPrep preparations, WLV-PTC also showed a significantly higher median number of lymphocytes within tumor clusters (p = .008), in the background (p = .008), and was significantly associated with higher lymphocytes within tumor clusters (p = .008) and the background (p = .008) compared with PTC. WLV-PTC showed a tendency for association with higher lymphocytes within tumors, in the background, and with higher histiocytes. WLV-PTC showed a significantly higher median number of histiocytes per one HPF (p = .048).

As an incidental finding, PTC-LT showed a neutrophilic smear with a higher median number compared with WLV-PTC or PTC (Tables 2, 3, Fig. 1G–J); however, the result was not statistically significant.

DISCUSSION

WLV-PTC is a rare variant of PTC having characteristic histologic features; therefore, histologic diagnosis of this tumor is usually straightforward. However, preoperative diagnosis using conventional or liquid-based cytology techniques is complicated because several diseases resemble each other based on cytologic features. The first description of WLV-PTC cytologic features
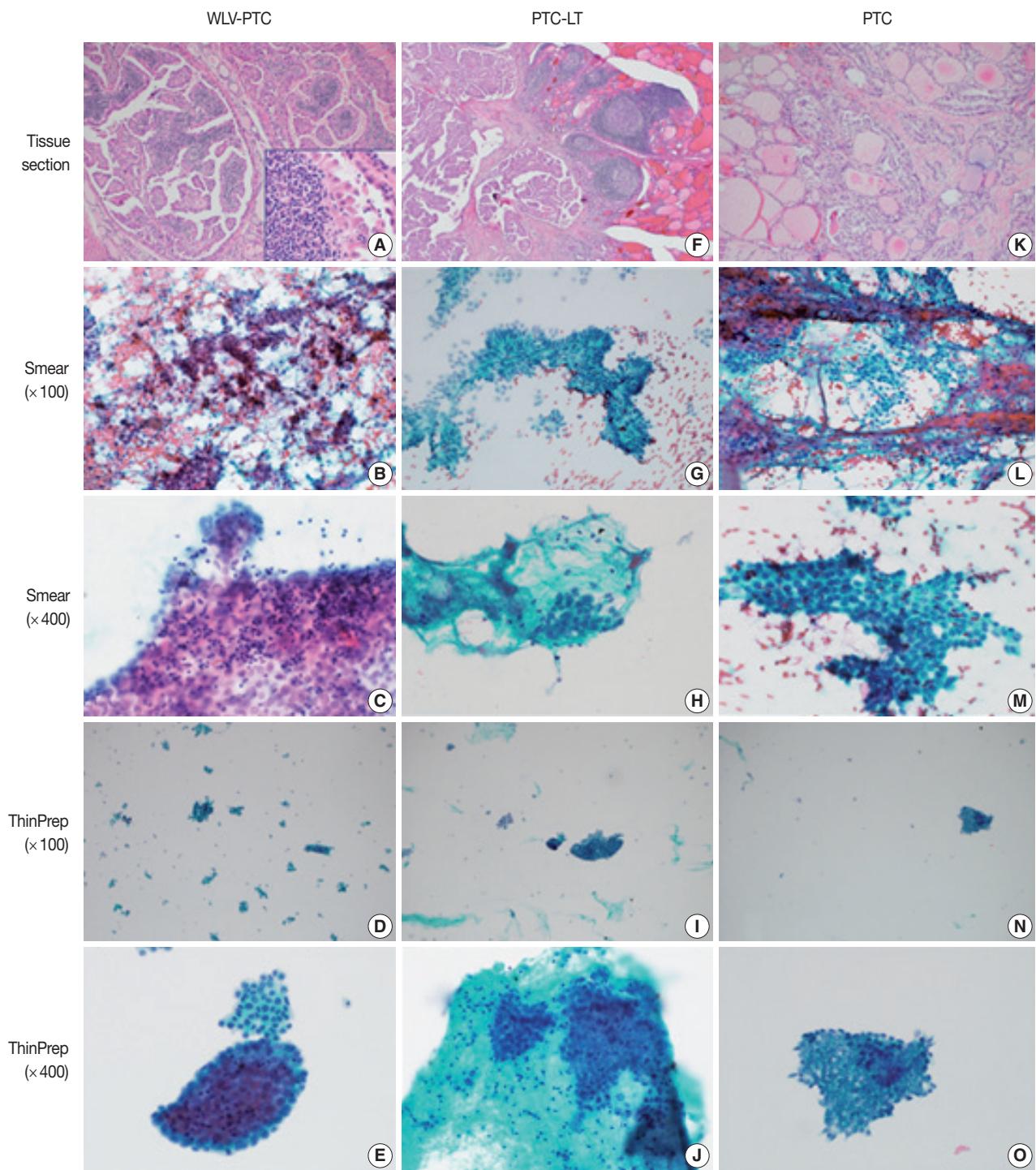
Fig. 1. Microscopic findings of Warthin-like variant of papillary thyroid carcinoma (WLV-PTC), conventional papillary thyroid carcinoma with lymphocytic thyroiditis (PTC-LT), and conventional papillary thyroid carcinoma without lymphocytic thyroiditis (PTC). (A) Histologic findings of WLV-PTC. WLV-PTC is composed of atypical follicular cells with abundant oxyphilic cytoplasm and nuclear grooves (inset) showing papillary structures with abundant lymphoid stroma. (B, C) Conventional smear of WLV-PTC showing irregular papillary clusters and numerous lymphocytes in tumor clusters in the bloody background. (D, E) Inflammatory and multinucleated giant cells are rather evenly distributed and hypercellular relative to the conventional smear. Intratumoral lymphocytes are easily seen. (F) Histologic findings of PTC-LT. (G, H) Conventional PTC-LT smear showing papillary tumor clusters without intratumoral lymphocytes, but some neutrophils seen around the tumor clusters in the lymphocytic background. (I, J) Peritumoral neutrophils seen in the lymphocytic background. (K) Histologic findings of PTC. (L–O) Hypercellular smear showing classic cytologic features of papillary carcinoma without inflammatory cells in background in both the conventional smear (L, M) and in ThinPrep (N, O) preparations.

was done by Yousef *et al*. in 1997.[6] Since then, nuclear features typical of PTC combined with oncocytic cytoplasm and lymphocytic background were considered to be the cytologic features of WLV-PTC. Therefore, every tumor or tumor-like condition having both nuclear pseudoinclusions in follicular cells and lymphocytic background should be included on the list of differential diagnoses. This list includes Hashimoto's thyroiditis, follicular neoplasm with oncocytic change, oncocytic variant of PTC,[7] PTC in the background of Hashimoto's thyroiditis, and tall cell variant of PTC.[8] Paker *et al*.[8] said the most important differential point is mixture of lymphocytes and oncocytic follicular cells, tissue fragments, and papillary structures. However, distinguishing these diseases by cytologic examination is not always clear cut. Especially in liquid-based cytology, cell clusters are easily dissolved during preparation, which can confer further diagnostic difficulty.[7]

In this study, we selected WLV-PTC, PTC-LT, and conventional PTC cases of which the diagnosis was confirmed by postoperative pathological examination. We compared preoperative cytology slides and investigated whether specific clues other than nuclear feature and lymphocytic background could distinguish these diseases. We focused on the component and amount of background and intratumoral inflammatory cells.

Although limitations of our study include relatively small WLV-PTC sample size due to the rarity of the disease, WLV-PTC was associated with higher lymphocytes and histiocytes within tumor clusters and within the background as well. The difference was more distinct in ThinPrep preparations.

Our investigation implies that analyzing inflammatory components in preoperative cytologic diagnosis could be helpful in the differential diagnosis between WLV-PTC and conventional PTC without lymphocytic thyroiditis. If lymphocytes within tumor clusters are also considered, the preoperative diagnosis of this rare WLV-PTC variant is possible; however, further multi-institutional studies including a large number of WLV-PTC cases will be needed.

Conflicts of Interest

No potential conflict of interest relevant to this article was reported.

REFERENCES

1. Apel RL, Asa SL, LiVolsi VA. Papillary Hurthle cell carcinoma with lymphocytic stroma: "Warthin-like tumor" of the thyroid. Am J Surg Pathol 1995; 19: 810-4.

2. Jun HH, Kim SM, Hong SW, Lee YS, Chang HS, Park CS. Warthin-like variant of papillary thyroid carcinoma: single institution experience. ANZ J Surg 2016; 86: 492-4.

3. D'Antonio A, De Chiara A, Santoro M, Chiappetta G, Losito NS. Warthin-like tumour of the thyroid gland: RET/PTC expression indicates it is a variant of papillary carcinoma. Histopathology 2000; 36: 493-8.

4. Ludvíková M, Ryška A, Korabečná M, Rydlová M, Michal M. Oncocytic papillary carcinoma with lymphoid stroma (Warthin-like tumour) of the thyroid: a distinct entity with favourable prognosis. Histopathology 2001; 39: 17-24.

5. Mai KT, Thomas J, Yazdi HM, Commons AS, Lamba M, Stinson AW. Pathologic study and clinical significance of Hürthle cell papillary thyroid carcinoma. Appl Immunohistochem Mol Morphol 2004; 12: 329-37.

6. Yousef O, Dichard A, Bocklage T. Aspiration cytology features of the warthin tumor-like variant of papillary thyroid carcinoma: a report of two cases. Acta Cytol 1997; 41(4 Suppl): 1361-8.

7. Chong Y, Suh S, Kim TJ, Lee EJ. Fine needle aspiration cytology of Warthin-like papillary thyroid carcinoma: a brief case report. Korean J Pathol 2014; 48: 170-3.

8. Paker I, Kokenek TD, Yilmazer D, Seker GE, Alper M. Oncocytic variant of papillary thyroid carcinoma with lymphocytic stroma (Warthin-like variant): report of a case with fine needle aspiration cytology and review of the literature. Cytopathology 2012; 23: 408-10.

■ ORIGINAL ARTICLE ■

Cytological Features That Differentiate Follicular Neoplasm from Mimicking Lesions

Kanghee Han · Hwa-Jeong Ha
Joon Seog Kong · Jung-Soon Kim
Jae Kyung Myung[1] · Jae Soo Koh
Sunhoo Park[1] · Myung-Soon Shin
Woo-Tack Song · Hye Sil Seol
Seung-Sook Lee[1]

Department of Pathology, Korea Cancer Center
Hospital, Korea Institute of Radiological and
Medical Sciences (KIRAMS), Seoul;
[1]Laboratory of Radiation Pathology, Korea
Institute of Radiological and Medical Sciences
(KIRAMS), Seoul, Korea

Corresponding Author
Seung-Sook Lee, MD, PhD
Laboratory of Radiation Pathology, Korea Cancer
Center Hospital, Korea Institute of Radiological and
Medical Sciences (KIRAMS), 75 Nowon-ro,
Nowon-gu, Seoul 01812, Korea
Tel: +82-2-970-1268
Fax: +82-2-970-2430
E-mail: sslee@kirams.re.kr

Background: It is difficult to correctly diagnose follicular neoplasms (FNs) on fine-needle aspiration cytology (FNAC) because it shares many cytological features with other mimicking lesions. The aim of this study was to identify the cytological features that differentiate FNs from mimicking lesions. **Methods:** We included the cytological slides from 116 cases of thyroid FN diagnosed on FNAC, and included their subsequent histological diagnoses. We evaluated the cytological architectural pattern and nuclear features of the lesions according to their histological groups. **Results:** The final histological diagnoses of the 116 cases varied, and included 51 FNs (44%), 47 papillary thyroid carcinomas (40%) including follicular variant, and seventeen cellular nodular hyperplasias (15%). Regardless of the final histological diagnosis, microfollicular pattern was observed in most cases. On the other hand, trabecular pattern was identified in 34% of FNs, but not in any other lesions. Additionally, elongated nuclei and ground glass chromatin were found in only some papillary thyroid carcinomas. **Conclusions:** This study shows that the trabecular pattern is a representative cytological feature of FNs that can be used to distinguish FNs from mimicking lesions. In addition, nuclear shape and chromatin pattern can be used to further confirm the diagnosis of FNs from mimicking lesions through FNAC.

Fine-needle aspiration cytology (FNAC) is an accurate and useful method for evaluating thyroid lesions and has been adopted as a tool for the diagnosis of thyroid nodules prior to surgery. This convenient tool could be used to reduce the rate of unnecessary treatments, such as surgery, for benign lesions.[1,2] More rapid and accurate diagnoses will also increase the effectiveness of treatments.[3] Moreover, because of the recent normalization of regular health checkups, the diagnosis of thyroid lesions has increased and FNAC is used more frequently to identify indeterminate nodules in the thyroid. Although FNAC is an excellent diagnostic tool for identifying thyroid nodules, the accuracy of diagnosis remains an issue in diagnosing follicular neoplasms (FNs) including follicular adenoma (FA), follicular carcinoma (FC), and Hurthle cell carcinoma (HC) and cytologically similar lesions.

In general, FNAC diagnosis of FNs depends on highly cellular

aspirate composed of uniform follicular cells arranged in microfollicular pattern and crowded clusters. However, because FNs display cytological features similar to other lesions including cellular nodular hyperplasia (NH), follicular variant of papillary thyroid carcinoma (FVPTC), and classic papillary thyroid carcinoma (PTC), correctly distinguishing FNs from these mimicking lesions through FNAC can be difficult. For these reasons, to correctly diagnose FNs in the thyroid using FNAC is a great challenge in clinical practice. Therefore, in this study, we investigated the cytological features of FNs to clearly distinguish it from other mimicking lesions by comparing features such as cytological architecture and detailed nuclear features, as well as histological diagnosis.

MATERIALS AND METHODS

We searched for cytology cases that were diagnosed as or suspected to be FNs through FNAC at the Department of Pathology, Korea Cancer Center Hospital (KCCH, Seoul, South Korea) between January 2010 and June 2015, using the pathology database of KCCH. We selected 116 cases where the thyroid was subsequently removed. The slides were reviewed by two pathologists and one cytotechnician.

Aspirations were performed with a 22–25-gauge needle attached to a 10-mL disposable syringe. The collected samples were placed onto slides, fixed with 95% ethyl alcohol, and stained with the Papanicolaou stain. Surgically resected tissues were embedded in paraffin, sectioned into 4-μm slices and stained with hematoxylin and eosin (H&E).

Diagnoses of the 116 cases through FNAC were compared with the histological diagnoses. The cytological analysis focused on both cytomorphological architecture and individual nuclear features. The architectural features evaluated were microfollicular architecture, multilayer rosettes, branching monolayer sheets, syncytial fragments, and trabecular pattern. Nuclear characteristics were analyzed based on chromatin clearing, nuclear grooves, intranuclear inclusions, anisonucleosis, and nuclear shape in each tissue-proven diagnostic group.

Definition of diagnostic terms

The FNAC cases in this study belong to the diagnostic category IV "FN or suspicious for FN" by the Bethesda system[3] which refers to a cellular aspirate composed of follicular cells showing significant cell crowding and/or microfollicular pattern without nuclear features of papillary carcinoma. Here, we tried to identify whether the diagnostic category IV by the Bethesda system is correlated with the histological diagnosis of FNs and, if there is a discrepancy, what would be helpful findings to differentiate them. Thus, the term "FN" in this study was used as a word collectively referred to as FA, FC, and HC by histological diagnosis. Therefore, FNs used in this study is different in meaning from the FN used in the Bethesda system.

Here, the term "PTC" refers to a classic papillary thyroid carcinoma having papillary architecture and characteristic nuclear features such as chromatin clearing, nuclear grooves, and intranuclear inclusions. Additionally, in the present study, FVPTCs were subdivided into three subgroups by the histologic examination and diagnostic criteria proposed in previous studies[4,5]: noninvasive follicular thyroid neoplasm with papillary-like nuclear features (NIFTP),[4] invasive encapsulated follicular variant of papillary thyroid carcinoma (invasive EFVPTC), and infiltrative FVPTC.[5] We examined the difference between the subtypes of FVPTC.

Statistical analysis

All statistical analyses were performed using the SPSS ver. 18 (SPSS Inc., Chicago, IL, USA). A Pearson's chi-square test was performed to evaluate the relevance of correlation between cytological architecture, nuclear characteristics and categorical variables. For all analyses, a p-value < .05 was considered statistically significant.

This study was approved by the Institutional Review Board of Korea Cancer Center Hospital with a waiver of informed consent (IRB number: K-1710-002007).

RESULTS

Histological correlation

Table 1 shows the final histological diagnoses for the 116 cases diagnosed as Bethesda diagnostic category IV, "FN or suspicious for FN" using FNAC. The concordance rate between preoperative cytological diagnosis and histological diagnosis of FNs was only 44% (Table 1). Histological follow-up identified 40% of the cases diagnosed as FNs by preoperative cytology as FVPTC or PTC. The most commonly misdiagnosed lesion was FVPTC. The detailed results are as follows: 27 cases of FA (23%), 23 cases of FC (20%), one case of HC (1%), 35 cases of FVPTC (30%), 12 cases of PTC (10%), 17 cases of NH (15%), and one case of Hashimoto thyroiditis (HT; 1%). The representative histological and cytological features of the lesions are shown in Fig. 1.

Evaluation of cytological features

The aspirates of the lesions were generally cell-rich with an

Table 1. Histological categories of 116 cases diagnosed as Bethesda category IV, "FN or suspicious for FN" through fine-need aspiration cytology

	Histological diagnosis	No. of cases (%)
FN	FA	27 (23)
	FC	23 (20)
	HC	1 (1)
Non-FN	FVPTC	35 (30)
	PTC	12 (10)
	NH	17 (15)
	HT	1 (1)

FN, follicular neoplasm; FA, follicular adenoma; FC, follicular carcinoma; HC, Hurthle cell carcinoma; FVPTC, follicular variant of papillary thyroid carcinoma; PTC, classic papillary thyroid carcinoma; NH, nodular hyperplasia; HT, Hashimoto thyroiditis.

abundance of follicular cell groups showing microfollicular patterns, syncytial configurations, and/or abundant isolated cells, which was sufficient evidence to suspect FNs in FNAC smears.

To determine cytological features unique to FNs, we evaluated each case in terms of both cytological architecture and nuclear characteristics.
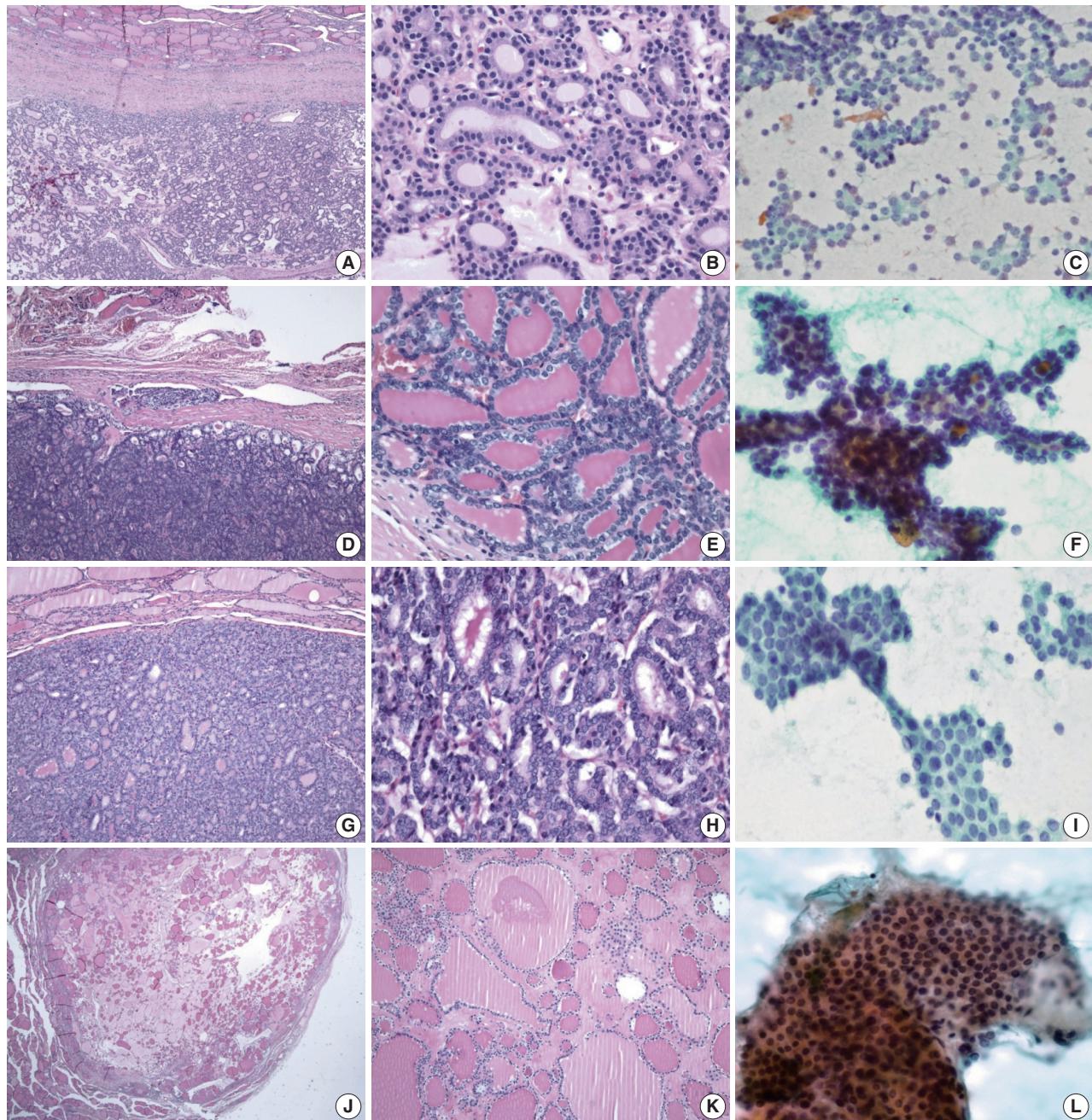

Fig. 1. Histological and cytological features of thyroid neoplasm. (A, B) Histological features of follicular adenoma. (A) The tumor is enclosed in a thick fibrous capsule. (B) The architectural pattern is follicular, and cells are uniform, round and dark. (C) Cytological features of follicular adenoma. Abundant follicular cells are seen, with little colloid. (D, E) Histological features of follicular carcinoma. (D) Vascular invasion in fibrous capsule of follicular carcinoma. (E) Colloid-containing well-formed follicles. (F) Cytological feature of follicular carcinoma. Note that microfollicles show three dimensional branching cellular clusters with trabecular pattern. (G, H) Histological features of follicular variant of papillary carcinoma. (G) The tumor resembles follicular neoplasm. (H) Nuclei are round to ovoid, similar to follicular neoplasm but show slight enlargement and overlapping. (I) Cytoloigcal feature of papillary carcinoma. Monolayer branching sheet of papillary carcinoma is compared with three-dimensional branching cluster of follicular carcinoma. (J, K) Histological features of nodular hyperplasia. Follicles are of varying sizes with abundant colloid. (L) Aspirate of nodular hyperplasia shows flat sheets of uniform follicular cells and colloid.

Cytological architecture

We reviewed the cytology smears, focusing on cytological architectures generally regarded as features of FNs such as microfollicular patterns, the trabecular pattern, multilayer rosettes, branching sheets, and syncytial fragments, and analyzed the frequency of these findings in each histologically proven diagnosis (Table 2).

Regardless of the final histological diagnosis, the microfollicular pattern was observed in most cases (Table 2). The microfol-

Table 2. Cytological architecture on the aspirates according to histological diagnosis

Histological diagnosis	Cytological architecture				
	Microfollicular pattern	Multilayer rosettes	Trabecular pattern	Branching monolayer sheets	Syncytial fragments
FA (n=27)	27 (100)	4 (15)	9 (33)	3 (11)	26 (96)
FC (n=23)	23 (100)	8 (35)	8 (35)	1 (4)	22 (96)
HC (n=1)	1 (100)	0	0	0	0
FVPTC (n=35)	33 (94)	16 (46)	0	12 (34)	30 (86)
PTC (n=12)	10 (83)	5 (42)	0	0	12 (100)
NH (n=17)	17 (100)	1 (6)	0	3 (17)	11 (65)
HT (n=1)	1 (100)	0	0	0	1 (100)
Total (n=116)	112 (97)	34 (29)	17 (15)	19 (16)	101 (87)

Values are presented as number (%).
FA, follicular adenoma; FC, follicular carcinoma; HC, Hurthle cell carcinoma; FVPTC, follicular variant of papillary thyroid carcinoma; PTC, classic papillary thyroid carcinoma; NH, nodular hyperplasia; HT, Hashimoto thyroiditis.
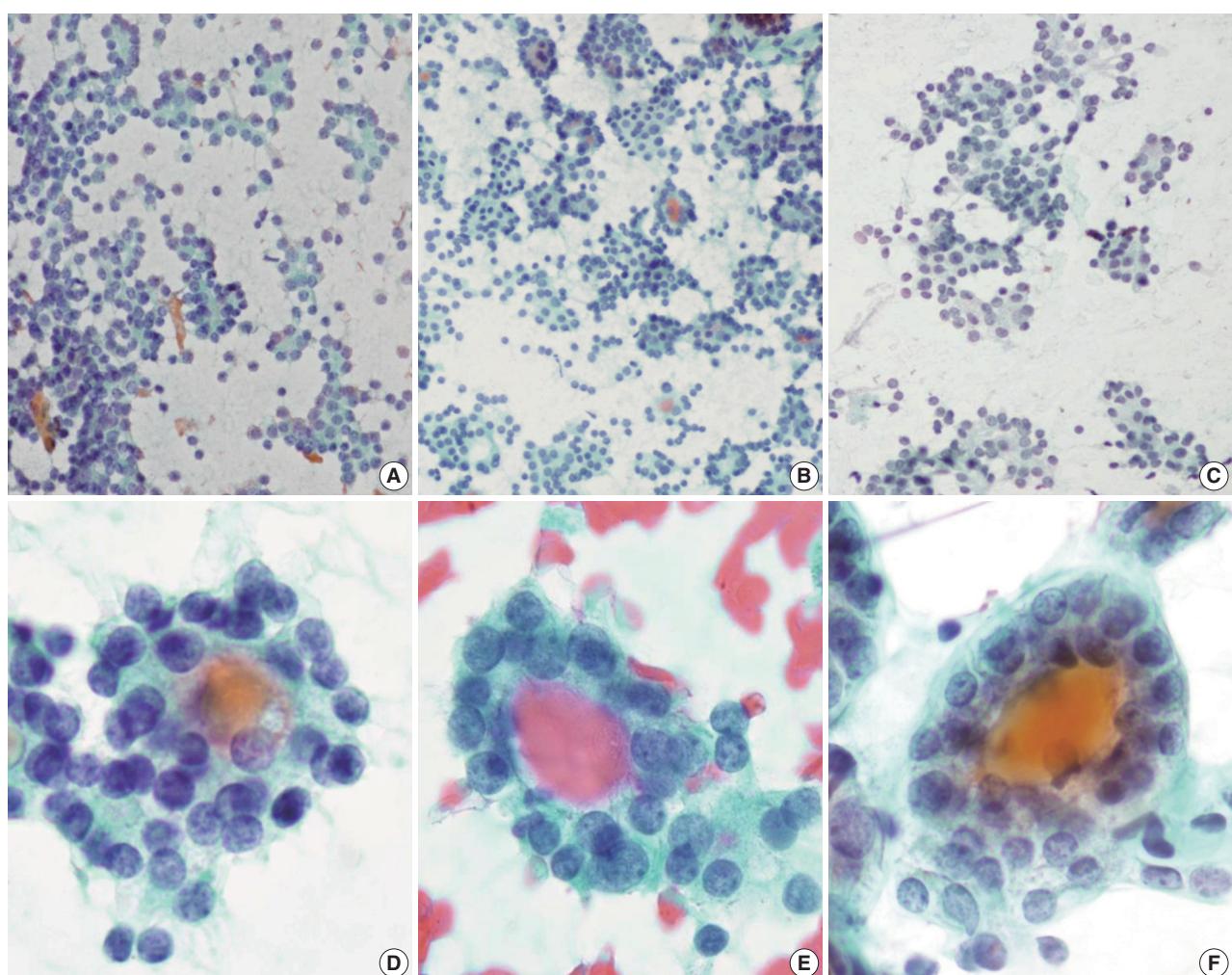

Fig. 2. Microfollicular pattern (A–C) and multilayer rosettes (D–F) are found not only in follicular neoplasm but also in nodular hyperplasia or follicular variant of papillary carcinoma. (A, D) Follicular neoplasm. (B, E) Follicular variant of papillary carcinoma. (C, F) Nodular hyperplasia.

licular pattern was found not only in FNs, but also in PTC/FVPTC and NH. Based on this finding, PTC/FVPTC and NH might be mistaken for FNs through FNAC. The observation rates of the microfollicular pattern in each disease entity are as follows: 100% of FNs cases (FA, FC, and HC), 94% of FVPTC cases (33/35), 83% of PTC cases (10/12), 100% of NH cases, and 100% of HT cases (Table 2, Fig. 2A–C). These results suggest that the presence of microfollicles is not specific to FNs.

The presence of the multilayer rosette, which is thought to be a representative cytological feature of FNs, was limited to 15% of FA cases (4/27) and 35% of FC cases (8/23). Moreover, multilayer rosettes were found more frequently in FVPTC or PTC than in FA or FC (46% of FVPTC cases [16/35] and 42% of PTC cases [5/12]) in this study (Fig. 2D, E). Multilayer rosettes were also found in cases of NH (Fig. 2F). Based on these data, the presence of multilayer rosettes in thyroid FNAC smears
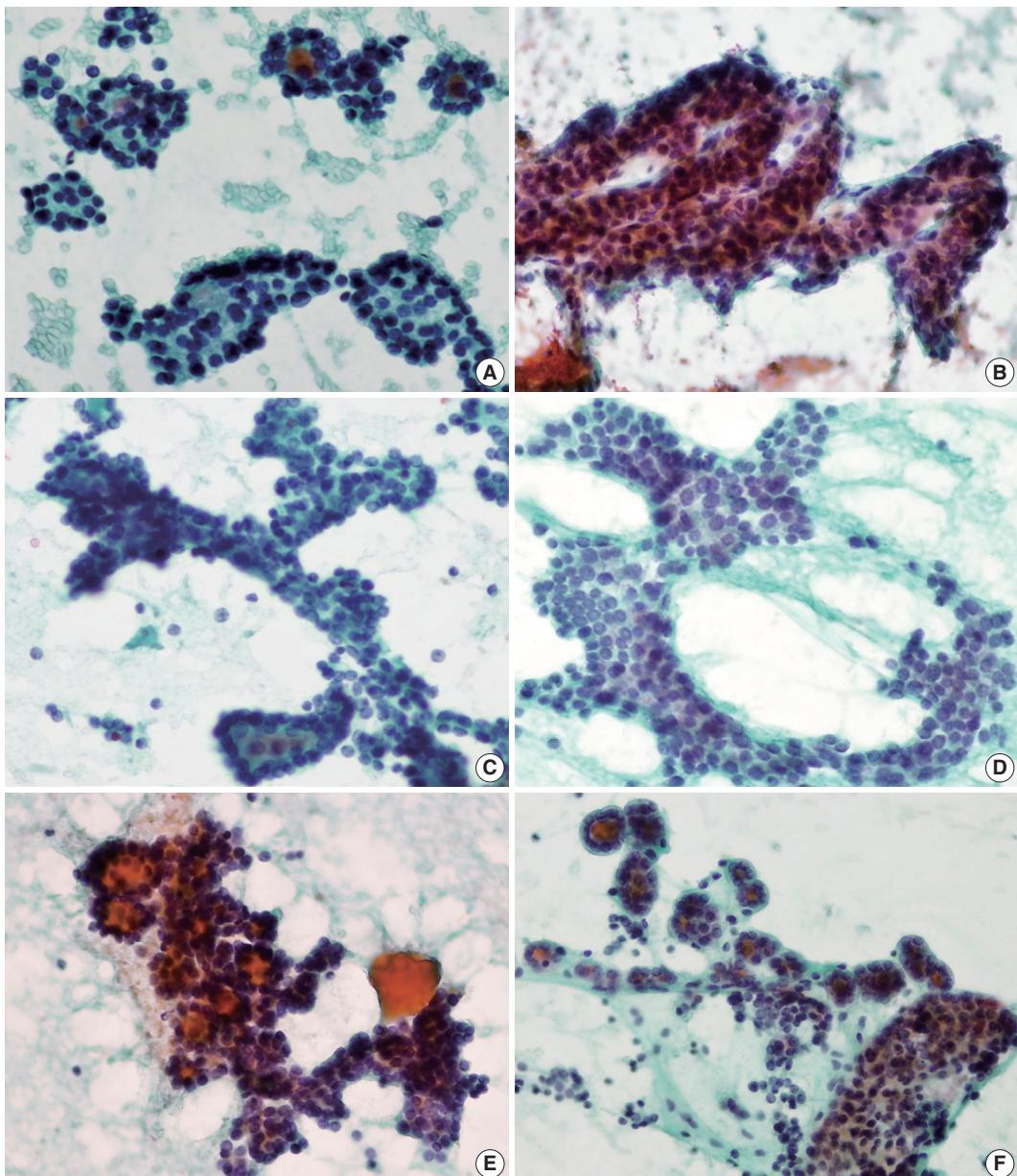
Fig. 3. Different features of cell clusters in follicular neoplasm (FN), follicular variant of papillary thyroid carcinoma (FVPTC), and nodular hyperplasia. (A, B) Trabecular pattern in FN. (C) Branching cell sheets in FN. Branching fragments of FN show ribbon-forming overlapped follicular cells. Note the three-dimensional arrangement of follicular cells of FN (C), which is contrasted with monolayer branching sheet of FVPTC (D). (E) Multilayered cellular ball clusters of FN show branching and trabecular pattern. (F) On the other hand, cell ball clusters in NH show no branching pattern with large non-branching cellular sheet in the colloid background.

should be considered a feature of both FNs and PTC.

Syncytial cellular fragments were common in FNs, FVPTC, PTC, and NH (Table 2). Interestingly, the trabecular pattern was exclusively observed in FNs (33% of FA cases and 35% of FC cases) (Table 2, Fig. 3A–C, E). In FVPTC, branching cellular fragments tended to appear as monolayer sheets; this is in contrast to the cellular overlapping observed in FNs cells (Fig. 3C, D). Branching monolayer sheets were more common in FVPTC (12/35 cases, 34%) than in FNs (FA [3/27 cases, 11%], FC [1/23 cases, 4%], and HC [0/1 case]) (Table 2). Multilayered cellular ball clusters were also observed in NH, but in contrast to FNs, no branching trabecular pattern was seen (Fig. 3E, F).

Cytological nuclear characteristics

Next, we analyzed and compared the nuclear features of each disease (Table 3). Chromatin clearing was observed in 86% of FVPTC cases (30/35) and 75% of PTC cases (9/12). In contrast, much lower frequencies were observed in FNs cases; only 4% of FA cases (1/27), 17% of FC cases (4/23), and 0% of HC cases (0/1) displayed chromatin clearing. The nuclei of FNs and NH were slightly more hyperchromatic than those of PTC or FVPTC, and were found to contain microgranular chromatin (Fig. 4). In addition, nuclear grooves were observed in all histological groups except HT, and their observation rates ranged from 22% to 100% (Table 3, Fig. 4). Intranuclear inclusions, another

Table 3. Cytological nuclear characteristics on the aspirates according to histological diagnosis

Histological diagnosis	Nuclear characteristic			
	Chromatin clearing	Nuclear groove	Intranuclear cytoplasmic inclusion	Anisonucleosis
FA (n=27)	1 (4)	11 (41)	2 (7)	7 (26)
FC (n=23)	4 (17)	5 (22)	3 (13)	20 (87)
HC (n=1)	0	1 (100)	0	0
FVPTC (n=35)	30 (86)	32 (91)	17 (49)	32 (91)
PTC (n=12)	9 (75)	4 (33)	2 (17)	10 (83)
NH (n=17)	0	8 (47)	1 (6)	4 (24)
HT (n=1)	0	0	0	1 (100)

Values are presented as number (%).
FA, follicular adenoma; FC, follicular carcinoma; HC, Hurthle cell carcinoma; FVPTC, follicular variant of papillary thyroid carcinoma; PTC, classic papillary thyroid carcinoma; NH, nodular hyperplasia; HT, Hashimoto thyroiditis.
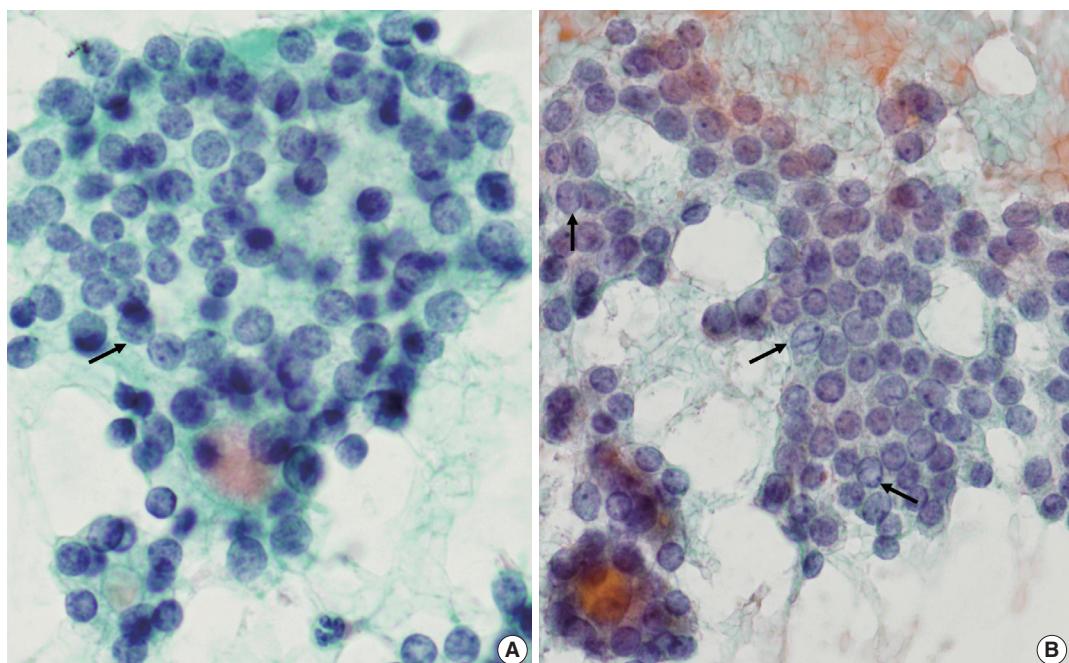
Fig. 4. Nuclear features of follicular neoplasm (FN) and nodular hyperplasia (NH). The nuclear features of FN (A) and NH (B) are similar. Both have round nuclei with microgranular chromatin and nuclear grooves (arrows). However, note the difference that FN (A) shows a three-dimensional arrangement and slightly hyperchromatic nuclei but NH (B). NH has monolayer honeycomb sheets of follicular cells that do not overlap.
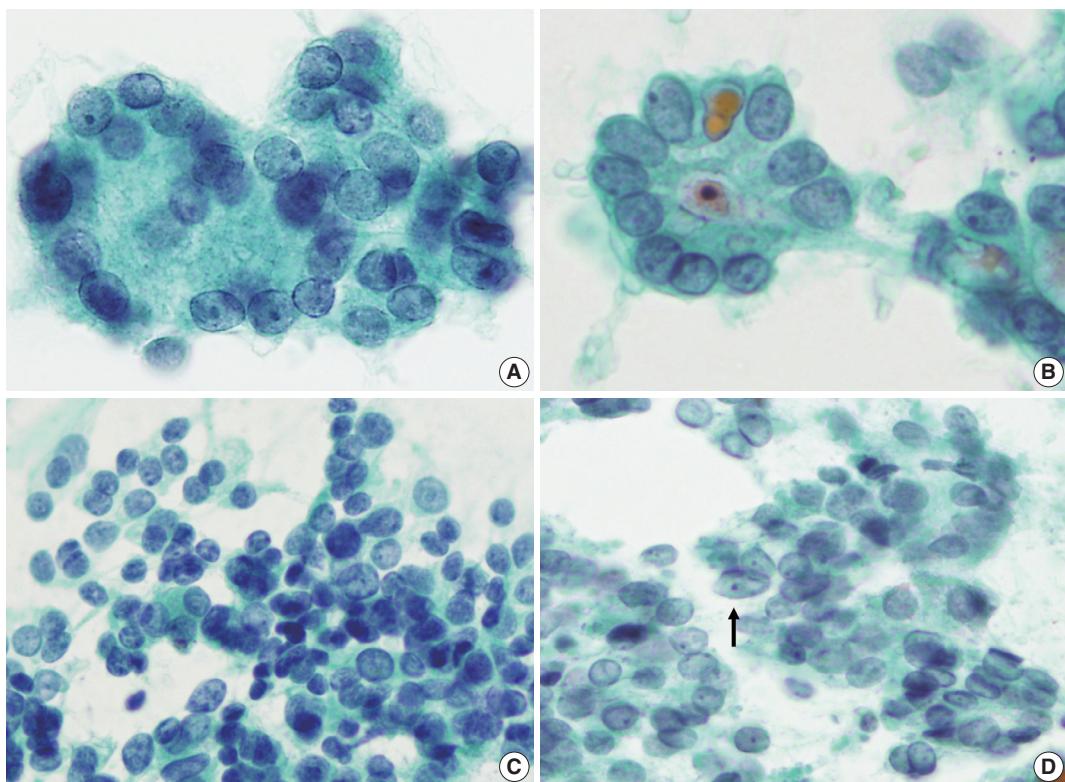
Fig. 5. Nuclear features of follicular neoplasm (FN) and follicular variant of papillary thyroid carcinoma (FVPTC). Please note the subtle difference of nuclear shape and chromatin between follicular carcinoma (A, C) and FVPTC (B, D). (A, C) In FN, nuclei are round to ovoid and chromatin is finely granular rather than ground glass or vesicular pattern. (B, D) Nuclei in FVPTC are slightly elongated (arrow) and have a ground-glass appearing chromatin pattern.

nuclear characteristic of papillary carcinomas, were found in 49% of FVPTC cases (17/35) and 17% of PTC cases (2/12), as well as in 7%, 13%, and 6% of FA, FC, and NH cases, respectively.

Regarding nuclear size variation, FVPTC, PTC, and FC showed anisonucleosis in most cases (91% of FVPTC cases [32/35], 83% of PTC cases [10/12], and 87% of FC cases [20/23]), except for FA and NH, where it was observed less frequently (26% [7/27] and 24% [4/17], respectively). We noticed that, in some cases, the nuclear shape was different for each disease. While approximately half of the FVPTC/PTC cases showed round-to-oval or oval-to-elongated nuclei, most FNs and all NH cases showed round nuclei (Figs. 4, 5). Round-to-oval nuclei were commonly observed in FNs and FVPTC/PTC cases, but elongated nuclei were only observed in FVPTC cases (Table 4, Fig. 5). From these observations, a combination of nuclear shape and nuclear chromatin pattern analysis would be useful for differentiating between FNs and PTC/FVPTC through FNAC.

Statistical significance

Categorizing the cases into FNs and thyroid diseases other

Table 4. Analysis of nuclear shape on the aspirates according to histological diagnosis

Histological diagnosis	Round	Round-to-oval	Oval-to-elongated
FA (n = 27)	19 (70)	8 (30)	0
FC (n = 23)	21 (91)	2 (9)	0
HC (n = 1)	1 (100)	0	0
FVPTC (n = 35)	15 (43)	7 (20)	13 (37)
PTC (n = 12)	9 (75)	3 (25)	0
NH (n = 17)	16 (94)	1 (6)	0
HT (n = 1)	1 (100)	0	0

Values are presented as number (%).
FA, follicular adenoma; FC, follicular carcinoma; HC, Hurthle cell carcinoma; FVPTC, follicular variant of papillary thyroid carcinoma; PTC, classic papillary thyroid carcinoma; NH, nodular hyperplasia; HT, Hashimoto thyroiditis.

than follicular neoplasm (non-FN), the statistical significance of various variables was examined. For the cytological architecture, trabecular pattern (p < .001) and branching monolayer sheets (p = .028) were statistically associated with histological diagnosis FN or non-FN, respectively. On the other hand, there was no significant correlation between histological diagnosis and other cytological architectures such as microfollicular pattern, multilayer rosettes and syncytial fragments (Table 5). Regarding nuclear fea-

Table 5. Differentiation between FN and non-FN

	FN (n=51)	Non-FN (n=65)	χ^2	p-value
Cytological architecture				
Microfollicular pattern				.071
Present	51 (100)	61 (94)	3.251	
Absent	0	4 (6)		
Multilayer rosettes				.226
Present	12 (24)	22 (34)	1.468	
Absent	39 (76)	43 (66)		
Trabecular pattern				<.001
Present	17 (33)	0	22.037	
Absent	34 (67)	65 (100)		
Branching monolayer sheets				
Present	4 (8)	15 (23)	4.842	.028
Absent	47 (92)	50 (77)		
Syncytial fragments				
Present	48 (94)	54 (83)	3.283	.070
Absent	3 (6)	11 (17)		
Nuclear characteristics				
Chromatin clearing				<.001
Present	5 (10)	39 (60)	30.584	
Absent	46 (90)	26 (40)		
Nuclear groove				<.001
Present	17 (33)	44 (68)	13.531	
Absent	34 (67)	21 (32)		
Intranuclear cytoplasmic inclusion				
Present	5 (10)	20 (32)	7.430	.006
Absent	46 (90)	45 (68)		
Anisonucleosis				.048
Present	27 (53)	46 (71)	3.894	
Absent	24 (47)	19 (29)		

Values are presented as number (%).
FN, follicular neoplasm; Non-FN, disease other than FN.

tures, chromatin clearing (p < .001), nuclear groove (p < .001), intranuclear cytoplasmic inclusion (p = .006) and anisonucleosis (p = .048) were statistically associated with non-FN.

Cytological architecture and nuclear characteristics of subtypes of FVPTC

We subdivided FVPTC cases into three subtypes: NIFTP, invasive EFVPTC, and infiltrative FVPTC. Of the 35 FVPTCs, NIFTP accounted for 20 cases (57%), invasive EFVPTC for 12 cases (34%), and infiltrative FVPTC for three cases (9%). As shown in Table 6, there were no significant differences between the three subtypes in the cytological architecture and nuclear features, but the reliability is limited due to the small number of cases.

DISCUSSION

For preoperative evaluation of thyroid nodules, FNAC is a valuable and reliable method for the majority of thyroid lesions. However, FNs and similar lesions such as FVPTC or cellular NH are difficult to differentiate from each other using FNAC.[3] For this reason, the Bethesda system proposed a flexible framework for reporting thyroid cytopathology, and the general category IV "FN or suspicious for a FN" was provided for follicular adenomas and cytomorphologically similar lesions.[3] It is convenient for preoperative cytological diagnosis and can lead to a definitive diagnostic procedure, usually lobectomy, to identify carcinoma. However, the general category IV includes not only FA and FC but also hyperplastic nodules and FVPTC,[3] therefore more efforts needs to be made to achieve a precise diagnosis. In the current study, we investigated 116 cases initially diagnosed as Bethesda diagnostic category IV "FN or suspicious for FN" using FNAC, and determined the cytological features that can distinguish FNs from similar lesions. Based on our observations, we suggest that trabecular patterns and cellular overlapping of the branching sheets are the most clearly characteristic cytological features of FNs, in addition to round nuclei with a granular chromatin pattern.

In this study, the FNAC-histology concordance rate for FNs was only 44%, and the most common erroneous diagnosis was FVPTC (35/116 cases; 30%), followed by NH (17/116 cases, 15%) and classic PTC (12/116 cases, 10%). As the current study is a retrospective study of cases diagnosed by several pathologists, it has limitations of interobserver variations.

Many studies have also revealed discrepancies between the final histological and initial cytological diagnoses for cases diagnosed as FNs using FNAC, showing a concordance rate ranging from 32% to 62% (Table 7).[6-10] Similar to our results, other studies reported that NH and FVPTC/PTC were most often mistaken for FNs by FNAC (Table 7).[6-10] As FVPTC mimics FNs cytologically and architecturally, even in histological sections, it is commonly confused with FNs by FNAC.[11-13] It might be because the nuclear changes in FVPTC can be more subtle than classic PTC.[11,12,14] According to Bizzarro *et al.*,[12] 70% of noninvasive FVPTC cases demonstrated a nuclear size of < 20 μm, and rarely exhibited grooves compared to invasive FVPTCs. To overcome the limitations of morphology, the application of ancillary tests such as immunohistochemistry or molecular studies have been encouraged.[13] However, these are not always available on aspirates; therefore, the cytomorphological approach is still valuable.

Recently, there has been a paradigm shift on the clinical sig-

nificance of noninvasive EFVPTC, and nomenclature for this tumor was revised as "noninvasive follicular thyroid neoplasms with papillary-like nuclear features (NIFTP)."[4] It is because that noninvasive EFVPTC shows indolent behavior with a very low risk of adverse outcome and therefore should not be named carcinoma.[4] By adopting this new terminology, patients with NIFTP only require lobectomy and can avoid unnecessary overtreatment such as total thyroidectomy and radioactive iodine therapy.[4,15]

Table 6. Cytological architecture and nuclear characteristics of subtypes of FVPTC

	NIFTP (n=20)	Invasive EFVPTC (n=12)	Infiltrative FVPTC (n=3)	p-value for NIFPT vs infiltrative FVPTC	p-value for NIFPT vs infiltrative	p-value for invasive EFVPTC vs infiltrative FVPTC
Microfollicular pattern				.619	.104	.038
Present	19 (95)	12 (100)	2 (67)			
Absent	1 (5)	0 (0)	1 (33)			
Multilayer rosettes				.305	.385	.605
Present	8 (40)	6 (50)	2 (67)			
Absent	12 (60)	6 (50)	1 (33)			
Trabecular pattern				-	-	-
Present	0	0	0			
Absent	20 (100)	12 (100)	3 (100)			
Branching monolayer sheets				.039	.214	.292
Present	6 (30)	4 (33)	2 (67)			
Absent	14 (70)	8 (67)	1 (33)			
Syncytial fragments				.016	.472	.448
Present	17 (85)	10 (83)	3 (100)			
Absent	3 (15)	2 (17)	0			
Chromatin clearing				.059	.328	-
Present	15 (75)	12 (100)	3 (100)			
Absent	5 (25)	0	0			
Nuclear groove				.876	.567	.605
Present	18 (90)	11 (92)	3 (100)			
Absent	2 (10)	1 (8)	0			
Intranuclear cytoplasmic inclusion				.465	.484	.792
Present	11 (50)	5 (42)	1 (33)			
Absent	9 (45)	7 (58)	2 (67)			
Anisonucleosis				.876	.567	.605
Present	18 (90)	11 (92)	3 (100)			
Absent	2 (10)	1 (8)	0			

Values are presented as number (%).
FVPTC, follicular variant of papillary carcinoma; NIFTP, noninvasive follicular thyroid neoplasm with papillary-like nuclear feature; EFVPTC, encapsulated follicular variant of papillary carcinoma.

Table 7. Review of the literature of cytological-histological correlations in cases of diagnosed as follicular neoplasm in fine needle aspiration cytology

Histological diagnosis	Greaves *et al.* (2000)[6]	Deveci *et al.* (2006)[7]	Wu *et al.* (2012)[8]	Faquin (2009)[9]	Yang *et al.* (2007)[10]
FA	25/96 (26)	145/339 (43)	35/65 (54)	88/251 (35)	109/326 (33)
FC	6/96 (6)	21/339 (6)	5/65 (8)	22/251 (9)	16/326 (5)
HA	NA	NA	NA	NA	48/326 (15)
HC	NA	9/339 (3)	NA	NA	13/326 (4)
FVPTC	6/96 (6)	36/339 (11)	7/65 (11)	40/251 (16)	71/326 (22)
PTC	16/96 (17)	8/339 (2)	1/65 (1.5)	NA	NA
NH	36/96 (38)	120/339 (35)	16/65 (24)	100/251 (40)	53/326 (16)
HT	6/96 (6)	NA	NA	NA	11/326 (3)
Other malignancy	1/96 (1)	NA	NA	1/251 (0.3)	5/326 (2)

Values are presented as number (%).
FA, follicular adenoma; FC, follicular carcinoma; HA, Hurthle cell adenoma; NA, not applicable; HC, Hurthle cell carcinoma; FVPTC, follicular variant of papillary thyroid carcinoma; PTC, classic papillary thyroid carcinoma; NH, nodular hyperplasia; HT, Hashimoto thyroiditis.

For the cytological diagnosis regarding a new entity, NIFTP, more experience and consensus about NIFTP needs to be achieved for practical application.[15] In case of NIFTP, there would be no clinical problem even if it is not distinguished from FA in the preoperative diagnosis, because both will be treated with lobectomy. However, in this study, there were no significant differences on cytological findings between NIFTP and invasive FVPTC. Similar results have been recently reported on cytomorphological distinction between non-invasive and invasive EFVPTC.[16] In this context, it is imperative to make efforts to better differentiate FVPTC from FNs by FNAC because invasive EFVPTC and NIFTP cannot be reliably differentiated preoperatively.

As we selected the cases diagnosed as or suspected to be FNs by FNAC for the current study, all cases included in this study had moderate to high cellularity, frequently showing a well-known microfollicular pattern.[3] Usually, most PTCs contain some follicular structures in addition to conventional papillary configurations;[17] therefore, it is not surprising that microfollicular patterns were identified in the aspirates of PTC and FVPTC. Furthermore, a rosette appearance with small droplets of central dense colloids was also observed not only in FNs, but also in FVPTC/PTC or NH in this study. Thus, microfollicular patterns and multilayer rosettes, which are generally accepted to be cytological characteristics of FNs, do not seem to be important in distinguishing FNs from mimicking lesions. Interestingly, the trabecular pattern was only found in the aspirates of FNs, although the positive rates were limited to 33% and 35% of FA and FC cases, respectively. The trabecular pattern differs from the microfollicular pattern and multilayer rosettes in that it has a branching pattern. FNs have a three-dimensional multilayered branching structure, which could be distinguished from the monolayer appearance of the branching sheets of FVPTC (Fig. 3). When distinguishing between NH and FNs, some multilayered cellular ball clusters in NH differed from the trabecular pattern of FNs in that no branching pattern was found. Therefore, the trabecular pattern was identified as a specific feature for the differential diagnosis of FNs from mimicking lesions. Regarding cytological architecture, microfollicular patterns should no longer be considered important in the cytological diagnosis of FNs. Rather, trabecular clusters and multilayered patterns of branching cellular groups are more suitable for the proper diagnosis of FNs.

Based on our observations, the nuclear chromatin pattern and nuclear shape are considered to be important nuclear features for differential diagnosis. Because nuclear grooves were observed in NH or FNs as well as PTC, and because intranuclear inclusions were visible in less than half of the FVPTC/PTC cases in this series, there was a limit to this method of distinction. On the other hand, the nuclear chromatin of PTC/FVPTC showed ground-glass or vesicular patterns, whereas that of FNs was finely granular and NH showed dense chromatin. Our results are supported by a recent report on the analysis of nuclear characteristics using nuclear morphometry and textural analysis by Deka *et al*.[18] They reported that PTC cases showed the largest perimeter and elongation factor and heterogeneous chromatin distribution compared to FNs and NH. However, it is not easy to distinguish the nuclear chromatin pattern in each case, because FVPTC lacks the unequivocal nuclear features of PTC; this may prevent a definitive diagnosis.[19-23] In addition, slightly elongated nuclei were found in FVPTC/PTC, but not in FNs or NH, suggesting that the presence of elongated nuclei in the aspirates would be helpful to differentiate PTC/FVPTC from FNs or NH. Thus, the presence of slightly elongated nuclei with chromatin clearing favors FVPTC/PTC over FNs.

In NH, follicular cells may form large monolayers that fold over on themselves. However, they are contrasted that FNs have three-dimensional arrangement and the branching patterns. The large cell groups of NH did not exhibit branching patterns unlike FNs.[10] Although the nuclear features were similar to those of FNs, as they showed granular chromatin patterns and occasional nuclear grooves, the nuclei of NH cells were slightly more hyperchromatic than those of FNs cells. Hence, we suggest that cytoarchitectural patterns of cell groups should be the main focus of differential diagnosis between FNs and NH.

In conclusion, the findings of the current study suggest that a combination of architectural features and nuclear characteristics may improve the ability of cytopathologists to differentiate FNs from similar thyroid lesions such as FVPTC and NH. Based on our data, we propose that pathologists should keep in mind that the most well-known cytological feature of FNs—the microfollicular pattern with high cellularity—is not a reliable factor in obtaining a definite diagnosis. Rather, the trabecular pattern and cell clusters with cellular overlapping should be examined, as they seem to be more specific to FNs. Additionally, if slightly elongated follicular cells and nuclear clearing are found, even in a small proportion of the cells, pathologists must raise the possibility of FVPTC/PTC.

Conflicts of Interest

No potential conflict of interest relevant to this article was reported.

REFERENCES

1. Hamberger B, Gharib H, Melton LJ 3rd, Goellner JR, Zinsmeister AR. Fine-needle aspiration biopsy of thyroid nodules. Impact on thyroid practice and cost of care. Am J Med 1982; 73: 381-4.

2. Yassa L, Cibas ES, Benson CB, *et al*. Long-term assessment of a multidisciplinary approach to thyroid nodule diagnostic evaluation. Cancer 2007; 111: 508-16.

3. Cibas ES, Ali SZ. The Bethesda System for Reporting Thyroid Cytopathology. Thyroid 2009; 19: 1159-65.

4. Nikiforov YE, Seethala RR, Tallini G, *et al*. Nomenclature revision for encapsulated follicular variant of papillary thyroid carcinoma: a paradigm shift to reduce overtreatment of indolent tumors. JAMA Oncol 2016; 2: 1023-9.

5. Liu J, Singh B, Tallini G, *et al*. Follicular variant of papillary thyroid carcinoma: a clinicopathologic study of a problematic entity. Cancer 2006; 107: 1255-64.

6. Greaves TS, Olvera M, Florentine BD, *et al*. Follicular lesions of thyroid: a 5-year fine-needle aspiration experience. Cancer 2000; 90: 335-41.

7. Deveci MS, Deveci G, LiVolsi VA, Baloch ZW. Fine-needle aspiration of follicular lesions of the thyroid: diagnosis and follow-up. Cytojournal 2006; 3: 9.

8. Wu HH, Rose C, Elsheikh TM. The Bethesda system for reporting thyroid cytopathology: An experience of 1,382 cases in a community practice setting with the implication for risk of neoplasm and risk of malignancy. Diagn Cytopathol 2012; 40: 399-403.

9. Faquin WC. Diagnosis and reporting of follicular-patterned thyroid lesions by fine needle aspiration. Head Neck Pathol 2009; 3: 82-5.

10. Yang J, Schnadig V, Logrono R, Wasserman PG. Fine-needle aspiration of thyroid nodules: a study of 4703 patients with histologic and clinical correlations. Cancer 2007; 111: 306-15.

11. Brandler TC, Zhou F, Liu CZ, *et al*. Can noninvasive follicular thyroid neoplasm with papillary-like nuclear features be distinguished from classic papillary thyroid carcinoma and follicular adenomas by fine-needle aspiration? Cancer Cytopathol 2017; 125: 378-88.

12. Bizzarro T, Martini M, Capodimonti S, *et al*. Young investigator challenge: the morphologic analysis of noninvasive follicular thyroid neoplasm with papillary-like nuclear features on liquid-based cytology: Some insights into their identification. Cancer Cytopathol 2016; 124: 699-710.

13. Rossi ED, Bizzarro T, Martini M, Larocca LM, Schmitt F, Vielh P. Cytopathology of follicular cell nodules. Adv Anat Pathol 2017; 24: 45-55.

14. Clark DP, Faquin WC. Thyroid cytopathology. New York: Springer, 2005; 131.

15. Krane JF, Alexander EK, Cibas ES, Barletta JA. Coming to terms with NIFTP: a provisional approach for cytologists. Cancer Cytopathol 2016; 124: 767-72.

16. Maletta F, Massa F, Torregrossa L, *et al*. Cytological features of "noninvasive follicular thyroid neoplasm with papillary-like nuclear features" and their correlation with tumor histology. Hum Pathol 2016; 54: 134-42.

17. Yoo C, Choi HJ, Im S, *et al*. Fine needle aspiration cytology of thyroid follicular neoplasm: cytohistologic correlation and accuracy. Korean J Pathol 2013; 47: 61-6.

18. Deka L, Gupta S, Gupta R, Gupta K, Kaur CJ, Singh SS. Nuclear morphometry and texture analysis on cytological smears of thyroid neoplasms: a study of 50 cases. Malays J Pathol 2017; 39: 33-7.

19. Ho AS, Sarti EE, Jain KS, *et al*. Malignancy rate in thyroid nodules classified as Bethesda category III (AUS/FLUS). Thyroid 2014; 24: 832-9.

20. Song JY, Chu YC, Kim L, Park IS, Han JY, Kim JM. Reclassifying formerly indeterminate thyroid FNAs using the Bethesda system reduces the number of inconclusive cases. Acta Cytol 2012; 56: 122-9.

21. Shi Y, Ding X, Klein M, *et al*. Thyroid fine-needle aspiration with atypia of undetermined significance: a necessary or optional category? Cancer 2009; 117: 298-304.

22. Horne MJ, Chhieng DC, Theoharis C, *et al*. Thyroid follicular lesion of undetermined significance: Evaluation of the risk of malignancy using the two-tier sub-classification. Diagn Cytopathol 2012; 40: 410-5.

23. Dincer N, Balci S, Yazgan A, *et al*. Follow-up of atypia and follicular lesions of undetermined significance in thyroid fine needle aspiration cytology. Cytopathology 2013; 24: 385-90.

■ CASE STUDY ■

Combined Adenosquamous and Large Cell Neuroendocrine Carcinoma of the Gallbladder

Jiyoon Jung · Yang-Seok Chae
Chul Hwan Kim · Youngseok Lee
Jeong Hyeon Lee · Dong-Sik Kim[1]
Young-Dong Yu[1] · Joo Young Kim

Departments of Pathology and [1]Surgery, Korea
University Anam Hospital, Korea University
College of Medicine, Seoul, Korea

Corresponding Author
Joo Young Kim, MD, PhD
Department of Pathology, Korea University Anam
Hospital, Korea University College of Medicine,
73 Inchon-ro, Seongbuk-gu, Seoul 02841, Korea
Tel: +82-2-920-6268
Fax: +82-2-920-6576
E-mail: lepetit80@hanmail.net

Large cell neuroendocrine carcinoma (LCNEC) of the gallbladder is extremely rare and usually combined with other type of malignancy, mostly adenocarcinoma. We report an unusual case of combined adenosquamous carcinoma and LCNEC of the gallbladder in a 54-year-old woman. A radical cholecystectomy specimen revealed a 4.3×4.0 cm polypoid mass in the fundus with infiltration of adjacent liver parenchyma. Microscopically, the tumor consisted of two distinct components. Adenosquamous carcinoma was predominant and abrupt transition from adenocarcinoma to squamous cell carcinoma was observed. LCNEC showed round cells with large, vesicular nuclei, abundant mitotic figures, and occasional pseudorosette formation. The patient received adjuvant chemotherapy. However, multiple liver metastases were identified at 3-month follow-up. Metastatic nodules were composed of LCNEC and squamous cell carcinoma components. Detecting LCNEC component is important in gallbladder cancer, because the tumor may require a different chemotherapy regimen and show early metastasis and poor prognosis.

Key Words: Carcinoma, adenosquamous; Large cell neuroendocrine carcinoma; Gallbladder; Prognosis

Large cell neuroendocrine carcinoma (LCNEC) of the gallbladder is an extremely rare malignancy, comprising 2% of all gallbladder cancers.[1] The prognosis of this tumor is poor and early metastasis is common.[2] To date, 18 cases of gallbladder LCNEC have been reported.[3,4] LCNEC of the gallbladder is usually combined with other types of malignancies, mostly adenocarcinoma. We present an unusual case of combined adenosquamous carcinoma (ASC) and LCNEC of the gallbladder.

CASE REPORT

A 54-year-old woman presented with a 4-month history of intermittent epigastric pain. Laboratory tests revealed elevated serum levels of alkaline phosphatase and gamma-glutamyltransferase, up to 161 IU/L (reference range, 30 to 120 IU/L) and 81 IU/L (reference range, 9 to 64 IU/L), respectively. The levels of other liver enzymes including aspartate aminotransferase, alanine aminotransferase, as well as total bilirubin and direct bilirubin levels, were within normal range. Serum carbohydrate-associated antigen (CA19-9) was 151.4 IU/mL (normal < 37 IU/mL), and

α-fetoprotein and carcinoembryonic antigen were within normal range. Abdominal computed tomography showed a 6.9 cm mass in the gallbladder fundus, with direct invasion of the adjacent liver (Fig. 1A). Biopsy of the liver mass showed poorly differentiated carcinoma with extensive squamous differentiation.

Radical cholecystectomy was performed and gross examination revealed a 4.3×4.0 cm polypoid mass in the gallbladder fundus with infiltration of the adjacent liver parenchyma and multiple yellowish gallstones (Fig. 1B, C). An incidentally found 0.4-cm-sized nodule was also noted in the liver.

Microscopically, the tumor comprised two distinct components: ASC and LCNEC. The adenocarcinoma (AC) component of the ASC consisted of variable sized glands, lined by atypical columnar epithelium. The squamous cell carcinoma (SCC) component showed atypical stratified squamous epithelium with occasional keratin pearls. An abrupt transition from AC to SCC was observed (Fig. 2A, B). In addition, there was an area of LCNEC consisting of round cells with large, vesicular nuclei and frequent mitotic figures (33/10 high-power fields). Occasional rosette formation was found. The tumor cells were arranged in trabecular, palisad-

ing, or solid patterns, and mixed with an AC component in the periphery (Fig. 2C, D). These cells showed diffuse and strong positivity for synaptophysin and chromogranin, and focal positivity for CD56 immunohistochemistry (Fig. 3A–C). The Ki-67 proliferating labeling index was 25% (Fig. 3D). The tumor was largely composed of ASC, and the proportion of the SCC component was approximately 80%, whereas the area of LCNEC was small, constituting approximately 10% of the entire tumor. The

gallbladder wall was mainly composed of AC components, while the proportion of SCC and LCNEC components increased substantially as the tumor invaded into the liver parenchyma. Multifocal lymphovascular invasion by SCC and perineural tumor invasion by LCNEC were identified. Only a few foci of lymphovascular invasion were observed with an AC component. Chronic cholecystitis with intestinal metaplasia were identified in the remaining mucosa. No metastasis was present in the seven regional

Fig. 1. Imaging and gross findings. (A) On abdominal computed tomography, the tumor of the gallbladder shows direct invasion of the adjacent liver. (B) On opening the gallbladder, a fungating mass is observed in the fundus. (C) The cut surface shows a relatively well-circumscribed, yellowish fibrotic mass, with hemorrhage and necrosis, invading the liver parenchyma.
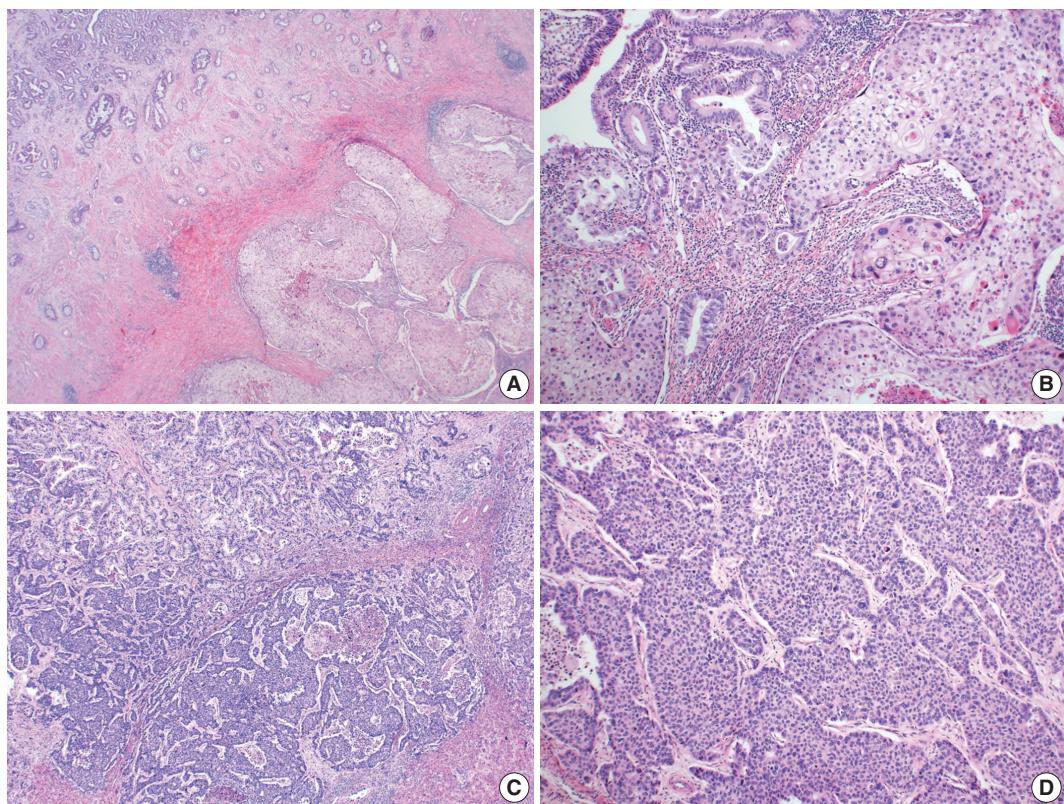

Fig. 2. Microscopic findings. (A, B) Adenosquamous carcinoma component consisted of variable-sized glands lined by atypical columnar epithelium (left) and atypical stratified squamous epithelium (right). (C) Neuroendocrine carcinoma component, transition from adenocarcinomatous component (left) and composed of large cells arranged in solid sheets (right). (D) The neuroendocrine component shows solid and pseudorosette patterns.
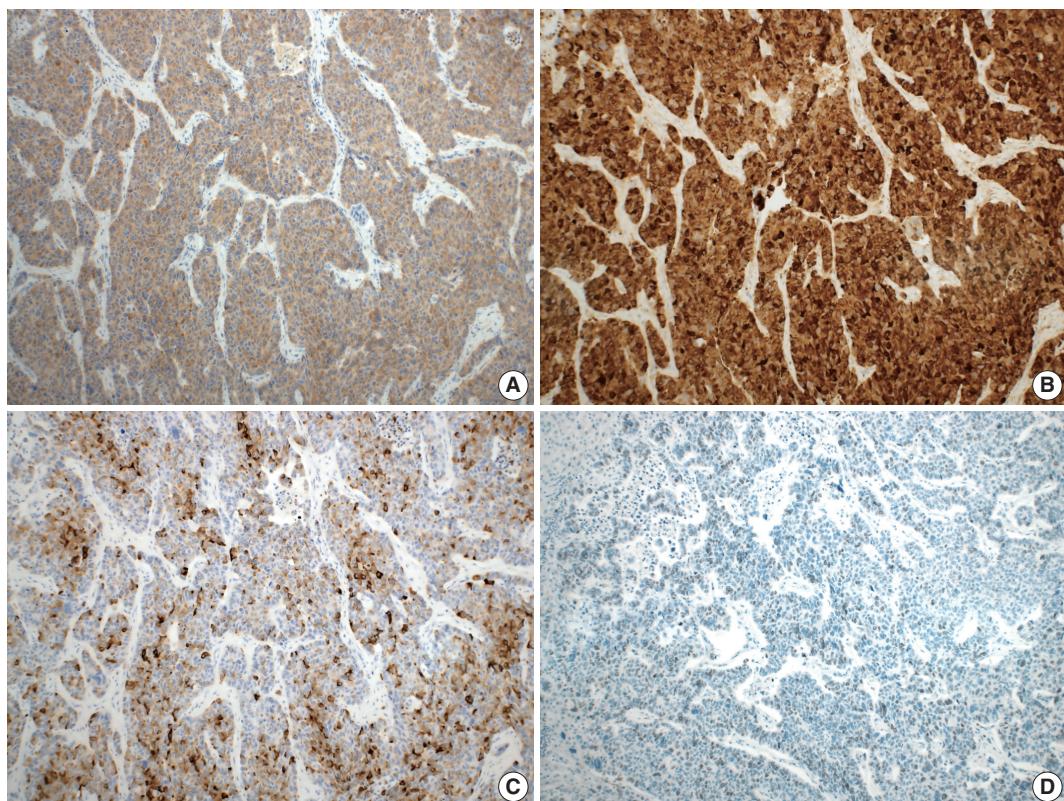
Fig. 3. Immunohistochemical findings. Large cell neuroendocrine carcinoma component was diffusely positive for synaptophysin (A), and chromogranin (B), and focal positive for CD56 (C). (D) The Ki-67 proliferating index was up to 25%.

lymph nodes. The metastatic nodule in the liver was composed purely of an LCNEC component. The final diagnosis of the gallbladder was confirmed as combined ASC and LCNEC. The patient received adjuvant chemotherapy post-operatively. However, magnetic resonance imaging revealed two liver metastases at the 3-month follow-up. Wedge resection of the liver was performed on the metastatic nodules, measuring 4.7 cm and 3.4 cm. Microscopically, the metastatic nodules were composed purely of an SCC component with no AC or LCNEC components. The patient was treated with chemotherapy (gemcitabine, cisplatin, and epirubicin) and radiotherapy after the operation, and died after 13 months from the initial diagnosis.

This study was approved by the Institutional Review Board of Korea University Anam Hospital, and informed consent was waived (ED17132).

DISCUSSION

The majority of carcinomas in the gallbladder are ACs, comprising up to 88%. Other carcinomas include ASC (5%), neuroendocrine carcinoma (NEC) (2%), SCC (1%), and undifferentiated carci-

noma (< 1%).[5] Identifying the exact histologic component of the tumor is important because the histologic type is associated with patient prognosis in gallbladder cancers. ACs have a relatively favorable prognosis, whereas tumors with squamous or neuroendocrine differentiation have a poor outcome (mean survival time, 50 vs 23 or 10 months, respectively).[2,6] LCNEC has been known to exhibit aggressive behavior and early metastasis.[4] Among the previously reported LCNEC cases, 53% had directly invaded the liver at the time of diagnosis, and 47% had been identified with locoregional or distant metastases involving bone, liver or lymph nodes.[3] In this case, the tumor showed direct invasion of the liver parenchyma at the time of initial diagnosis and additional multiple liver metastases afterwards, demonstrating aggressive behavior.

According to the recent 2010 World Health Organization classification, neoplasms, morphologically composed of both glandular epithelial cells and neuroendocrine cells with over 30% of each component are described as mixed adenoneuroendocrine carcinoma (MANEC).[7] The present case was predominantly composed of SCC (about 80%) and the amount of AC or NEC component was not enough for the criteria of MANEC.

The histogenesis of NEC in the gallbladder is still not clear, because neuroendocrine cells are not normally present in the gallbladder except for a few cells in the neck region. It has been postulated that they may arise from pluripotent precursor cells.[8] However, the pathogenesis of differentiation from stem cells to neuroendocrine cells remains unclear. Another hypothesis for the development of NEC of the gallbladder is through metaplastic change.[9] Intestinal or gastric metaplasia occurs as a result of cholelithiasis and chronic inflammation.[10] Argentaffin cells have been identified in the metaplastic mucosa and these cells have been suggested as precursors of neuroendocrine tumor in the gallbladder.[11] Almost all previously reported gallbladder LCNECs described coexisting cholelithiasis with chronic cholecystitis.[5] In this case, chronic cholecystitis with intestinal metaplasia associated with cholelithiasis was identified, which suggested a precursor lesion of the NEC.

It is noteworthy that metastatic nodules show two different histologic types. The incidentally identified, synchronous metastatic hepatic nodule was totally composed of an LCNEC component, whereas the metachronous metastatic nodules were composed entirely of an SCC component. The metastatic potential is different in each type of cancer cells.[12] The SCC component has higher proliferative activity than the AC component and more frequently observed in the invasive front of the tumor and in lymphovascular and perineural invasion in the gallbladder ASC.[13] This might contribute to the metastatic potential and tumor progression in ASC.[13] In the present case, the SCC component was frequently observed in lymphovascular invasion and caused multiple pure SCC metastatic nodules. Additionally, LCNEC has higher risk of metastasis through lymphatic invasion, compared to the AC.[14] Acosta and Wiley[15] reported that the majority of lymph node metastases shows only NEC components in primary MANECs of the biliary tree. This case is consistent with previous studies in that the metastatic nodules were composed of either SCC or NEC, without an AC component, and this might contribute to the metastatic potential and poor prognosis of ASC and NEC of the gallbladder.

There are also differences in chemotherapeutic agents between conventional AC and combined tumor of the gallbladder. Conventional AC is usually treated with gemcitabine and cisplantin, while combined ASC or NEC is treated with FOLFOX (leucovorin, fluorouracil, and oxaliplatin) or etoposide.[4,16]

This is an unusual case of LCNEC combined with ASC. The histologic types of the gallbladder carcinoma might contribute to the metastatic potential and poor prognosis. To detect an LCNEC or ASC component is important because the tumor may require

a different chemotherapy regimen and show early metastasis with poor prognosis.

Conflicts of Interest

No potential conflict of interest relevant to this article was reported.

REFERENCES

1. National Cancer Institute. SEER data, 1973-2005 [Internet]. Rockville: National Cancer Institute, 2008 [cited 2017 Sep 1]. Available from: http://seer.cancer.gov/.

2. Henson DE, Albores-Saavedra J, Corle D. Carcinoma of the gallbladder: histologic types, stage of disease, grade, and survival rates. Cancer 1992; 70: 1493-7.

3. Liu W, Wang L, He XD, Feng C, Chang XY, Lu ZH. Mixed large cell neuroendocrine carcinoma and adenocarcinoma of the gallbladder: a case report and brief review of the literature. World J Surg Oncol 2015; 13: 114.

4. Buscemi S, Orlando E, Damiano G, *et al*. "Pure" large cell neuroendocrine carcinoma of the gallbladder: report of a case and review of the literature. Int J Surg 2016; 28 Suppl 1: S128-32.

5. Eltawil KM, Gustafsson BI, Kidd M, Modlin IM. Neuroendocrine tumors of the gallbladder: an evaluation and reassessment of management strategy. J Clin Gastroenterol 2010; 44: 687-95.

6. Alpuerto AC, Mora ME, Robitsek RJ, Schubl SD. Primary pure squamous cell carcinoma of the gallbladder locally invading the liver, duodenum, and stomach: a case report and literature review. Case Rep Surg 2017; 2017: 2534029.

7. Bosman FT, Carneiro F, Hruban RH, Theise ND. WHO classification of tumours of the digestive system. 4th ed. Lyon: IARC Press, 2010; 274-6.

8. Noske A, Pahl S. Combined adenosquamous and large-cell neuroendocrine carcinoma of the gallbladder. Virchows Arch 2006; 449: 135-6.

9. Kanthan R, Senger JL, Ahmed S, Kanthan SC. Gallbladder cancer in the 21st century. J Oncol 2015; 2015: 967472.

10. Albores-Saavedra J, Nadji M, Henson DE, Angeles-Angeles A. Enteroendocrine cell differentiation in carcinomas of the gallbladder and mucinous cystadenocarcinomas of the pancreas. Pathol Res Pract 1988; 183: 169-75.

11. Christie AC. Three cases illustrating the presence of argentaffin (kultschitzky) cells in the human gall-bladder. J Clin Pathol 1954; 7: 318-21.

12. Hart IR, Fidler IJ. The implications of tumor heterogeneity for studies

on the biology of cancer metastasis. Biochim Biophys Acta 1981; 651: 37-50.

13. Hoshimoto S, Hoshi S, Hishinuma S, *et al*. Adenosquamous carcinoma in the biliary tract: association of the proliferative ability of the squamous component with its proportion and tumor progression. Scand J Gastroenterol 2017; 52: 425-30.

14. Chen C, Wang L, Liu X, Zhang G, Zhao Y, Geng Z. Gallbladder neuroendocrine carcinoma: report of 10 cases and comparision of

clinicopathologic features with gallbladder adenocarcinoma. Int J Clin Exp Pathol 2015; 8: 8218-26.

15. Acosta AM, Wiley EL. Primary biliary mixed adenoneuroendocrine carcinoma (MANEC): a short review. Arch Pathol Lab Med 2016; 140: 1157-62.

16. Verlicchi L, Blons H, Hannoun L, Bachet JB. Squamous-cell gallbladder carcinoma: how to treat? J Cell Sci Ther 2015; 6: 212.

■ CASE STUDY ■

Multiple Neuroendocrine Tumors in Stomach and Duodenum in a Multiple Endocrine Neoplasia Type 1 Patient

Bohyun Kim · Han-Kwang Yang[1]
Woo Ho Kim

Departments of Pathology and [1]Surgery, Seoul
National University College of Medicine, Seoul,
Korea

Corresponding Author
Woo Ho Kim, MD, PhD
Department of Pathology, Seoul National University
College of Medicine, 103 Daehak-ro, Jongno-gu,
Seoul 03080, Korea
Tel: +82-2-740-8269
Fax: +82-2-765-5600
E-mail: woohokim@snu.ac.kr

A 67-year-old woman with a history of subtotal parathyroidectomy, distal pancreatectomy, and total splenectomy 23 years prior underwent surgical gastric resection for neuroendocrine tumors of the stomach and duodenum. Meticulous examination of the entire stomach and duodenum revealed multiple scattered, minute neuroendocrine tumors. To the best of our knowledge, this is the first case report of a patient diagnosed with gastroduodenal neuroendocrine tumors associated with multiple endocrine neoplasia type 1 (MEN 1) in whom complete histologic mapping of the whole gastrectomy specimen was performed. The presence of MEN 1–associated neuroendocrine tumors in the stomach is very rare, but should be considered in patients diagnosed with MEN 1 who present with a new tumor in the stomach.

Multiple endocrine neoplasia (MEN) is a rare, autosomal-dominant disease caused by a genetic mutation and shows a familial tendency.[1,2] Various kinds of endocrine glands may be involved in this condition. According to the affected genes and the distribution of neuroendocrine tumor-involved organs, MEN is classified into types 1, 2, 3, and 4.[3] MEN 1 has a prevalence of 0.25% in postmortem studies, and is found in patients of all ages.[4] MEN 1 can be diagnosed based on three different criteria. First, a clinical diagnosis can be made if two or more MEN 1–associated tumors are found. Second, a familial diagnosis can be made if a MEN 1 patient who has been clinically diagnosed has a first-degree family member with a history of MEN 1. Finally, a genetic diagnosis can be made if a MEN 1 germ-line mutation is confirmed, even in the absence of clinical and biochemical manifestations.[5]

CASE REPORT

A 67-year-old woman visited Seoul National University Hospital after an abnormal finding was detected on esophago-gastroduodenoscopy (EGD) performed as part of a routine medical examination at another hospital. She previously underwent right thyroidectomy with subtotal parathyroidectomy, distal pancreatectomy, and total splenectomy 23 years prior. Pathological evaluation at that time resulted in the diagnosis of parathyroid gland hyperplasia, thyroid adenomatous goiter, and pancreas islet cell adenomas. The clinical diagnosis was MEN 1. The patient's younger sister was also diagnosed with MEN 1.

Laboratory studies from 23 years prior showed preoperative and postoperative serum gastrin levels of 222 and 143 ng/dL (normal range, < 90 ng/dL), respectively, and calcium levels of 10.7 and 7.9 mg/dL (normal range, 8.4 to 10.2 mg/dL), respectively. Thus, the patient was clinically diagnosed with MEN 1. One year prior, two adenocarcinoma lesions were found on the posterior wall of the stomach antrum, and they were successfully removed via endoscopic submucosal dissection.

The patient underwent EGD, which revealed a subepithelial mass with an approximate size of 0.5 cm in the stomach cardia and 1 cm sized multiple subepithelial masses in the second portion of the duodenum (Fig. 1A). Biopsy was performed and immunohistochemical evaluation revealed tumor cells positive for chromogranin A, synaptophysin, and cytokeratin. The pathological diagnosis was neuroendocrine tumor for all lesions (Fig. 1B–D).
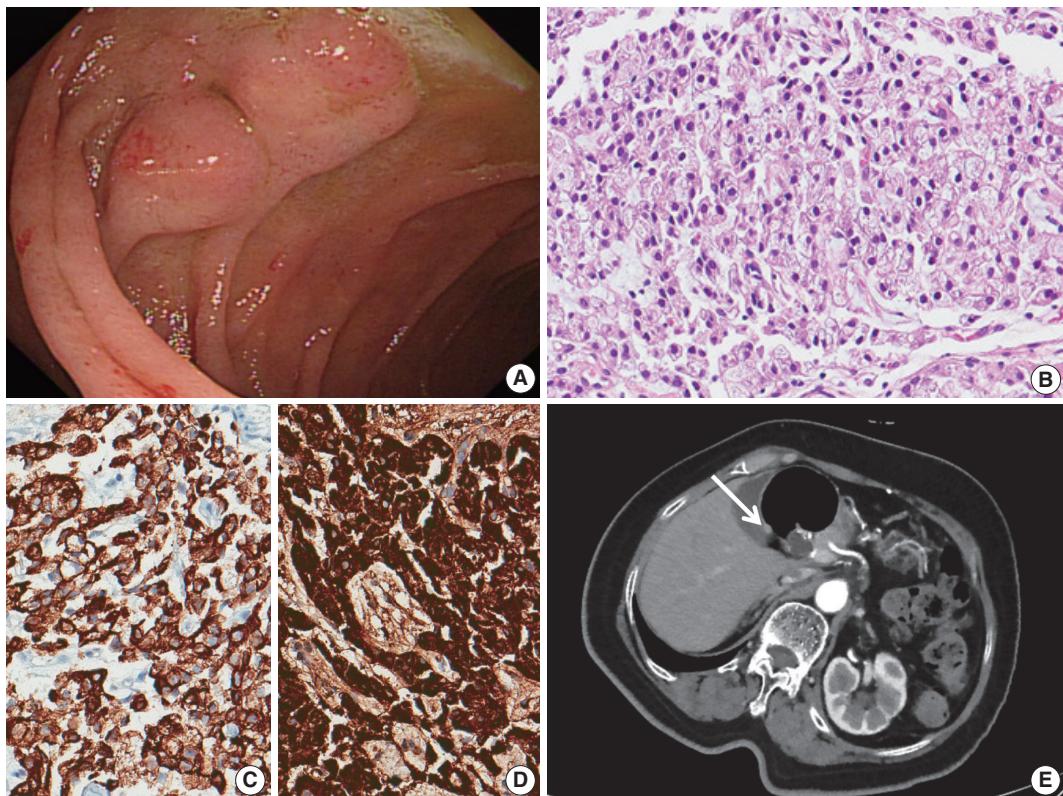
Fig. 1. (A) Two subepithelial masses were found in the duodenum on esophagogastroduodenoscopy. (B) A neuroendocrine tumor with a diffuse pattern. (C) Immunohistochemistry of cytokeratin. (D) Immunohistochemistry of chromogranin A. (E) Abdominal computed tomography reveals a 6-mm-sized nodule (arrow) in the duodenal bulb.

On three-dimensional computed tomography of the stomach, a definite subepithelial tumor could not be observed in the stomach cardia, but a 6-mm-sized subepithelial tumor was found in the duodenal bulb (Fig. 1E). Three additional tiny, hyperenhanced lesions were found in the uncinate process of the pancreas. Considering her medical history, the possibility of the lesions being neuroendocrine tumors could not be excluded. No lesions were found in the pituitary gland or adrenal gland.

Total gastrectomy with extended resection of the proximal duodenum was performed. On macroscopic examination, three polypoid lesions were identified in the duodenum. They consisted of multiple polypoid submucosal nodules covered by centrally umbilicated hyperemic mucosa, each with a size of less than 1 cm. Polypoid lesions were macroscopically not visible in the stomach cardia, where the neuroendocrine tumor was diagnosed. To evaluate the lesion in the stomach cardia, which was confirmed on EGD, and identify additional neuroendocrine lesions in the stomach, the entire resected specimen was subjected to a histologic mapping procedure. Two hundred seventeen sections were mounted in 109 each formalin-fixed, paraffin-embedded blocks. Meticulous microscopic examination of the entire specimen

revealed 14 neuroendocrine lesions in the duodenum and five neuroendocrine lesions in the anterior and posterior walls of the stomach cardia. Among the 14 lesions in the duodenum, 10 had the greatest dimension > 0.5 mm and the remaining four lesions represented neuroendocrine dysplasia with the greatest dimension > 150 μm but < 500 μm (Fig. 2A).[6] All five lesions in the stomach had the greatest dimensions > 0.5 mm. Among the 19 lesions, only three were identifiable on macroscopic examination, and these were located in the duodenum as multiple nodules.

Microscopically, the neuroendocrine tumors in this case showed histopathologic features that were identical to those of sporadic neuroendocrine tumors. Duodenal lesions were all located in the mucosa or submucosa, with the greatest lesion being $0.8 \times 0.8 \times 0.3$ cm in size. All lesions in the stomach were located in the lamina propria or submucosa, with the size of the greatest lesion being $0.3 \times 0.2 \times 0.2$ cm (Fig. 2B). Immunohistochemical analysis revealed that the neuroendocrine markers synaptophysin and chromogranin A were positive. Lymphatic invasion, vascular invasion, and perineural invasion were not observed. Thirty regional lymph nodes were identified, and metastasis was confirmed in one lymph node in station 3 (lymph
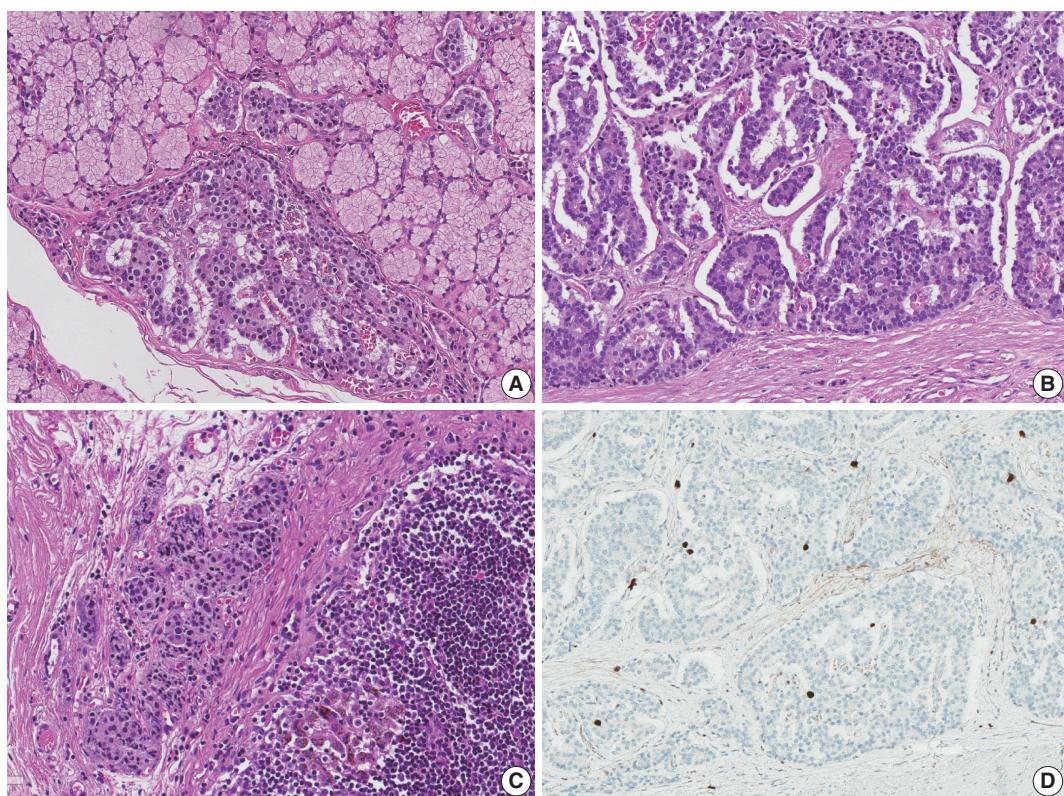
Fig. 2. Histologic features of neuroendocrine tumors. (A) Neuroendocrine dysplasia in the submucosal layer of the duodenum. (B) Neuroendocrine tumor in a ribbon-like growth pattern. (C) Metastatic lymph node in station 3. (D) Immunohistochemistry of Ki-67.
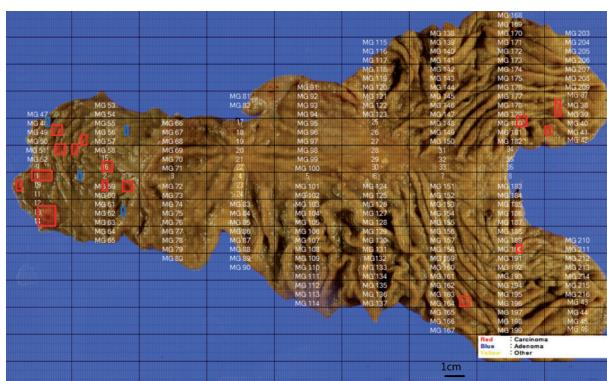

Fig. 3. Histologic mapping of the entire specimen revealed 19 neuroendocrine lesions in the stomach and duodenum (red, neuroendocrine tumor; blue, neuroendocrine dysplasia).

nodes along the lesser curvature). The size of the metastatic lymph node was 0.4 mm (Fig. 2C). On the histologic mapping procedure, 16 additional lesions were found (Fig. 3).

According to the 8th edition of the TNM staging system of the American Joint Committee on Cancer, neuroendocrine tumors of the stomach were stage T1, as they invaded the lamina propria or submucosa and were ≤ 1 cm in size. Neuroendocrine tumors

in the duodenum were also stage T1, as they invaded only the mucosa or submucosa and were ≤ 1 cm in size. Both could be staged as N1 because of regional lymph node metastasis and as grade 1, as they showed a Ki-67 index of < 1% and mitotic activity of < 1/10 high-power field (Fig. 2D).

The patient underwent follow-up abdominal computed tomography, and a small enhanced nodular lesion in the second portion of the duodenum and three enhanced lesions in the uncinated process of the pancreas were found. The possibility of additional neuroendocrine tumors could not be excluded. No recurrence was observed at the surgery site.

The study was approved by the Institutional Review Board of Seoul National University Hospital (IRB No. H-1706-098-860) and performed in accordance with the principles of the Declaration of Helsinki. The informed consent was waived.

DISCUSSION

MEN 1 is a rare autosomal-dominant disease caused by a mutation in the *MEN1* gene (chromosome 11) encoding the tumor suppressor protein menin.[7,8] MEN 1 is suspected when two

or more of the most common neuroendocrine tumors (parathyroid tumor, pancreatic islet cell tumor, and pituitary gland tumor) are found. Approximately 80%–90% of patients diagnosed with MEN 1 show a *MEN1* gene mutation.[9] However a genetic evaluation to confirm *MEN1* gene mutation was not performed in this patient.

The incidence of gastrointestinal neuroendocrine tumors is increasing, and they account for 1% of all stomach tumors.[10] Stomach neuroendocrine tumors can be subclassified into types I, II, and III. Type I neuroendocrine tumors accounts for 70%–80% of stomach neuroendocrine tumors and primarily occur in patients with chronic atrophic gastritis, such as autoimmune gastritis and *Helicobacter pylori*–associated atrophic gastritis. Type III neuroendocrine tumors account for 10%–15% of stomach neuroendocrine tumors. These are sporadic tumors and are not associated with enterochromaffin cell hyperplasia. Finally, type II neuroendocrine tumors account for 5%–6% of stomach neuroendocrine tumors and are associated with MEN 1 and Zollinger-Ellison syndrome. In previous studies, 5%–10% of MEN 1 patients exhibited neuroendocrine tumors in the stomach, thymus, and lung. Type II neuroendocrine tumors are associated with hypergastrinemia, and they originate from enterochromaffin cells.[11,12]

This report described a patient with a clinical diagnosis of MEN 1 and neuroendocrine tumor involvement of the stomach and duodenum, in whom whole-stomach histologic mapping was performed on a gastrectomy specimen. After mapping, multiple small lesions were detected that had not been observed on prior radiologic and macroscopic examinations.

In conclusion, we report a rare case of multiple gastric and duodenal neuroendocrine tumors associated with MEN 1. Histologic mapping was conducted using the entire resected specimen. This case shows that some patients with stomach neuroendocrine tumors associated with MEN 1 can develop multiple lesions in the stomach and duodenum, which can be overlooked on radiologic or endoscopic evaluation. Further studies are needed to assess the pathological characteristics of inherited stomach neuroendocrine tumors.

Conflicts of Interest

No potential conflict of interest relevant to this article was reported.

REFERENCES

1. Kouvaraki MA, Lee JE, Shapiro SE, *et al*. Genotype-phenotype analysis in multiple endocrine neoplasia type 1. Arch Surg 2002; 137: 641-7.
2. de Laat JM, van der Luijt RB, Pieterman CR, *et al*. MEN1 redefined, a clinical comparison of mutation-positive and mutation-negative patients. BMC Med 2016; 14: 182.
3. Thakker RV. Multiple endocrine neoplasia type 1 (MEN1) and type 4 (MEN4). Mol Cell Endocrinol 2014; 386: 2-15.
4. Feliberti E, Perry RR, Vinik A. Multiple endocrine neoplasia type I and MEN II. In: De Groot LJ, Chrousos G, Dungan K, *et al.*, eds. Endotext. South Dartmouth: MDText.com Inc., 2000.
5. Turner JJ, Christie PT, Pearce SH, Turnpenny PD, Thakker RV. Diagnostic challenges due to phenocopies: lessons from multiple endocrine neoplasia type1 (MEN1). Hum Mutat 2010; 31: E1089-101.
6. Grin A, Streutker CJ. Neuroendocrine tumors of the luminal gastrointestinal tract. Arch Pathol Lab Med 2015; 139: 750-6.
7. Wang GG, Yao JC, Worah S, *et al*. Comparison of genetic alterations in neuroendocrine tumors: frequent loss of chromosome 18 in ileal carcinoid tumors. Mod Pathol 2005; 18: 1079-87.
8. Christopoulos C, Papavassiliou E. Gastric neuroendocrine tumors: biology and management. Ann Gastroenterol 2005; 18: 127-40.
9. Falchetti A. Genetic screening for multiple endocrine neoplasia syndrome type 1 (MEN-1): when and how. F1000 Med Rep 2010; 2: 14.
10. Tsikitis VL, Wertheim BC, Guerrero MA. Trends of incidence and survival of gastrointestinal neuroendocrine tumors in the United States: a seer analysis. J Cancer 2012; 3: 292-302.
11. Li TT, Qiu F, Qian ZR, Wan J, Qi XK, Wu BY. Classification, clinicopathologic features and treatment of gastric neuroendocrine tumors. World J Gastroenterol 2014; 20: 118-25.
12. Sato Y, Hashimoto S, Mizuno K, Takeuchi M, Terai S. Management of gastric and duodenal neuroendocrine tumors. World J Gastroenterol 2016; 22: 6817-28.

Osteosarcomatous Differentiation in Rebiopsy Specimens of Pulmonary Adenocarcinoma with EGFR-TKI Resistance

Hyein Ahn · Hyun Jung Kwon · Eunhyang Park[1] · Hyojin Kim · Jin-Haeng Chung

Department of Pathology, Seoul National University Bundang Hospital, Seongnam; [1]Department of Pathology, Seoul National University Hospital, Seoul, Korea

Histological transformation of adenocarcinoma such as transformation into small cell carcinoma (SCC) and epithelial to mesenchymal transition (EMT) is one of the discovered mechanisms of the acquired resistance to epidermal growth factor receptor–tyrosine kinase inhibitor (EGFR-TKI). We report two cases of EGFR-TKI resistant pulmonary adenocarcinoma associated with EMT features that showed osteosarcomatous differentiation in rebiopsy specimens.

CASE REPORT

Case 1

A 55-year-old female, non-smoker presenting chronic cough was found to have a mass in the right upper lobe of lung with disseminated intrapulmonary metastasis on computed tomography (CT). CT-guided biopsy of the pulmonary mass revealed a moderately differentiated adenocarcinoma (Fig. 1A) harboring *EGFR* exon 19 deletion. The initial positron emission tomography–CT and brain magnetic resonance imaging showed metastatic lesions in the left ilium and bilateral cerebral cortex. As first-line therapy, she received one cycle of conventional chemotherapy for 8 days, and then started gefitinib as second-line therapy. After 1 year of continuous gefitinib treatment, radiologic evaluation showed a larger number of metastatic nodules in lung and increased extent of the left iliac metastases with extraosseous ossification (Fig. 2A).

Corresponding Author
Jin-Haeng Chung, MD, PhD
Department of Pathology, Seoul National University Bundang Hospital, 82 Gumi-ro 173beon-gil, Bundang-gu, Seongnam 13620, Korea
Tel: +82-31-787-7713, Fax: +82-31-787-4012, E-mail: chungjh@snu.ac.kr

Case 2

A 58-year-old man who had undergone right upper lobectomy of lung was diagnosed as adenocarcinoma (Fig. 1B) with pT-1N0M0 harboring an *EGFR* exon 19 deletion mutation. Three years after surgery, metastatic lesions were detected in the right lower lobe and pleura on radiologic findings. He received conventional chemotherapy for 3 months, and then started gefitinib. After 15 months of continuous gefitinib treatment, second biopsy for the pulmonary lesion confirmed T790M mutation, and additional metastatic lesions found in T2 and T5 vertebral bodies (Fig. 2B) were removed by surgical curettage.

Rebiopsy of the metastatic bone lesions of these two patients was performed. Microscopic findings of the tumor showed adenocarcinoma merging with poorly differentiated sarcomatous components. Remarkably, there were spindle shaped sarcomatous tumor cells with eosinophilic cytoplasm producing ill-defined pink acellular lace-like osteoid. These osteoid components were closely associated with the tumor cells and deposited as disorganized features. The sarcomatous neoplastic cells intermingled with osteoid demonstrate unequivocal features of malignancy, which is different from reactive osteoid or callus formation (Fig. 1C, D). *EGFR* mutation status was same as that of primary lung specimen, and immunohistochemistry showed vimentin expression and decreased E-cadherin.

DISCUSSION

It is known that the resistance to EGFR-TKI is due to various mechanisms. Rebiopsy is usually used to detect the underlying molecular mechanism of resistance; however, meticulous histologic examination is very important to identify the change in cancer phenotype. Histological transformation of adenocarcinoma such
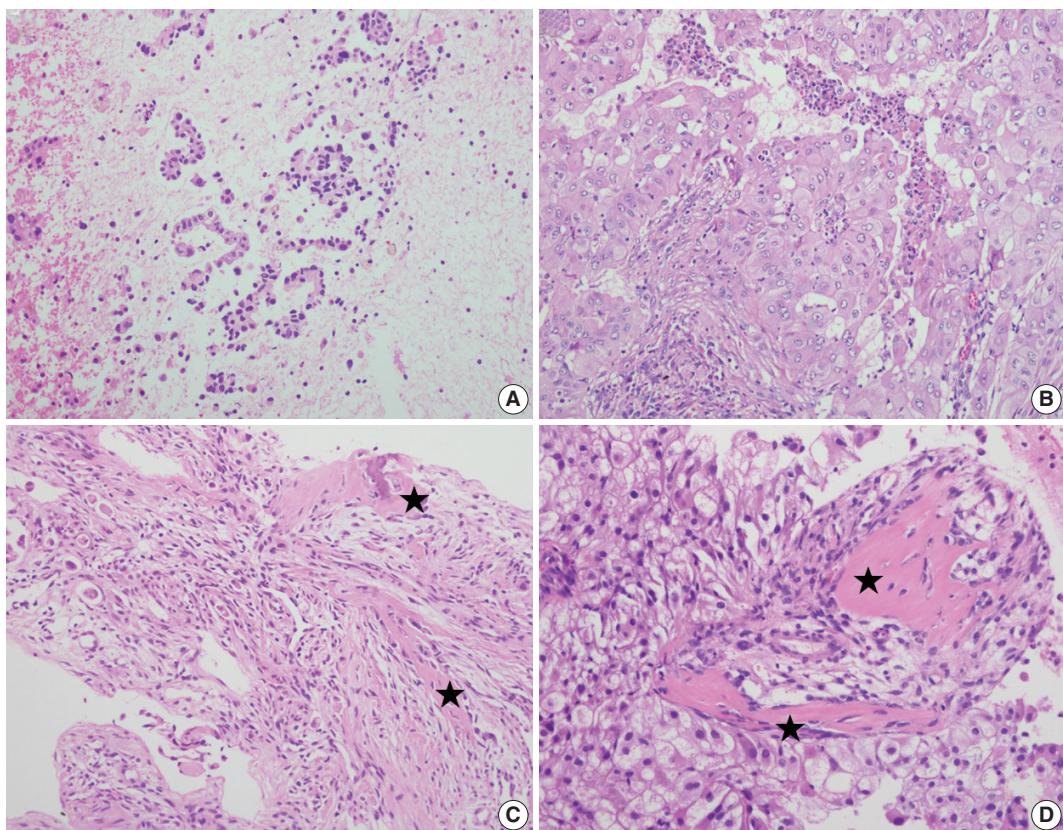
Fig. 1. Histologic findings. First biopsy of case 1 (A) and case 2 (B). Microscopic finding of first biopsy reveals adenocarcinoma showing glandular differentiation. Rebiopsy of case 1 (C) and case 2 (D). Microscopic finding shows sarcomatous tumor cells producing osteoid (asterisks).
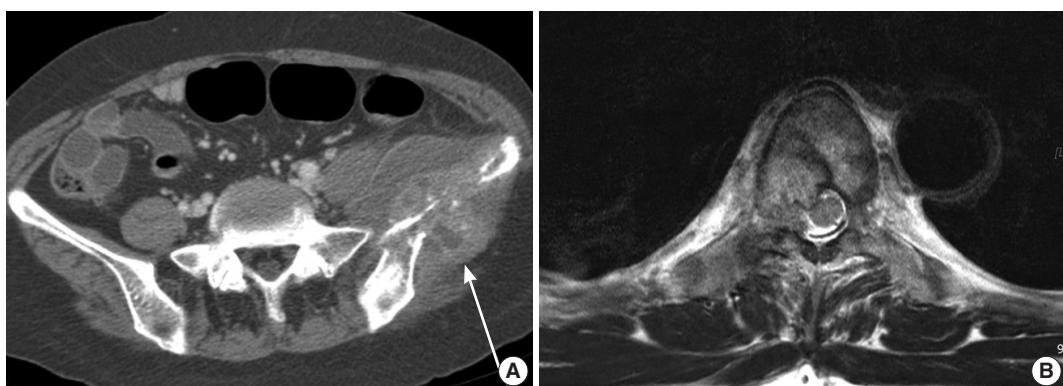

Fig. 2. Radiologic findings. Case 1 (A). Pelvic magnetic resonance imaging demonstrates left iliac metastases with ossification at the extraosseous soft tissue (arrow). Case 2 (B). Computed tomography reveals T2 and T5 vertebral bodies metastases.

as transformation into SCC and EMT is one of the discovered mechanisms in the acquired resistance to EGFR-TKI.[1] EMT is characterized by loss of cell adhesion and acquisition of mesenchymal features, showing morphological change from the epithelial phenotype to the mesenchymal fibroblastoid phenotype. Osteosarcomatous differentiation highly represents EMT features which may contribute to the acquired resistance to EGFR-

TKIs. To the best of our knowledge, this is the first report to describe pulmonary adenocarcinoma with osteosarcomatous differentiation in rebiopsy specimens of EGFR-TKI resistant patients.

Here, we describe two cases showing osteosarcomatous differentiation with sarcomatoid features after EGFR-TKI treatment. The malignant osteoid components were distinguished from destroyed and/or regenerating bone elements by their morphol-

ogy and surrounding poorly differentiated sarcomatous cells in histologic findings. In addition, the ossification of extraosseous sites in radiologic findings is helpful. As the evaluation of metastatic sites for rebiopsy were bone lesions in both patients, the tumor microenvironment may have contributed to the transformation from adenocarcinoma to osteosarcomatous phenotype.[2] A few previous studies suggested that a bone environment is essential for osteosarcoma development from transformed mesenchymal stem cells.[3] Our findings suggest that the differences of the intrinsic nature between epithelial and osteosarcomatous mesenchymal cancers may be the cause of the acquired resistance to EGFR-TKI.[4] In addition, Mink *et al.*[5] demonstrated that the tumor stroma having cancer-associated fibroblast related to EMT plays an important role in limiting responsiveness to EGFR-TKI.

The phenotypic change in cancer including EMT and histological transformation has been identified as a mechanism of resistance to EGFR-TKI; however, the specific underlying biologic mechanism remains unclear. Further investigations are needed to explain the mechanism of EMT and tumor microenvironment involved in EGFR-TKI resistance.

Conflicts of Interest

No potential conflict of interest relevant to this article was reported.

REFERENCES

1. Sequist LV, Waltman BA, Dias-Santagata D, *et al*. Genotypic and histological evolution of lung cancers acquiring resistance to EGFR inhibitors. Sci Transl Med 2011; 3: 75ra26.
2. Quail DF, Joyce JA. Microenvironmental regulation of tumor progression and metastasis. Nat Med 2013; 19: 1423-37.
3. Rubio R, Abarrategi A, Garcia-Castro J, *et al*. Bone environment is essential for osteosarcoma development from transformed mesenchymal stem cells. Stem Cells 2014; 32: 1136-48.
4. Byers LA, Diao L, Wang J, *et al*. An epithelial-mesenchymal transition gene signature predicts resistance to EGFR and PI3K inhibitors and identifies Axl as a therapeutic target for overcoming EGFR inhibitor resistance. Clin Cancer Res 2013; 19: 279-90.
5. Mink SR, Vashistha S, Zhang W, Hodge A, Agus DB, Jain A. Cancer-associated fibroblasts derived from EGFR-TKI-resistant tumors reverse EGFR pathway inhibition by EGFR-TKIs. Mol Cancer Res 2010; 8: 809-20.

■ BRIEF CASE REPORT ■

Denosumab-Treated Giant Cell Tumor of the Bone Mimicking Low-Grade Central Osteosarcoma

Chang-Che Wu · Pin-Pen Hsieh

Department of Pathology and Laboratory Medicine, Kaohsiung Veterans General Hospital, Kaohsiung, Taiwan

Giant cell tumor of the bone is a benign but locally aggressive bone tumor. In recent years, denosumab, a receptor activator for nuclear factor-κβ ligand (RANKL) inhibitor has emerged as a treatment alternative, especially when surgical clearance cannot be obtained or for frequent recurrence. However, treatment-related histologic changes have been rarely documented in the literature until recently and show substantial overlap with other primary tumors of bone such as low-grade central osteosarcoma, which can easily lead to a misdiagnosis. Here we present a typical case of denosumab-treated giant cell tumor of the bone confirmed by detection of an *H3F3A* (histone H3 family 3A protein) mutation, which we believe is the first case report in Taiwan.

CASE REPORT

A 50-year-old female patient visited our clinic complaining of left knee pain that had been present for 4 months. The condition was aggravated during ambulation and worsened as time went by. There was no trauma history or any significant past medical history of note. She had gone to another hospital first where a left distal femur osteolytic tumor was found. Needle biopsy was performed there, and the pathology revealed giant cell tumor of the bone (Fig. 1A). She was then given subcutaneous injections of denosumab (120 mg) every 4 weeks for 3 months. Due to personal reasons, she visited our clinic thereafter. Magnetic resonance imaging showed a 4.1-cm expansile, eccentric osteolytic

Corresponding Author
Pin-Pen Hsieh, MD
Department of Pathology and Laboratory Medicine, Kaohsiung Veterans General
Hospital, 386, Ta-Chung 1st Rd., Kaohsiung 813, Taiwan
Tel: +886-7-3422121 (ext. 6306), Fax: +886-3422288, E-mail: pinpenh@gmail.com

bone tumor around the epiphysis and metaphysis of the left distal femur; the lesion manifested low T1 weighted image and T2 weighted image with strong contrast enhancement (Fig. 1B). Relatively well-defined margins with cortical thinning were noted. No conspicuous tumor regression was noted, and the lesion was still radiologically classified as grade II using the Campanacci classification. After 3 months of denosumab treatment, adequate curettage and adjuvant cryotherapy with liquid nitrogen and bone graft implantation were performed.

A brownish circumscribed tumor, 5 cm in size, was found during the operation, with no soft tissue or joint involvement. The curettage specimen was sent for pathologic examination. Light microscopy showed that the tumor was composed mostly of woven bone, with a small amount of aggregated mononuclear cell foci and scattered osteoclast-like giant cells (< 10%). Compared with ordinary giant cell tumors of the bone before denosumab treatment (Fig. 1A), this post-treatment specimen showed decreased cellularity, reduced number and size of osteoclast-like giant cells, and abundant new bone deposition as broad, rounded cords, or long, curvilinear arrays (Fig. 1C, D). Only minimal cytological atypia and occasional mitoses were noted. Focal necrosis was identified. Immunohistochemically, the tumor cells were negative for cyclin-dependent kinase 4 (1:200, ZETA Corporation, Arcadia, CA, USA), and murine double minute 2 (MDM2; 1:50, ZETA Corporation) (Fig. 1E). The genetic study was negative for *MDM2* amplification. In addition, the *H3F3A* gene mutation was assessed with polymerase chain reaction and direct sequencing which showed hotspot mutation c.100G > T (G34W) (Fig. 1F).

After the operation, the range of motion (ROM) for the left knee gradually improved from partial to full ROM at 6-month follow-up. No evidence of tumor recurrence was noted.

This study was approved by the Institutional Review Board of Kaohsiung Veterans General Hospital (IRB No. VGHKS18-CT2-01) with a waiver of informed consent.

DISCUSSION

Giant cell tumor of the bone is composed of a proliferation of mononuclear cells amongst which are scattered numerous macrophages and large osteoclast-like giant cells. It is thought that the numerous large osteoclast-like giant cells are not neoplastic but reactive in nature.[1] These neoplastic mononuclear cells exhibit mutations to the *H3F3A* gene,[2] and express high levels of RANKL,[3] which binds to RANK, a receptor expressed on the surface of multinucleated osteoclast-like giant cells and their precursors. This results in the activation and proliferation of these cells, leading to bone resorption.[4] Denosumab, a RANKL inhibitor, has been shown to retard or arrest tumor growth.[5] Denosumab-treated tumors can be devoid of giant and mononuclear cells and are composed of abundant woven bone and fibrous tissue.

Wojcik *et al.*[6] reported nine cases and demonstrated that all treated giant cell tumors of the bone showed marked giant cell depletion. A gradual decrease in stromal cellularity and increased
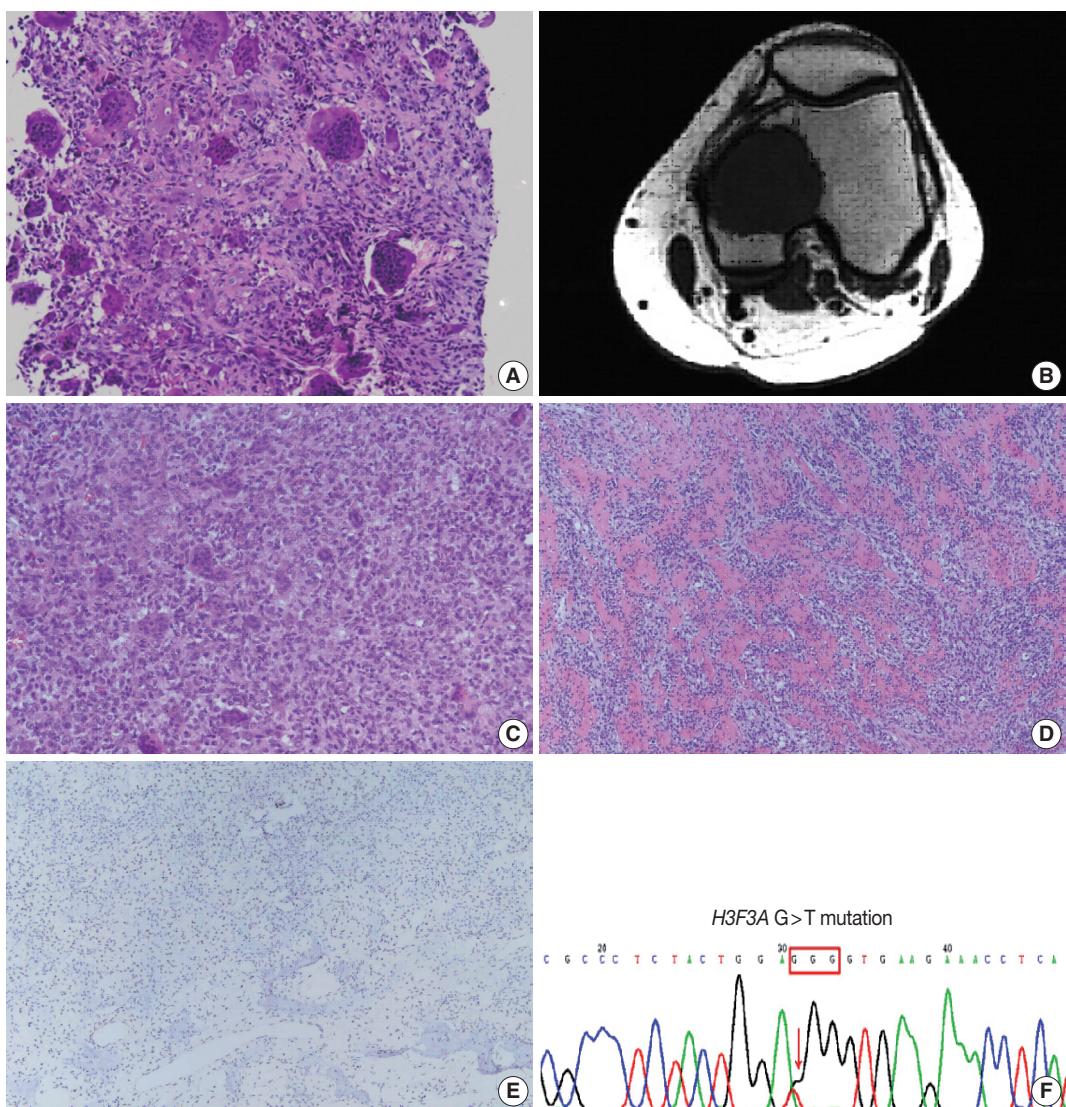

Fig. 1. (A) The typical picture of giant cell tumor before treatment shows "giant" osteoclasts with >20 and sometimes >50 nuclei. (B) Magnetic resonance imaging reveals an expansile, eccentric osteolytic bone tumor around epiphysis and metaphysis of left distal femur. (C, D) Compared with ordinary giant cell tumor, this case exhibits reduced number and size of osteoclast-like giant cells and also abundant new bone deposition, mimicking low-grade central osteosarcoma. (E) The immunohistochemical result shows negative for MDM2. (F) *H3F3A* hotspot mutation (G34W) is detected.

new bone formation appeared to correlate with treatment. Denosumab shifts the balance of physiological bone formation away from RANK-mediated osteoclastic bone resorption toward osteoprotegrin-induced bone formation. However, it seems that this shift does not reflect terminal differentiation, as the morphology reverts to classic giant cell tumor histopathology upon denosumab therapy cessation.

The combination of relatively bland-looking tumor cells with minimal cytological atypia, as well as abundant new bone formation in curvilinear arrays within a fibrous background, produced a resemblance to low-grade central osteosarcoma.[6] In addition, benign multinucleated giant cells have been reported in up to 36% of low-grade central osteosarcomas,[7] making the distinction more challenging. Recently, Rekhi et al.[8] also reported that after denosumab treatment, giant cell tumors of the bone can appear as low-grade osteosarcomas on histopathologic examination, but lack the clinical behavior of an osteosarcoma.

In terms of differential diagnoses, giant cell-rich conventional osteosarcoma and malignancy in giant cell tumor of the bone are characterized by more severe cytological atypia and more prominent mitotic activity, which were not seen in this case. Low-grade central osteosarcoma was also excluded due to the lack of an infiltrative growth pattern and negative MDM2 amplification. Finally, we performed a genetic test and an H3F3A hotspot mutation (G34W) was detected. This finding supported the diagnosis of giant cell tumor of the bone.

In summary, we present a case of giant cell tumor of the bone with typical morphologic changes after denosumab treatment, including giant cell depletion and abundant new bone formation. Detection of an H3F3A hotspot mutation (G34W) also confirmed the diagnosis. This is the first case report in Taiwan. Because denosumab-treated tumors bear little resemblance to their pretreatment counterparts and have substantial histologic overlap with other primary tumors of the bone, it is important for pathologists to understand the differences between treatment-related histologic changes and morphologic mimics. Due to the increasing use of denosumab in recent years, it is crucial to pay careful attention to the history of denosumab administration to avoid a misdiagnosis.

REFERENCES

1. Fletcher CD, Bridge JA, Hogendoorn PC, Mertens F. WHO classification of tumours of soft tissue and bone. 4th ed. Lyon: IARC Press, 2013; 321-4.

2. Behjati S, Tarpey PS, Presneau N, et al. Distinct H3F3A and H3F3B driver mutations define chondroblastoma and giant cell tumor of bone. Nat Genet 2013; 45: 1479-82.

3. Zheng MH, Robbins P, Xu J, Huang L, Wood DJ, Papadimitriou JM. The histogenesis of giant cell tumour of bone: a model of interaction between neoplastic cells and osteoclasts. Histol Histopathol 2001; 16: 297-307.

4. Cowan RW, Singh G. Giant cell tumor of bone: a basic science perspective. Bone 2013; 52: 238-46.

5. Thomas D, Henshaw R, Skubitz K, et al. Denosumab in patients with giant-cell tumour of bone: an open-label, phase 2 study. Lancet Oncol 2010; 11: 275-80.

6. Wojcik J, Rosenberg AE, Bredella MA, et al. Denosumab-treated giant cell tumor of bone exhibits morphologic overlap with malignant giant cell tumor of bone. Am J Surg Pathol 2016; 40: 72-80.

7. Kurt AM, Unni KK, McLeod RA, Pritchard DJ. Low-grade intraosseous osteosarcoma. Cancer 1990; 65: 1418-28.

8. Rekhi B, Verma V, Gulia A, et al. Clinicopathological features of a series of 27 cases of post-denosumab treated giant cell tumors of bones: a single institutional experience at a tertiary cancer referral centre, India. Pathol Oncol Res 2017; 23: 157-64.

Fine-Needle Aspiration Cytology of Carcinosarcoma in the Salivary Gland: An Extremely Rare Case Report

Hyo Jung An[1] · Hye Jin Baek[2,3,4]
Jin Pyeong Kim[2,3,5] · Min Hye Kim[6]
Dae Hyun Song[1,2,3]

[1]Deparment of Pathology, Gyeongsang National University Changwon Hospital, Changwon; [2]Gyeongsang National University School of Medicine, Jinju; [3]Gyeongsang Institute of Health Science, Jinju; Departments of [4]Radiology and [5]Otorhinolaryngology, Gyeongsang National University Changwon Hospital, Changwon; [6]Department of Pathology, Gyeongsang National University Hospital, Jinju, Korea

Corresponding Author
Dae Hyun Song, MD
Department of Pathology, Gyeongsang National University School of Medicine, 15 Jinju-daero 816beon-gil, Jinju 52727, Korea
Tel: +82-55-214-3150
Fax: +82-55-214-3174
E-mail: golgy@hanmail.net

Carcinosarcoma of the salivary gland is an extremely rare tumor that is composed of both malignant epithelial and mesenchymal components. Diagnosing carcinosarcoma with fine-needle aspiration cytology is challenging because of its overlapping cytomorphologic characteristics with other high-grade malignant salivary gland tumors. Among the many features, including pleomorphic oncocytoid epithelial components, necrotic background, and mitoses, recognizing the singly scattered atypical spindle cells is most essential in carcinosarcoma. We present a case of a 66-year-old male patient with characteristic features of carcinosarcoma, who was successfully treated by wide local excision and subsequent radiation therapy.

The term carcinosarcoma of the salivary gland, which means a tumor consisting of both carcinomatous and sarcomatous elements, was first used by King[1] in 1967. The three distinct histologic types of malignant mixed tumor are carcinoma ex pleomorphic adenoma, which accounts for most malignant mixed tumors, metastasizing mixed tumor, and carcinosarcoma, also known as true malignant tumor. To the best of our knowledge, approximately 60 cases of carcinosarcomas of the salivary glands have been reported in the English literature. Patients with carcinosarcoma of the salivary gland should be considered for additional chemotherapy or radiotherapy.[2] Its differential diagnosis is extremely important. However, making a correct diagnosis on an aspirated cytologic specimen is a challenge for pathologists because of various histologic features. Herein, we present a case of carcinosarcoma of the salivary gland diagnosed by preoperative fine-needle aspiration cytology (FNAC).

CASE REPORT

A 66-year-old man presented with a mass in the right submandibular gland that had been rapidly enlarging for several months. His medical history included hypertension, cardiovascular attack, and unstable angina. The computed tomography scan showed a 5-cm-sized movable mass with sialolithiasis in the right submandibular area (Fig. 1A). The FNAC specimen contained numerous single malignant epithelial cells that had marked nuclear pleomorphism, increased nuclear-cytoplasmic ratio, and coarse chromatin pattern with prominent nucleoli (Fig. 1C). Additionally, a few atypical mucin-containing cells, reminiscent of mucoepidermoid carcinoma, were found. Abundant necrotic debris and a mixture of inflammatory cells were scattered in the background of dispersed atypical spindle cells (Fig. 1D). There were sheet-like fragments, which showed

squamous differentiation with a few mitosis in only one out of ten FNAC slides (Fig. 1E). The patient underwent surgery to remove the mass and stones at Gyeongsang National University Changwon Hospital.

Overall, the cut surface showed a relatively well-circumscribed, ivory, heterogeneous mass that measured 5.5×4 cm and extended to the extra-parenchymal area (Fig. 1B). Microscopically, the tumor was mainly composed of two components—undifferentiated carcinoma (UC) and undifferentiated pleomorphic sarcoma (UPS) with a central necrosis (Fig. 1F). Under higher magnification, the carcinomatous component was haphazardly arranged with numerous mitoses. The sarcomatous components were permeating to the UC (Fig. 1G). The immunohistochemical findings were in a sharp contrast in these two components. Carcinoma cells were positive for cytokeratin (Fig. 1H), whereas sarcoma cells were negative for cytokeratin and positive for vimentin (Fig. 1I). Focal areas mimicking epithelial-myoepithelial carcinoma were observed (Fig. 1J).

All dissected 11 lymph nodes had no metastatic focus. The patient was successfully managed by wide local excision and subsequent radiation therapy. This study was approved by the Institutional Review Board of Gyeongsang National University Changwon Hospital with a waiver of informed consent (GNUCH 2017-09-009).

DISCUSSION

FNAC is a simple, safe, cost-effective, well-tolerated, and in particular, minimally invasive method.[3] On average, the salivary gland FNAC has high specificity (97%), but the sensitivity is relatively low (80%).[4] This means that the diagnosis on FNAC is very reliable, but the false-negative rate associated with FNAC (20%) may not be acceptable.[4] FNAC determines the extent of surgery needed after malignant tumor is diagnosed. It helps in deciding whether the facial nerve can be spared during the surgery and therefore, it is still important.[3] Diagnosing a high-grade salivary gland tumor, especially carcinosarcoma, on FNAC is challenging; thus, we should approach more systematically. Griffith et al.[5] proposed a risk stratification of FNAC in salivary gland tumors, which are classified as non-neoplastic and neoplastic. Among the neoplastic lesions, they proposed using the term oncocytoid and basaloid neoplasm rather than pleomorphic adenoma and Warthin tumor, the two most common tumors of the salivary gland. They also subdivided the oncocytoid and basaloid groups based on their nuclear grade (as monomorphic and pleomorphic groups), background characteristics, and stromal features. The pleomorphic oncocytoid neoplasm group was universally high-grade malignancies (21/21) and most of these 21 cases were of salivary duct carcinomas and several other
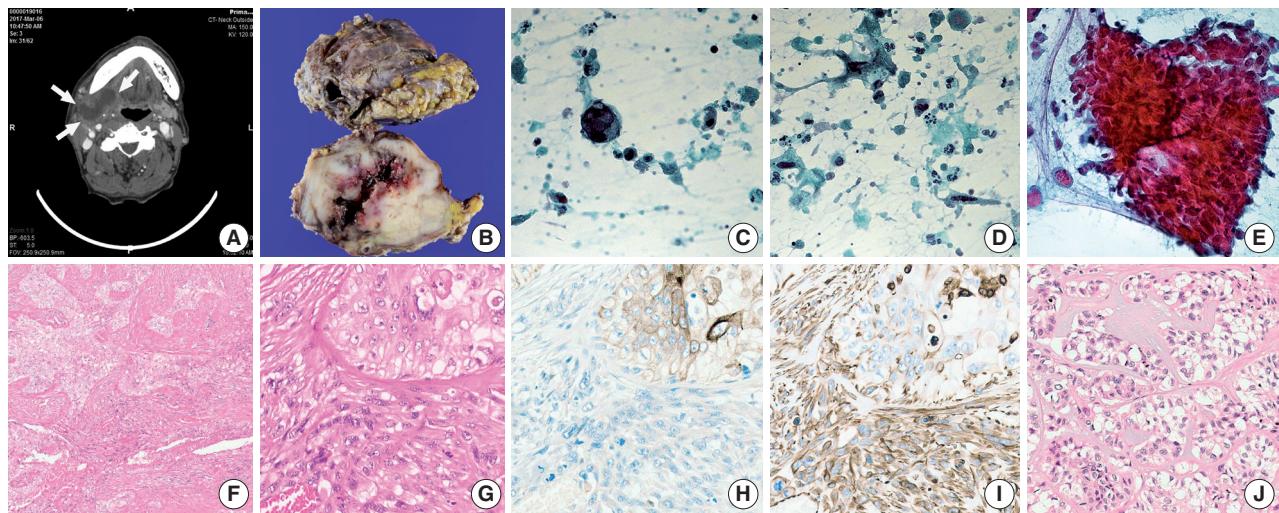

Fig. 1. Computed tomography image of the patient and gross examination, fine-needle aspiration specimen, and microscopic and immunohistochemical findings of carcinosarcoma. (A) Computed tomography scan shows a movable mass with sialolithiasis in the right submandibular area. (B) A well-circumscribed, ivory, heterogeneous mass is extended to the extra-parenchymal area. (C) A single malignant epithelial cell with marked nuclear pleomorphism, increased nuclear-cytoplasmic ratio, coarse chromatin pattern, and prominent nucleoli. (D) Abundant necrotic debris and a mixture of inflammatory cells are scattered in the background of dispersed atypical spindle cells. (E) Sheet-like fragments show squamous differentiation with a few mitosis. (F) Tumor is mainly composed of two components-undifferentiated carcinoma and undifferentiated pleomorphic sarcoma. (G) Under higher magnification, the carcinomatous component is haphazardly arranged with numerous mitoses and the sarcomatous components are permeating to the undifferentiated carcinoma. (H) Carcinoma cells are positive for cytokeratin. (I) Sarcoma cells are positive for vimentin. (J) Focal area mimicking epithelial-myoepithelial carcinoma.

high-grade carcinoma types including three high-grade muco-epidermoid carcinoma, one poorly differentiated carcinoma, and one UC.[5]

Based on the criteria of abundant cytoplasm, high nuclear grade with pleomorphism and hyperchromasia, and increased mitotic activity, the "pleomorphic oncocytoid neoplasm" was very identical to the carcinomatous components in our case. In addition, some other findings were observed, including isolated giant cells with vesicular nuclei and macronucleoli and isolated atypical spindle cells with hyperchromatic nuclei. These two different cells were classified as atypical because they had variations in size and shape more than three times the normal.[6] When FNAC findings were correlated with histological findings, the giant epithelial cells seemed to have come from the UC component, and the atypical spindle cells, either isolated or clustered with epithelial cells, seemed to have been exfoliated from the UPS component. In histologic section, UPS and UC were intermingled, showing different patterns of immunohistochemical staining for cytokeratin and vimentin, which is the key finding in confirming carcinosarcoma.

Because there were squamoid clusters without keratinization in the FNA specimen, mucoepidermoid carcinoma (MEC) with squamous elements and moderate to poorly differentiated squamous cell carcinoma (SCC) were included in differential diagnosis. If it were MEC, there must be numerous tumor cell clusters due to its hard and solid consistency in high-grade types.[6] Also, non-keratinizing, moderate to poorly differentiated SCCs usually exfoliate in clusters or sheets. Rapidly growing tumors like our case frequently produce central necrosis and often show cellular debris with necrotic background in their aspirates.[6] In our case, there were plenty of individual pleomorphic cells in abundant necrotic background. Only up to 23 cell clusters were contained in 10 aspirated slides. We suggest that more aggressive tumors including malignant mixed tumor and carcinosarcoma must be considered, if there are fewer carcinomatous clusters and abundant individual pleomorphic cells in necrotic background.

The sarcomatous components in our case occupied nearly 40% of the total tumor volume. However, these components were hardly seen in the FNAC. Both isolated spindle cells and sheet-like tissue fragments were found in one out of 10 FNAC slides. We hypothesized that matrix-forming characteristics of carcinosarcoma might have affected the hypocellularity of sarcomatous cells in the FNAC specimen. The malignant mesenchymal elements of carcinosarcomas are most commonly in the form of chondrosarcoma.[2,7,8] In the present case, however, features of chondrosarcoma were not observed in both cytologic and surgical speci-

mens. In addition, tumor cells in sheets were not as pleomorphic as the isolated atypical spindle cells in the FNAC specimen. We should be concentrating on the scattered atypical cells or matrix-forming cells when we approach high-grade pleomorphic salivary gland tumors in FNAC. Frequently, isolated cells, which accurately reveal their characteristic morphologic features, are more important than three-dimensional clusters in cytologic specimens.

The histogenesis and pathogenesis of the carcinosarcoma are still under discussion. Some authors insist that pleomorphic adenoma and carcinosarcomas may share a common precursor cell in which the myoepithelial cell is a major component in their development.[8,9] In the present case, approximately 20% of the total volume of epithelial myoepithelial carcinoma-mimicking area was observed in the histologic specimen. However, these components did not show any immunoactivities for smooth muscle actin and S100, a marker of myoepithelial cells. Furthermore, histologic evidence of a preexisting or coexisting pleomorphic adenoma was not observed. These findings may indirectly prove that myoepithelial cells may not be the sole origin of carcinosarcoma. We agree with Kwon and Gu[10] that the primitive mesenchymal cells, which can be differentiated in diverse directions, may contribute to the development of different types of sarcomas in carcinosarcomas; thus, they have heterogeneous combinations of both epithelial and mesenchymal components.[7]

Although carcinosarcoma is an extremely rare tumor, pathologists should be aware of this entity because the diagnosis of carcinosarcoma warrants concurrent radiation therapy extended to regional lymph nodes even if those lymph nodes are not metastatic.

We described the cytologic features of carcinosarcoma arising in the submandibular salivary gland. In FNAC of the salivary gland tumor, carcinosarcoma should be considered if atypical spindle cells and highly pleomorphic epithelial cells are identified in abundant necrotic background.

Conflicts of Interest

No potential conflict of interest relevant to this article was reported.

REFERENCES

1. King OH Jr. Carcinosarcoma of accessory salivary gland: first report of a case. Oral Surg Oral Med Oral Pathol 1967; 23: 651-9.
2. Keh SM, Tait A, Ahsan F. Primary carcinosarcoma of the parotid gland. Clin Pract 2011; 1: e117.

3. Schmidt RL, Hall BJ, Wilson AR, Layfield LJ. A systematic review and meta-analysis of the diagnostic accuracy of fine-needle aspiration cytology for parotid gland lesions. Am J Clin Pathol 2011; 136: 45-59.

4. Schmidt RL, Hunt JP, Hall BJ, Wilson AR, Layfield LJ. A systematic review and meta-analysis of the diagnostic accuracy of frozen section for parotid gland lesions. Am J Clin Pathol 2011; 136: 729-38.

5. Griffith CC, Pai RK, Schneider F, et al. Salivary gland tumor fine-needle aspiration cytology: a proposal for a risk stratification classification. Am J Clin Pathol 2015; 143: 839-53.

6. Naib ZM. Cytopathology. 4th ed. New York: Little Brown & Company, 1996.

7. Marcotullio D, de Vincentiis M, Iannella G, Cerbelli B, Magliulo G.

Mucoepidermoid carcinoma associated with osteosarcoma in a true malignant mixed tumor of the submandibular region. Case Rep Otolaryngol 2015; 2015: 694684.

8. Stephen J, Batsakis JG, Luna MA, von der Heyden U, Byers RM. True malignant mixed tumors (carcinosarcoma) of salivary glands. Oral Surg Oral Med Oral Pathol 1986; 61: 597-602.

9. Bleiweiss IJ, Huvos AG, Lara J, Strong EW. Carcinosarcoma of the submandibular salivary gland. Immunohistochemical findings. Cancer 1992; 69: 2031-5.

10. Kwon MY, Gu M. True malignant mixed tumor (carcinosarcoma) of parotid gland with unusual mesenchymal component: a case report and review of the literature. Arch Pathol Lab Med 2001; 125: 812-5.